DEVELOPMENT OF BUBBLE AND LIGAND-BASED TARGETED NANOPARTICLES FOR SOLID TUMOR THERAPY

By

MICHAEL-JOSEPH GORBET, B.S.

Bachelor of Science in Chemistry
Southwestern Oklahoma State University
Weatherford, OK
2016

Submitted to the Faculty of the
Graduate College of the
Oklahoma State University
in partial fulfillment of
the requirements for
the Degree of
DOCTOR OF PHILOSOPHY
December, 2021

DEVELOPMENT OF BUBBLE AND LIGAND-BASED TARGETED NANOPARTICLES FOR SOLID TUMOR THERAPY

Dissertation Approved:

Dr. Ashish Ranjan

Dissertation Adviser

Dr. Jerry Malayer

Dr. Clinton Jones

Dr. Steven Hartson

ACKNOWLEDGEMENTS

I would like to humbly thank all those that have been a part of my journey during my Ph.D. I am truly grateful for not only my extremely supportive family, but also all professional support I have received during my time at Oklahoma State University. During my time as a graduate student, I have gotten married, witnessed the beauty of the birth of my first child, and had many wonderful experiences. While cancer affects many of us, it has directly impacted my family in many ways. I am very happy to contribute in any way I can to furthering our understanding of the topic towards options that are much more clinically effective.

My Ph.D. advisor, Dr. Ashish Ranjan, has been extremely supportive and helped me through some of the most difficult, yet most fulfilling years of my life. I am extremely grateful to all my committee- Dr. Jerry Malayer, Dr. Clinton Jones, and Dr. Steven Hartson for all your guidance, suggestions, and help throughout my Ph.D. Thank you kindly for taking time out of your busy schedules to be willing to discuss my data, seminars, qualifiers, etc. and helping to mold me into the scientist I am today. My special thanks to Dr. Hartson for the extra time and effort put forth in assisting writing.

I am extremely thankful for all my lab members, past and present, that helped me both during my transition into a new field entirely and my continued time into the program—Nandhini, Mohit, Kalyani, Josh, Cristina, Sarang, Akansha, and Harshini. Many of us grew very close, and I thoroughly enjoyed getting to know all of you. It really has felt like a family, and for that, I thank all of you. It is much easier to get work and inner collaborations done efficiently when colleagues are as such. I am especially thankful for Kalyani for teaching me everything I needed to know about coming into a predominantly biological lab. I am also very thankful for Sarang, who mentored me about modern cancer immunology advances, immunotherapy principles, and mouse models. My many thanks to Mohit as well for showing me the routes of synthesis for nanoparticles. Without these three mentoring me within my time, my Ph.D. would have been much, much more difficult.

My dearest thanks to all my professors throughout my Ph.D. I feel that I learned very valuable information in every class, but especially thank you to Dr. Pamela Lovern, Dr. Tom Oomens, Dr. Joao Lemos Brandao, and Dr. Joshua Butcher, who structured the seminar classes every semester for Ph.D. students. I do not think enough credit is given for this class and how much it truly does help students with their presentations. They always give insightful critiques and help to improve every student. I was extremely thankful for these seminars throughout my Ph.D.

My deepest thanks to my undergraduate adviser, Dr. Timothy Hubin, who gave me a job in research when I was such a young kid with little to no knowledge, a dream, and a thirst for knowledge. He guided me at a time that many would have refused me, and he helped me through many tough years in college as an advisor and mentor. I was truly blessed to have met him at the time I did as he played a very large role in preparing me for the rigors of graduate school.

My thanks extend to all my friends and family that have been patient with me during my Ph.D. My brother helped me realize I was interested in science before I even knew simple math, and for that, I thank you. My dearest wife, Madison, I thank you from the bottom of my heart for all your love, patience, and hard work during these tough times. I truly could not have done this without you. I would like to dedicate this dissertation to my baby daughter, Eliora Robin. Throughout the countless tough times we have already endured and will inevitably continue to go through, being your father is and always will be the proudest accomplishment of my life. I am indebted to all of you for the rest of my days.

Name: MICHAEL-JOSEPH GORBET

Date of Degree: DECEMBER, 2021

Title of Study: DEVELOPMENT OF BUBBLE AND LIGAND-BASED TARGETED NANOPARTICLES FOR SOLID TUMOR THERAPY

Major Field: COMPARATIVE BIOMEDICAL SCIENCES

Abstract: The use of nanoparticles to enhance targeted chemotherapeutic delivery and efficacy against solid tumors is on the rise. Conventional chemotherapy can be associated with deleterious systemic side effects and limited efficacy, due in part to the insufficient drug delivery to the tumor site following systemic injections. Chemotherapy can also be limited by its adverse effects and tumor hypoxia that reduces the overall therapeutic outcomes and patient survival rates. To overcome these barriers, this project aimed to develop targeted nanoparticles (NPs) for systemic chemo-immunotherapy of both treated and untreated solid tumors. We hypothesize that combining *in-situ* delivered ligand- and bubble-based nanoparticles with high intensity focused ultrasound (HIFU) will enhance chemotherapy efficacy and induce immune-mediated clearance of untreated cancer cells, thereby significantly improving treatment outcomes. As model drugs, we chose doxorubicin (DOX) and mitoxantrone (MTX) from the anthracycline/anthraquinone class of chemotherapies for encapsulation into NPs. These chemotherapies are known inducers of immunogenic cell death (ICD). For bubble-based NP synthesis, polymeric NPs incorporating perfluoropentane, a known ultrasound contrast agent, and chemotherapies (i.e., DOX & MTX) were developed. Biophysical characterizations of the polymeric NPs showed controlled chemotherapy release *in vitro* and enhanced stability within serum with a targeted delivery in presence of HIFU via the "micro/nanobubble" effect. This resulted in an enhanced chemotherapy effects and extended survival following *in-situ* therapy of murine colon tumor *in vivo* compared to controls. We also similarly generated ligand-based NPs targeting CXCR4 receptors. We demonstrated the successful synthesis of these NPs loaded with chemotherapies in thermally sensitive formulations. Future studies are under planning to utilize these to test their targeting capabilities and therapeutic efficacy in comparison to free drug controls. Our data suggests that targeted NPs in combination with HIFU may be an innovative chemo-immunotherapeutic treatment regimen to improve targeting of solid tumors.

TABLE OF CONTENTS

Chapter Page

LIST OF TABLES

Table Page

Schemes

LIST OF FIGURES

Figure Page

CHAPTER I

REVIEW OF LITERATURE

ROLE OF NANOMEDICINES IN IMPROVING ANTI-CANCER THERAPIES

Abstract

Conventional chemotherapy is non-specific and non-targeted in nature, achieving moderate drug delivery to poorly vascularized solid tumors. One approach to overcome this challenge can be encapsulating drugs in nanoparticles (NPs). Physicochemical properties of NPs allow their enhanced accumulation in solid tumors. Further targeting (e.g., physical, device-directed, and ligand etc.) can increase the accumulation of chemotherapeutics, thereby allowing superior outcomes. A variety of NP properties, including i) drug loading, ii) functionalization, and iii) some form of tumor targeting (e.g., internal or external) are currently under investigation to improve solid tumor therapeutic efficacy. Herein, we discuss the various targeted approaches, their potential advantages and drawbacks, our perspectives, and dissertation objectives.

1. Cancer therapy outcomes continue to improve but still presents multiple clinical challenges

The decline of cancer death rates since 1991 through 2018 has been an impressive 31%, suggesting drastic improvements in the technologies related to early detection and development of therapeutics[1]. Despite this, the current data for 2021 projects an estimated ~1.8 million new cases and ~600,000 cancer deaths in the U.S alone, according to the National Center for Health Statistics. Moreover, the recent coronavirus disease 2019 (COVID-19) pandemic has limited the medical availability to many throughout the world. While this might lead to a lower than expected annual number, it may lead to a higher incidence rate of advanced cases in a number of years[1].

The survival rates of patients are highly dependent on the location of the tumor, and whether tumor cells have migrated beyond the primary locale. For instance, colorectal cancers have a 90% five-year relative survival rate if found while they are localized, 72% while they are regional, whereas there is only a 14% chance of survival in cases with distant tumors (U.S., 2010-2016) [1]. This trend is similarly seen in many other tumor types clinically, thereby a logical advance for cancer therapeutics would be aiming to effectively treat local as well as distant, secondary metastatic tumors. There is some anecdotal evidence that treating a solitary tumor can alter their immune environment to induce clearance of untreated masses. This phenomenon first postulated by R.H. Mole in 1953, is called the 'abscopal effect'[2]. Abscopal effect has extended the efficacy of treatments to distant, non-treated tumors by enhancing cell-mediated immunity by 'eliciting augmented tumor surveillance, tumor growth inhibition, and tumoricidal effects[3]. While there have been cases of abscopal effects reported in malignant melanoma[4,5], lymphoma[6], renal cell carcinoma[7,8], hepatocellular carcinoma[9-11], lung cancer[12,13], uterine cervical carcinoma[14], and breast

cancer[15], it remains controversial and elusive in many cases[3]. To even further complicate this narrative, many different tumor cell types display differing levels of immunogenicity[16] to evade immune detection and clearance through a variety of mechanisms (e.g., IFNγ has been described to be a determinant of solid tumor immunogenicity[17]). Based on these cellular differences, many ongoing immunotherapy trials are demonstrating differences in overall response rates (ORR) within the same tumor type (e.g., 30-50% in lung cancer, Non-Hodgkin lymphoma, melanoma; >50% in colon and rectal cancer; <10% in leukemia and pancreatic, and brain & CNS cancers)[18].

Multi-, or multiple, drug resistance (MDR) is another mechanism by which tumors gain resistance to drug molecules[19]. MDR is one of the biggest hurdles of cancer chemotherapies in preventing the successful clearance of solid tumors in patients. MDR can be mainly divided into primary and acquired forms, based on whether it is naturally-occurring or pre-existing, or gained from exposure to chemotherapies, respectively[20]. Many types of cancer cells attain resistance of chemotherapies when simply cultured with sub-lethal concentrations over time. A few notable examples of this include DOX-resistant cell lines that have been developed: chronic myelogenous leukemia, leukemia CME, gastric cancer SGC7901, hepatocellular carcinoma HepG2, colon cancer SW620, small cell lung cancer H6, and ovarian cancer OVCAR8[21]. Therefore, combating effective therapeutic clearance of solid tumors should focus on modulating their microenvironments to optimize outcomes.

2. Monotherapy of solid tumors attain sub-optimal efficacy

2.1 Radiotherapy generates variable outcomes in patients

Radiotherapy can be administered by means of external beam radiotherapy[22-24], or internally via brachytherapy[25-28] or selective internal radiation therapy (SIRT)[29-33]. Ionizing radiation causes cellular damage via DNA damage- the most potent being double-stranded DNA breaks (DSBs)[34]. Clusters of DSBs are more cytotoxic to cancerous cells generally due to their lessened ability to apply DNA repair mechanisms, yet there are many tumors types (i.e., breast, rectal, anal, cervix, head and neck, lung, bladder, endometrial, & CNS carcinomas, lymphomas, soft tissue sarcomas and pediatric tumors) display a decreased sensitivity to radiotherapy that can enhanced by combining with other therapies[35].

Overall, however, radiation as a monotherapy is highly variable dependent on tumor type. For example, as an average across the United States, United Kingdom, Australia, and Sweden, the utilization of radiotherapy is 52.3%. Upon further inspection, however, it revealed, liver cancer patients were recommended radiotherapy 0% of the time while CNS tumors were recommended 92%[36]. Generally, these optimal utilizations were calculated based on 'indications for radiotherapy taken from evidence-based treatment guidelines'[36]. These were ranked based on their levels of evidence starting at a systematic review of all randomized studies as 'I' to a case series being done as 'IV'[36]. Molecularly, however, most problems are seen in tumor types that display abnormal response to therapies by altering metabolism, increasing hypoxia (i.e., HIF-1α), increasing antioxidant levels and others to support tumor growth. These alterations promote tumor survival via reduction of ROS pressures elicited by radiotherapy, promoting tumors towards more aggressive phenotypes that favor metastasis or radio-/drug-resistance[37]. Further, a new identification of varied levels of radioimmunogenicity in tumor models display responses to immunotherapies only when paired with radiation. Examples include Pan02 pancreatic cancer,

MOC1 oral cell carcinomas, MC38 colorectal carcinoma[38], and TSA mouse mammary carcinoma cells[39]. This logically lends to the idea that radiotherapy might be a component in effective combination therapies, however, as a monotherapy it seems to be limited.

2.2 Immunotherapy is yet to become a standard of care for cancer therapy

The foundation of the field of cancer immunotherapy was led by Coley almost an entire century ago (1891)[40]. He used bacteria or bacterial products, which were later dubbed "Coley's toxins," as an anti-cancer therapy against bone and soft-tissue sarcomas, and superficial bladder cancers[41,42]. More recently, immunotherapies have evolved to encompass mechanistic links between various immune cells: examples include, i) M1-tumor macrophage polarization has proved to be vital in eliciting a more pro-inflammatory, anti-tumoral response[43-45], ii) dendritic cell-activation of natural killer cells has potent anti-tumoral effects that are independent of IL-12, and type-I interferons[46], iii) immune checkpoint inhibitors reversing immunosuppression via PD-1, PD-L1, and CTLA-4 inhibition[47,48]. A major flaw of existing and newly emerging immunotherapies, however, is the need for an inflamed tumor microenvironment cells for the therapy to be effective. In fact, the percentage of patients eligible for this therapy was 43.63% in 2018 with only a 12.46% response rate[49]. Even worse, further complications arise that seem to be linked with resistance-driven cancer progression[50]. These are important to consider in order to fully utilize the potentials of immunotherapies[51,52].

2.3 Chemotherapies are effective, but are not cancer cell specific

Chemotherapy's history has been excellently reviewed by *Chabner et al*.[53] Chemotherapeutic use against cancer started in the 1940s with the discovery and application of 'nitrogen mustards' (1949)

and antifolates[54,55]. It since then rapidly evolved with the discovery of anthracyclines and other topoisomerase II poisons to prevent DNA replication[56]. While chemotherapies can affect cancer cells in many different ways, the goal of targeting cancer cells and protecting healthy tissue remains constant. Chemotherapies tend to target rapidly dividing cells preferentially including healthy cells (e.g., cells in the oral cavity, digestive tract, reproductive system, hair follicles, and immune cells)[53]. While this might be a small price to pay for the eradication of a life-threatening tumor, full tumor clearance is rarely achieved in advanced metastatic cases.

Major downfalls within the use of chemotherapy-based cancer regimens include, i) the drastically lowered drug concentration within the tumor microenvironment, TME, (>1%)[57], ii) the potential of drug resistance via natural means or by selective pressure[58], and iii) detrimental, dose-limiting side effects[59]. These seemingly inescapable limitations have pushed researchers to investigate targeted therapies via multiple routes (e.g., physical, device-directed, and chemical targeting) to both limit systemic toxicity, and augment clinical efficacy by enhancing delivered drug to the TME. Simply, the enhancement of amount of drug that is delivered does not always correlate with the removal of solid tumors (e.g., natural resistance seen in cells without previous exposure). Further, there are intricacies and complications within cancer treatment regimens that can arise that must be addressed (i.e., acquired drug resistance).

Chemotherapy-resistance and MDR, in general, can be displayed and exacerbated via multiple pathways- high ABC transport efflux-pump expression, apoptosis resistance, autophagy induction, hypoxia induction, epigenetic regulation, and many more[60]. General understanding of MDR begins with the primary mechanism that resistance is achieved for a particular drug. For example, resistance against doxorubicin (DOX), a particular drug of interest in our case, can be mediated by

many mechanisms[61]. These include blocking of the nuclear translocation of DOX by the P-glycoprotein (P-gp) and high MRP1 expressions. DOX treatment elevates MRP1 in a variety of cancers including 7/7 Ewing's Sarcoma Family of Tumor, 2/2 thyroid carcinoma, 1/1 hemangioma, 2/2 melanomas, and 1/1 soft tissue rhabdomyosarcoma[62]. MRP and MRP-3 mRNA specifically is especially elevated with heightened DOX resistance in SCLC (small cell lung cancer) and NSCLC (non-SCLC) cell lines[63]. One approach can be to supplement the primary therapy with an additional therapy (e.g. verapamil, a known P-gp inhibitor via competitive or non-competitive inhibition of ABCs) to synergize efficacy and reduce the occurrence of MDR[64]. In the case of acquired resistance, maximizing the delivered drug to produce a higher internal drug concentration within the tumor (i.e., incorporating NPs), physically injecting drugs directly into the tumor to the hypoxic environment of the tumor microenvironment (TME), passively targeting via the enhanced permeability and retention (EPR) effect, or by active receptor-targeting can be employed. Each of these have their own inherent advantages and disadvantages along with the chemistry of NPs normally used with each of these motifs. (*Section 5).*

In contrast to DOX that was isolated from *Streptomyces peucetius* (i.e., daunorubicin, DOX)[65,66], this dissertation also focuses on mitoxantrone (MTX), a synthetic anthraquinone, or anthracenedione, that was chemically synthesized to improve the therapeutic profile of anthracyclines like DOX. While DOX is still used clinically to-date, it is accompanied by one major drawback-- a dose-limiting, irreversible cardiotoxicity that is thought to be tied to its lipid peroxidation properties. While the connection between induced cardiac dysfunction and drug administration has been elusive for many years, recent studies have attempted to explain it in greater detail. Examining the cellular mitochondria in the heart specifically, since the energy requirements

are vast, has revealed that MTX modifies the electron transport chain (ETC) by increasing complex IV and V activity early while decreasing complex V activity late. Meanwhile, DOX increases complex IV and V expression while decreasing complex I activity[67]. Due to the fact that the heart has the highest volume density of mitochondria, any mitochondrial malfunctions elicited would impair the heart drastically[68]. Furthermore, the heart has been shown to be particularly susceptible to xenobiotic oxidative-stress related injury based on the simple fact that it has a dampened ability to repair oxidative stress[69]. More specifically, DOX was shown to cause, i) reduced cardiomyocyte contractive function, ii) downregulation of the SERCA pump, and iii) decreased sarcoplasmic reticulum-calcium loading[70].

While MTX has displayed less cardiotoxicity than its anthracycline predecessor[71], it might seem counterintuitive since MTX's cytotoxicity is cell-cycle independent[72]. Additional studies show that one of the main metabolic contributors to DOX's toxicity is the semiquinone radical produced via reductive metabolism. This pathway differs from the enzymatically driven metabolism of MTX by cytochrome P-450, or peroxidase-driven oxidation via horseradish, lacto- or lignin peroxidase[67,73]. While MTX is different in these ways, it still does cause oxidative stress and cardiotoxicity[74,75]. This might be due to interactions with iron in blood[76], thus monitoring patients receiving these therapies is a clinical necessity. Likewise, the need for targeted therapies to increase intratumoral drug concentrations and decrease systemic and healthy tissue concentrations is an urgent endeavor that could save many lives clinically. This is crucial since MTX concentrations are generally lower intratumorally than surrounding healthy tissue when administered clinically[77]. For these reasons, we chose to use a murine CT26 colon carcinoma cancer cell line that is highly immunogenic[78]. The immunogenic nature of this tumor model hypothetically would pair well with both MTX to study

primary and abscopal effects[79]. Therefore, utilizing MTX in a nanomedical approach, can answer some of these fundamental questions related to its chemoimmunotherapeutic effects[80].

3. Role of nanoparticles in cancer therapy

3.1 Differing chemistries of nanoparticles elicit dramatically different cellular responses

There are two main types of nanoparticles- inorganic-derived and organic-based nanoparticles (NPs). Example of inorganic NPs include gold, silver, gadolinium etc. Organic NPs are made from carbon, hydrogen, sulfur, nitrogen, phosphorus-containing molecules (Fig. 1). NPs are biocompatible and can vary widely in both geometry and size, with a typical accepted range being within the "nanometer-range" of 100-200 nm. They have high surface area to volume ratios that allow chemical modification and functionalization via proteins, antibodies, antigens, and many kinds of small molecules. They are easily translatable for nanomedical applications due to their ease of synthesis, ability to passively- and actively-load drugs, and attain their targeted accumulation by EPR effects (the tendency of ~sub 200 nm-sized particles to accumulate in the leaky vasculature of tumors)[81-83]. In addition to loading drug payload[84], NP formulations can also be utilized for imaging (e.g., MRI, CT, ultrasound, optical imaging, photoacoustic imaging, PET, and single photon emission CT)[85].

Some NPs demonstrate immunomodulatory effects and can be used as adjuvants to advance T-helper cell activation (Th1 or Th2) to promote cell-mediated immunity or humoral immunity. NPs can interact with cells via pattern recognition receptors (PRRs)[86] and are preferentially endocytosed based on size if not specifically modified otherwise. Smaller NPs (sub-200 nm) tend to be endocytosed via the clathrin-mediated pathway while 200-500 nm particles prefer caveolae-

mediated endocytosis. Beyond this, sequestration by lysosomes is generally no longer observed[87]. Surface charge also is a major factor in determining route of endocytosis/phagocytosis of NPs. Generally, anionic NPs show less cellular interactions and increased 'stealth' due to their negatively charged cellular phospholipids. This lack of interaction gives less inflammatory properties than their cationic counterparts. Cationic NPs are rapidly taken up by phagocytic cells (i.e., macrophages) and produce an inflammatory response[88]. Both macrophages and DCs internalize NPs, however, the antigen presentation can be influenced by particle composition[89]. In one study with amphiphilic poly(γ-glutamic acid) (γ-PGA) NPs containing variable levels of hydrophobic amino acid ethyl esters, the hydrophobic segments were found to induce cellular and humoral immunity by dendritic cells[90]. Similarly, *Moyano et al.* investigated gold NPs with various levels of surface hydrophobicity to show production of pro-inflammatory cytokines from the splenocytes was proportional to the hydrophobicity of the NPs *in vitro* and *in vivo*[91].

The clearance of NPs via the corona effect[92,93] can generally be mitigated by increasing the stealth of NPs by using PEG. For cancer chemotherapy, the goal of NPs is to avoid clearance by immune cells. To do so, NPs are commonly modified via 'PEGylation' to prevent opsonization, immune detection and clearance[94]. Polyethylene glycol (PEG) is a hydrophilic surfactant molecule with low toxicity. Polyethylene oxide, PEO, a high molecular weight PEG, is also similarly utilized and has similar effects. The only real difference between the two being their differing size. The threshold for being qualified as PEO instead of PEG is if the polymer is larger than 20,000 g/mol (20 kDa). In general, a broad term of POE is used for any weight[95]. POE enables NPs such as liposomes enhanced circulation longevity[96]. For example, in one study, the PEGylation of liposomes increased

the circulation $t_{1/2}$ from <30 min without PEG to 5h with PEG. Presence in the blood was 85% and 18% in the liver and spleen at 1h while there was still 49% in the blood and 38% in the RES at 5h[96].

3.2 Liposome and polymeric nanoparticles can improve targeted drug delivery

Core-shell liposomes and polymeric structures are common organic NPs that can be used for targeted drug delivery purposes. Liposomes have an internal water-soluble cavity with a phospholipid bilayer membrane[97]. A meta-analysis of 10 randomized controlled trials showed that water-soluble agent, such as DOX, could be encapsulated in a liposome to lower cardiotoxicity[98]. Altering the lipid profile of liposomes lends the ability to burst them in response to hyperthermic conditions and aids in the concept of a targeted, deliverable payload[99]. Additionally, manipulation of the surface with proteins or ligands to target certain processes or cell types further enhances the specificity of targeted delivery for a desired effect. In addition to be being used as a hollow transportation vessels for chemotherapies, some formulations (e.g., cationic liposomes) can also have immunomodulatory effects via stimulation of the antigen presenting dendritic cells (DC) leading to the expression of co-stimulatory molecules, CD80 and CD86[100]. *Collins et al.* showed that ovalbumin (OVA)-encapsulated acid-resistant liposomes could generate class I MHC-restricted T cell responses *in vivo* by lysosomal processing and recycling of immunogenic peptides[101,102]. *Suzuki et al.* used unmethylated cytosine-phosphorothioate-guanine oligodeoxynucleotide (CpG-ODNs)-encapsulated cationic liposomes as an adjuvant to actively target antigen presenting cells (e.g., dendritic cells) by binding to TLR9 to increase type I innate immunity[103]. Data suggested that liposome encapsulation of unmodified CpG-ODN enhanced the dendritic cell uptake and IL-12 production. Additionally, this approach induced IFN-γ but not IL-

4 production by natural killer cells: features essential for Th1-dependent cytotoxicity against OVA-expressing tumor cells.

If used in combination with nucleic acids such as RNA, mRNA, DNA, etc., liposomes can further be used for non-viral gene transfection as lipoplexes[104]. Stimulatory RNA or DNA lipoplexes can also be used for targeted epitope expression and activation of T-cells. RNA encoding tumor associated, or tumor specific epitopes, were encapsulated in liposomes to enhance the targeting of antigen-presenting cells (i.e., splenic macrophages, dendritic cells, Kupffer cells) for epitope encoded activation of the T cell[105]. An even more recent example is the mRNA LNP (lipid nanoparticle) COVID-19 vaccine that has been used worldwide in the last year. Different nucleic acids can be utilized for their cellular roles and targeted to undergo cellular modifications (DNA) or simply to be included in translation with mRNA vaccines to encode the relevant protein (viral Spike (S) glycoprotein of SARS-CoV-2 in COVID's case)[106]. Liposomes and/or liposome-type NPs have also shown to deliver plasmid DNAs that normally would be very difficult to achieve clinically[107]. Cationic formulations were shown to enhance the delivery of plasmid DNA to elicit antitumor immunity in murine model of cervical cancer[105]. Unlike viral vectors that risk mutagenic integration with host cells, liposomes are a promising and safer gene drug delivery technology[108], and thus, have widely employed in clinical trials for immunotherapy investigations[109-112]. Studies are currently underway to further improve the transfection and expression efficiencies in a targeted manner in tumor cells while reducing side effects to healthy organs and induction of autoimmunity. A key challenge of liposomal formulation is lower stability, susceptibility to ester hydrolysis, peroxidation, fusion, aggregation, and/or loss of encapsulated material. The inclusion of cholesterol

can be employed to help increase stability, however, that sometimes clashes with the whole concept of being stimuli-sensitive[113-115].

One solution to the liposomal stability dilemma has been the expansion into synthesis of polymersomes. Generally, polymersomes have higher chemical versatility and stability due to their thickened membrane layer[116]. Additionally, the PEGylation that is done in liposomes to avoid immune clearance is molecularly integrated much easier into a polymersome, which is already an amphiphilic co-block polymer. These have shown a higher capacity for greater PEG content and >two-fold increased stealth via enhanced circulation in rats in comparison to their PEG-liposomal counterparts. Although, with the enhanced stability, there generally needs to be some expanded nature of delivery in formulation since degradability of the relatively thick (2-50 nm) membranes can be exceedingly strong in comparison[117].

Polymersomes can similarly be utilized as targeted drug vehicles[118-120] and for non-viral gene transfection[121-123]. They also have low toxicity and enhanced biocompatibility[124]. The enhanced chemical versatility enables more chemical modifications via functionalization, or using alternate di-block, tri-block or grafted polymers[116]. Polymers can range from anionic to cationic[121] and can be even made into hybrid lipid-polymer NPs to expand utility[125-127]. While there has been a plethora of LNP research, there is more polymer NP research in the recent years that have begun trying to address clinical problems that arose in lipid formulations (i.e., lack of stability and premature release of drug payload). More recently, *Wei et al.* synthesized a pH- and ultrasound-responsive polymersome made of poly(ethylene oxide)-block-poly(2-(diethylamino)ethyl methacrylate)-stat-poly(methoxyethyl methacrylate) [PEO-b-P(DEA-stat-MEMA)] and loaded with DOX[128]. They

uniquely modified polymersomes to release drug via PMEMA molecule in response to ultrasound exposure.

Others have primarily targeted ultrasound-targeted release by micro/nanobubbles. Microbubbles have been the predominant way for ultrasound-targeted release[129]. In recent times, there have been other methods of achieving these goals, including *Wei et al.*'s method listed above and the newer incorporation of nanobubbles instead of microbubbles[129]. We and others have investigated nanobubbles and their effectiveness when paired with ultrasound[130-132]. These bubbles are generally made from fluoroalkanes with a boiling point within a clinically relevant temperature. For example, perfluorohexane, perfluorobutane, and perfluoropentane have been used. Encapsulating these bubbles within NPs increases their boiling point by Laplace pressure. Further, the utilization of these combined tends to increases the sonoporation effects and causes holes in the cellular membrane from bubble oscillation and acoustic cavitation[133]. The current work in this dissertation similarly expands current knowledge with echogenic polymersomes loaded with MTX to determine their clinical safety and efficacy. Further, we hypothesize that MTX delivery with NPs in combination with HIFU will improve nuclear localization to enhance cytotoxicity against cancer cells.

4. Current limitations of systemically administered lipo- and polymeric-NPs

Although efficient in delivering drugs to tumors, limited NP perfusion into tumor interstitium can limit their efficacy. *Perrault et al.* demonstrated the size differential of permeation away from the blood vessel center with NPs ranging from 20 nm to 100 nm. As a general rule, the smaller the NP, the further distance from the capillary center was traveled[134]. Increased circulation and decreased

uptake in liver macrophages are observed when PEGylation is utilized for NPs[135], however, there both seems to be an over-reliance on the under-performing EPR effect and lack of information answering *in vivo* behavior of NPs versus *in vitro*. This is highly significant since currently it is known that NPs can continuously be moved from organ to organ, meanwhile *in vitro* studies are confining NPs to interacting with a small subset of cells in comparison[81]. The lack of EPR effect observed throughout the entire tumor microenvironment (TME) is a highly limiting factor, especially considering 50-60% of solid tumor tissue is hypoxic/anoxic[136]. Moreover, the overselling of the EPR effect as a targeted delivery component is somewhat misleading in some cases. The actual delivered dose, many times, is <5% of administered dose of drug[137]. While this is an improved delivery in comparison to free drug, it still demonstrates the clearance of >90% of drug and the accumulation in organs (i.e., liver and spleen)[137].

The lack of a real NP 'targeting mechanism' was nicely reviewed by *Albanese et al.* and was attributed to an over-reliance on the EPR effect, the lack of a universal tumor antigen, active targeting flaws, and <10% accumulation of drug administered in tumors[81]. There have been significant preclinical-clinical advancements in the last ~10 years to address some of the NP limitations. These include development of tumor-responsive formulations or targeted therapies to improve the aspects of the limited EPR effect, TME perfusion, altered hypoxia, and more[132,138-140]. (*Section 5)*.

Another NP limitation is their toxicities (acute and chronic) via necrotic and/or apoptotic mechanisms[141,142]. In general, oral dosages are significantly less toxic in comparison to the inhalation route of exposure, and metal NPs tend to display higher toxicity profiles at reduced sizes

compared to lipid/polymer NPs[143]. Organic NPs are derived from natural, biocompatible materials and chemical modifications with PEG or proteins minimize acute interactions with cells.

Finally, mistimed release of drug payload is a major concern in the field. Both the premature release of drug payload and the tendency to retain drug when release is desired are problems that mirror each other but represent a similar problem that requires integrity modification of NP formulation. For example, gadolinium-labeled, DOX-loaded, temperature-sensitive liposomes were prepared and monitored to determine the drug release in combination with hyperthermia. While there was an increase in percentage of injected dose within the tumor and less in blood in groups that received hyperthermia, the best value for concentration of DOX was <2% injected dose/g of tumor. These do correspond to increases by a factor between 2 and 10, showing marked DOX enhancement, however, the differences between *in vitro* and *in vivo* conditions also showed differing speeds of clearance. This suggests leakage of drug out of NPs prior to delivery into the tumor microenvironment and needs to be appropriately addressed for cancer therapy[144]. Therefore, modern approaches must look to address stability and drug release concerns. Our current methodology looks to answer these concerns by taking an inert co-block polymer formulation and adding ultrasound-sensitivity by adding nanobubbles.

5. Can we assimilate the characteristics of liposomes and polymersome, and translate them for *in-situ* and parenteral therapy via targeted approaches?

The concept of targeting a therapy to the tumor microenvironment primarily means drugs (i.e., chemotherapies, immunotherapies, etc.) are specifically delivered to the tumor site while avoiding deleterious side effects from prolonged systemic circulation. This can be accomplished by various

methodologies, i) physically injecting into the site (direct intratumoral injection, *in-situ* vaccination, NP-ISV), ii) device-directed targeting via external stimulus to aid in achieving successful delivery, iii) chemically targeting of the tumor via functionalization of the NPs (Fig. 1). While each of these approaches represent a version of targeting, they all differ in their inherent strengths and weaknesses. Beyond physically targeting via intratumoral injection, which is not always clinically available to deep-seated tumors, device-directed and chemically targeted NPs are the much more sought-after method. These modalities can use triggers (e.g., devices- HIFU, high intensity focused ultrasound, PTT, photothermal therapy, AMF, alternating magnetic field, and/or hyperthermia; chemical- pH-sensitivity, hypoxia-sensitivity, receptor-mediated interactions) to achieve proper release of NPs in the desired location. The subsequent sections will discuss the potentials for each more of these in-depth.

5.1 Physical targeting (intratumoral, direct injection, NP-ISV)

Physical targeting can be accomplished via direct, intratumoral injections. Direct, intratumoral injections, can also be called nanoparticle *in-situ* vaccinations (NP-ISVs). There are additional examples of liposomal formulations being administered via other routes (e.g., subcutaneous, intradermal, and intramuscular) (Fig. 2)[145-148]. These can enhance tumor cell recognition via multiple mechanisms. For example, a subcutaneous liposomal formulation, endowing continual release of IL-2, was synthesized and shown to extend IL-2 residence time in systemic circulation by 8-fold in comparison compared to free IL-2[146]. Unlike distant locations, a direct, intratumoral injection prevents interactions with serum proteins that can opsonize it for phagocytic uptake. The NPs, once administered into the TME, can also interact with tumor-specific

antigens and 'capture' them[149] to induce polarization and/or deplete tumor-associated macrophages (TAMs), activate dendritic cell maturation, and limit Tregs[150-152].

Both organic and inorganic formulations have been utilized as NP-ISVs. Tumor retention capabilities can also be enhanced by increasing the size of NPs or altering the surface charge to cationic. Typically, larger NPs (>200nm) are efficiently retained in the tumors. For example, PEGylated liposomes retain the encapsulated content in the tumor (~12-fold) compared to free form upon local injection[153]. Further, we showed the successful transfection of calreticulin (CRT) in murine melanoma tumors using a similar liposomal NP-ISV approach comprised of full-length cloned plasmid of CRT and cationic DOTAP-cholesterol liposomes combined with high intensity focused ultrasound (HIFU). This method involved the protection and targeted delivery of nucleic acids that would otherwise not achieve notable transfection, yet in our experiment CRT was successfully transfected and displayed properties along the lines of its normal physiological role after being translocated to the surface and, therefore increased immunogenic cell death (ICD)[154]. Enhanced expression of CRT, populations of melanoma specific CD4+ and CD8+ T cells, and polarization to M1 phenotype was observed in treated tumors. Notably, combination treatment CRT-NP/HIFU prevented tumor growth in the untreated secondary tumor locale, suggesting an abscopal effect. *Meraz et al.* developed an alternative liposomal NP-ISV approach by encapsulating monophosphoryl lipid A (MPL) and IL-12 in cationic liposomes to reduce systemic toxicity and achieve a more sustained local release of the cytokine[155]. The team found that following intratumoral injection in the orthotopic model of murine breast cancer, MPL acted as a pathogen-associated molecular pattern (PAMP), and activated the pattern recognition receptor (PRR) in the dendritic cell via IRAK and MyD88 adaptors. When combined with IL-12, it synergistically

enhanced the nitric oxide (NO) synthase (iNOS) expressions, resulting in high IL-2 and IFNγ expressions from T-cells, and a T helper (Th)-1 cell mediated local and systemic anti-tumor immunity.

In contrast to the toxicity of cationic lipids, neutral lipids are relatively safer to use. *Francian et al.* performed intratumoral NP-ISV vaccination with ovalbumin-loaded neutral liposomes decorated with endogenous C3 serum proteins in a murine model of lymphoma[156]. Data suggested an efficient targeting of the C3 receptors of macrophages and dendritic cells by the C3 proteins of liposomes. A drawback of neutral liposomes are their propensity to rapidly redistribute into the venous outflow[157], but a way to mitigate this can be to target draining lymph nodes via PEGylated liposomes.

Like cationic lipids, polymeric ISVs incorporating positively-charged moieties improve the cellular delivery of nucleic acids to tumors. For example, polycationic polyethylenimine (PEI) is highly unique in its ability to achieve intrinsic TLR activation activity of the tumor associated DCs. *Ruiz et al.* reported a PEI-based nanocomplex for nonviral siRNA therapy of murine ovarian cancer[158]. In another study, the intratumoral administration of PEI stimulated the expression of IL-12 and TNF-α from myeloid-derived suppressor cells (MDSCs) and caused the production of the tumor suppressive M1 phenotype[159]. *Nikitczuk et al.* developed PLGA-based NP-ISV encapsulating a tumor antigen and the TLR9 agonist CpG motif DNA. Intratumoral administration of the NP in a mouse model of T-cell lymphoma induced an IFNγ Th1 response, reducing local tumor growth[160]. PLGA-NPs also achieved concurrent chemo- and immune-therapy via co-loaded DOX, TLR3 agonist poly (I:C) and TLR7/8 activator (Resiquimod; R848). Intratumoral administration of the NP-ISV in treatment resistant TC-1 lung carcinoma and MC-38 colon adenocarcinoma induced

chemotherapeutic sensitization and enhanced the population of tumor-specific T-cells compared to the drug alone[161]. PLGA has also been found to capture released tumor antigens also. *Min et al.* modified NPs to show antigen capturing capacities of amine-polyethylene glycol (NH_2-PEG), (NH_2 AC-NP), and 1,2-Dioleoyloxy-3-(trimethylammonium)propane (DOTAP AC-NP) during radiation therapy in tumors. Data suggested efficient retention of damage associated molecule patterns (DAMPs) such as HMGB1 in NPs *in vitro*[162]. Also, when the NP-ISV was injected unilaterally in mice bearing bilateral melanoma, it induced an abscopal effect via improved APC presentation and T-cell cytotoxic effects. Thus, lipidic and polymeric NPs as NP-ISVs are being studied to improve availability to injected solid tumors. Therefore, we proposed and investigated the use of our targeted approach as an intratumoral approach.

5.2 External device-directed targeting (high intensity focused ultrasound, HIFU), photothermal therapy (PTT), alternating magnetic field (AMF) based hyperthermia can improve tumor therapy

In addition to physically targeting, the ability to target NPs by device-targeted stimulus can be utilized to expand the utility of NPs. These devices can be i) HIFU, ii) photothermal therapy, PTT, and iii) alternating magnetic field, AMF. The general physics behind each of HIFU[163], PTT[164,165], and AMF[166] are extensively covered in each of the referenced manuscripts. These work in different manners, however, the main goal is to selectively release payload. The latter method generally induces some level of stimuli-sensitivity through different kinds of physical phenomena that are currently beyond the scope of this review.

A key benefit of HIFU over PTT or AMF modalities is its ability to generate hyperthermia without NPs and its noninvasive, highly targeted capabilities. HIFU parameters are also tunable for various

types of immune priming or desired thermal/mechanical pressures. Low intensity HIFU (LOFU) modulates the expression of HSPs family protein (e.g., HSP 60, 70, and 90) and has been shown to augment radiotherapy in breast and prostate murine cancer[167]. Mild hyperthermia can be used for longer duration (~30 minutes-60 minutes) and in combination with temperature-sensitive NPs[132,168]. Thermal ablation by HIFU leads to cell fusion, necrosis, protein coagulation, coagulative necrosis,[169] and requires temperatures ranging from 60-85°C[170]. Treatment of liver tumors was the predominant role of thermal ablation, however, there has been recent extensions into wanting to use it for other tissues (e.g., lungs[171,172], kidney[173], etc.). A few marked problems with thermal ablation are defined as the need for complete and total ablation for proper efficacy, the 'escape' of heat into the "heat sink" of the vasculature", the potential for damage of surrounding tissue, or the possibility that it is not effective in clearing tumors[174]. Boiling histotripsy (BH) is achieved via high intensity millisecond intervals and can combine thermal and mechanical effects to effectively induce tissue disintegration[170]. The nonlinear propagation effects contributes to compressive pressure and the eventual tissue disintegrating effects of both cavitation and boiling histotripsy[175]. The stacking of these effects produce scattered shocks seen via 'cavitation clouds' in cavitation histotripsy meanwhile 'rapid tissue heating' by super focused shocks can be initiated in milliseconds in boiling histotripsy[175]. Cavitation histotripsy has been shown to have immunomodulatory properties in murine melanoma[176] and boiling histotripsy in renal cell carcinoma[177], but they also can be distinguished into their different effects more specifically. The presence or absence of heat can be inherently different in their downstream effects in immunogenic cell death (ICD) and other pro-inflammatory, and/or anti-tumoral processes. For example, one study showed that mechanical HIFU tends to release more endogenous danger signals (i.e., heat shock protein 60 and LDH) than thermal HIFU (hypothesized to be due to the denaturing potential

of temperatures of above 50°C). ATP was shown to be released to a greater degree in thermal HIFU treatments inversely in MC-38 tumor cells in the same study with a combined longer lasting ATP concentration in comparison[178].

Many ancient societies (i.e., Greek, Egyptian, and many more) have experimented with inducing a hyperthermic state for the treatment of diseases. Hyperthermia therapy, whether it is generated by ultrasound or some other external stimuli, is characterized by the raising of the tissue temperature to ~40-45°C for an extended amount of time 30-60 minutes. Hyperthermia has been studied in a phase III clinical trial combined with a neo-adjuvant chemotherapy to show regional hyperthermia adding to preoperative and postoperative chemotherapy compared to chemotherapy alone in a specific population of patients with high-risk soft-tissue sarcoma[179]. Thermal treatments have been studied extensively over the last few decades to better understand the effects of both low intensity heat (i.e., mild to moderate hyperthermia) and high intensity thermal ablation. Hyperthermia has been shown to resensitize cancer cells to, i) radiotherapy[180-185], and ii) chemotherapy[182,186-188]. A phase II clinical trial treated 37 prostate cancer patients at an average temperature of 41.2°C for an average of 62.8 minutes as a sensitization for radiation instead of chemotherapy, and while they did see benefits, they did specifically mention that both the suboptimal dose of radiation and thermal ablation may be required for full tumor clearance[189] More specifically, clinical endovesical thermochemotherapy proved more efficacious in the treatment of superficial transitional cell carcinoma of the bladder,[190] and it was further supported with long-term outcomes of thermochemotherapy disease free survival rates (53%) being significantly higher than chemotherapy alone (15%) with a p-value <0.001[191].

Other external devices (i.e., PTT, AMF) can similarly give expanded NP utility. These can also elicit hyperthermic conditions with NPs. PTT uses near infrared laser energy to excite NPs[192]. The activation/absorption of light energy by NPs (e.g., gold NPs, carbon nanotubes, indocyanine green (ICG), Prussian blue etc.) causes physical, hyperthermic, and ablative effects in tumors and a variety of downstream immune effects[193-196]. Gold[197] and Prussian blue[198] NPs are the primary NP modalities that have access to being 'activated' by the NIR laser of PTT. Similarly, AMF requires a magnetic NP formulation due to the magnetic properties utilized in the alternating magnetic field. This external magnetic gradient localizes NPs based on their magnetic properties. Hyperthermic conditions can be achieved if these are met with sufficiently magnetic NP formulations, such as SPIONs (superparamagnetic iron oxide NPs) or some version of iron oxide NPs[199].

These three main modalities, or devices, of targeting via HIFU, PTT, and AMF can target NPs mechanically. They can elicit their own immune effects, especially with HIFU's versatility without NPs present. While there are different immunomodulatory effects and NPs that can be used with each, they each represent a unique research goal. In the current work, we utilize a HIFU-targeted approach to develop a method that addresses some of the current problems in the field.

5.3 Chemical targeting (receptor-mediated, tumoral chemistry-targeting)

Specifically defining the target of a treatment to a tumor can be accomplished chemically. This can include developing a ligand-receptor interaction with a receptor that is overexpressed on the specific tumor type or aiming for drug release via tumor chemical conditions (e.g., hypoxic or pH conditions).

5.3.1 Receptor-Mediated Targeting

Various receptors and pathways can be hijacked by malignant cells for various purposes. These can include, i) enhancing tumor survival, ii) increasing cancer proliferation, iii) developing drug resistance, and more. These can be utilized as a target for therapeutic purposes (Fig. 3). Examples can be, i) urokinase-type plasminogen activator (uPa**)** in breast cancer[200], ii) epidermal growth factor receptor (EGFR) in lung cancer[201], iii) CD44 receptor in various cancer cell lines[202] (specifically used a HCT116 colon cancer cell line and Ehrlich's ascites carcinoma-bearing mice in the referenced study), iv) insulin-like growth factor 1-receptor (IGF1-R) in pancreatic cancer[203], CXCR4 in malignant hepatocellular carcinoma[204], and more.

Inhibition of CXCR4 has also been shown to sensitize cells to chemotherapies (e.g., acute lymphoblastic leukemia to nilotinib[205], prostate cancer to docetaxel[206], sorafenib in advanced hepatocellular carcinoma (HCC)[204,207]. This specific example of CXCR4 inhibition shows a good example of not only targeting tumoral receptors, but also utilizing a mechanistic understanding of the downstream side effects of the displayed receptor. CXCR4 plays key roles in tumoral neovascularization and angiogenesis, and additionally is tied to the JAK/STAT pathway. Specifically, JAK2 and JAK3 are associated and activated when stromal-derived factor 1-alpha (SDF-1a), also known as CXCL12, the natural ligand for CXCR4, causes CXCR4 receptor dimerization after binding. Then, the pathways of STAT1, -2, -3 and -5 are also associated[208]. There were further confirmations of these reports recently to show alternative implications of CXCR4/STAT3 linkage targeting being useful in small cell lung carcinomas due to anchorage and adhesion mechanisms of these studied lung carcinoma cell types[209]. A more recent formulation

utilized the NP alternative of delivering CXCR4 inhibition and sorafenib treatment regimens. As a basis, it is a known response that cancer cells, especially HCC, will develop drug resistance based on a hypoxic-derived mechanism in response to repeated sorafenib treatment. This HIF-1α- SDF1α-CXCR4 pathway of drug resistance can be alleviated via CXCR4 inhibition. This action was accomplished and enhanced via PLGA NPs that extended the circulation of the drug from getting almost completely cleared in ~1h to still maintaining ~10% after 4h with NPs[204]. This led to decreased tumor growth, lowered rate of metastasis, and increased survival *in vivo*. While this method is highly advantageous, many approaches simply rely on targeting the overexpression of receptors in certain ell types. This can be rather limiting based on the simple fact that there is no universally overexpressed receptor or tumor antigen. Therefore, there are other methods that target solid tumors more universally based on tumoral chemistry. We do believe, however, that utilizing the receptor-targeting approach in combination with other modalities (i.e., temperature-sensitive release) could greatly enhance applicability. For this reason, we investigated combining these methods as well in the presented work.

5.3.2 Tumoral chemistry targeting

It is well known that the tumor microenvironment (TME) is drastically different than normal tissue. The TME contains many alterations, such as i) leaky and irregular vasculature, ii) relatively acidic environment, iii) pockets of oxygen-deprivation to give hypoxia and anoxia within the tumor. While these alterations generally are used as tumor-promoting mechanisms, they can be utilized in tumor-targeting therapies to help spare healthy tissues due to their lack of similar features (Fig. 4). For example, the leaky and irregular vasculature of tumors has been extensively studied and

reviewed over the last few decades. It has been shown that most tumor vessels have abnormal branching patterns, disorder of cells, epithelial gaps (<2 μm), high expression of growth factors, and more[210]. These irregularities are used to maintain the high growth potential of solid tumors, however, they can also lead to the enhanced permeability and retention (EPR) effect to aid in macromolecule and NP drug delivery[211].

This phenomenon of NPs tending to deposit outside of the tumoral vasculature is generally restricted to the combination of this faulty vascularization and NP size (<100 nm). Albeit there have been investigations into what causes the EPR effect (i.e., bradykinin, ROS, and many others have been studied) and what could expand the possibilities of therapies relying on the EPR effect. For instance, a hypothesis is that the co-administration of vascular permeability mediators will potentially enhance the EPR effect, since in recent years, the EPR effect has demonstrated limitations[211-213].

The harsh limitation of various receptors being overexpressed in some cancers but not others is something that must be recognized. Even within the same cancer type, there is generally a large discrepancy between genotypes of patients, hence the push towards tumor marker identification and personal therapies. Instead of depending on receptor-targeting (previously discussed), many researchers have begun targeting therapies via tumoral chemistry (i.e., acidic or hypoxic TME). These forms of targeting can be more attractive due to the high specificity and lack of need of any sort of binding feature. Many newer NP formulations have investigated these kinds of triggers. These have enlisted the use of lowered extracellular pH values in tumors (pH 5.8-7.2)[214,215]. These can be more specifically broken into two main routes: i) pH sensitive-bonds being used to link

drugs to NPs that are disintegrated upon acidic degradation[216,217], ii) protonation of co-block polymers to alter the solubility of NPs, which reverses NP dissolution from deprotonation[218,219]. Both represent a method of delivery in response to lowered pH, which is only present in normal physiological conditions in saliva, gastric acid, skeletal muscle (via the Bohr effect involving the transportation of O_2 by different pH and O_2/CO_2 concentrations), or in endocytosis. While we were unable to find any current literature mentioning studies determining release of pH-sensitive NPs due to the Bohr effect, there are groups that are utilizing the Bohr effect with NPs. An example includes bicarbonate-loaded carbon NPs for composite hydrogels in response to light-triggered CO_2 for Bohr effect-triggered release of oxygen, and thus, the promotion of wound healing[220]. Thus, the targeting of tumors via pH is a clinically relevant modality.

A similar feature that is ubiquitous to solid tumors is the TME containing hypoxia. While many pathologies tend to display this property, hypoxia in cancer is associated with therapeutic resistance (i.e., radiotherapy and chemotherapy), angiogenesis, invasiveness, and metastasis[221]. Molecularly targeting hypoxia is a challenge. Due to the nature of hypoxic tissue resisting drugs from the vasculature, it also has varied levels of hypoxia patient to patient. Moreover, the differing kinds of approaches that target hypoxia involve using pro-drugs that are activated under moderate (e.g., tirapazamine drug being reported as 50-200-fold more toxic to hypoxic cells *in vitro*[222]) or severe hypoxia (i.e., PR-104, which is goes through selective reduction to increase toxicity to hypoxic cells[223]), both elicit their own kinds of issues however. Another kind of approach involves using inhibitory molecules for hypoxic factors or similar pathways, but these tend to be poorly defined[221]. Some NPs have been synthesized to utilize these mechanisms. For example, the carboxymethyl-dextran nitroimidazole, hypoxia-targeting NPs showed ~4-fold higher tumor targeting in

comparison to other surrounding tissues and a significant decrease in tumor volume in a SCC7 xenograft mouse model (n=5 per group)[224]. Imidazoles, more specifically nitroimidazoles, can generally be used for this type of application for their metabolism via one-electron reduction that is oxygen-derived and reversible (Fig. 4). This chemistry has been utilized in various NP approaches, even for combined theranostic or combination therapy applications[225,226]. While these methods of using pH- or hypoxia-targeting are an expanding new sub-topic that can be potentially used in the future. Even further, understanding the links between hypoxia and PFP nanobubbles could be highly applicable in our case since PFP bubbles have been shown capable of delivering oxygen to the TME[227].

In conclusion, nanoparticles have faced many levels of challenges since their conception, however, scientific advances involving them have expanded many current treatment modalities. Many data suggest nanomedical approaches have significantly improved therapeutic outcomes compared to free drug alternatives. The variety of targeting capabilities greatly expands the utility of NPs, and more research is being added to the field every year.

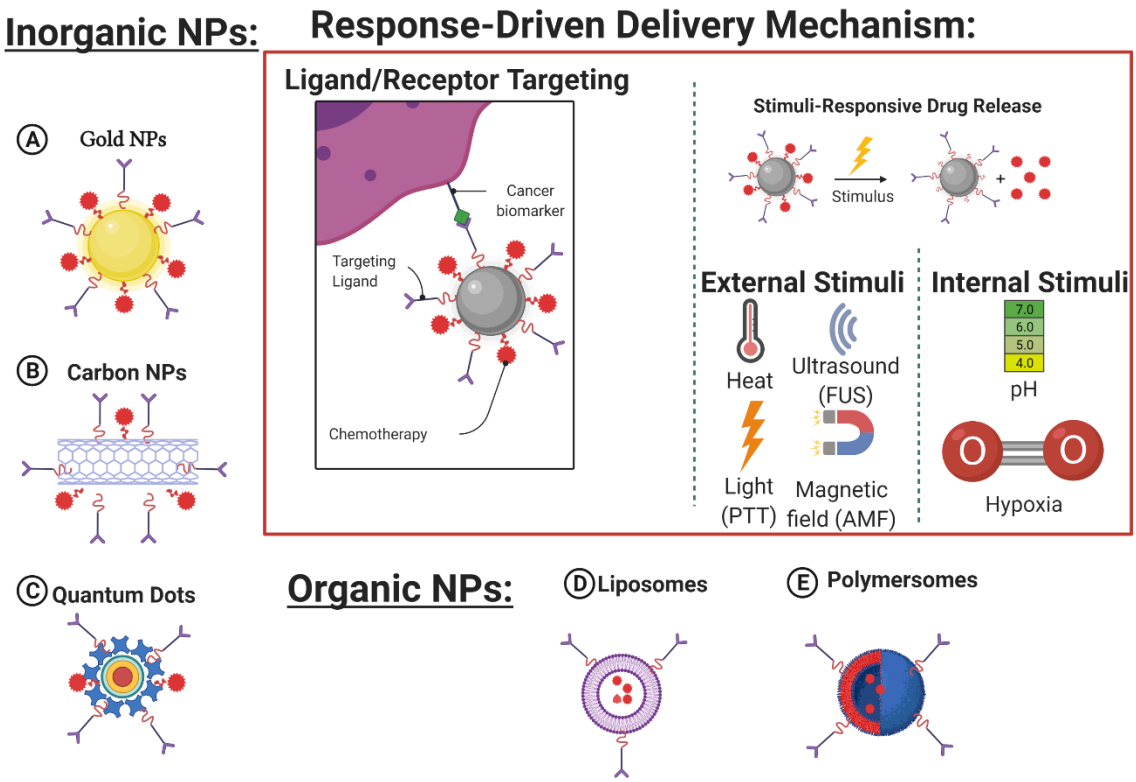

Figure 1. Nanoparticles' (NPs') chemistry and targeting capabilities

NPs can be made of inorganic material (A-C), or organic material (D-E). They can be targeted to the tumor via ligand-receptor targeting, (middle left), or via stimuli (middle right) (Created with BioRender.com)

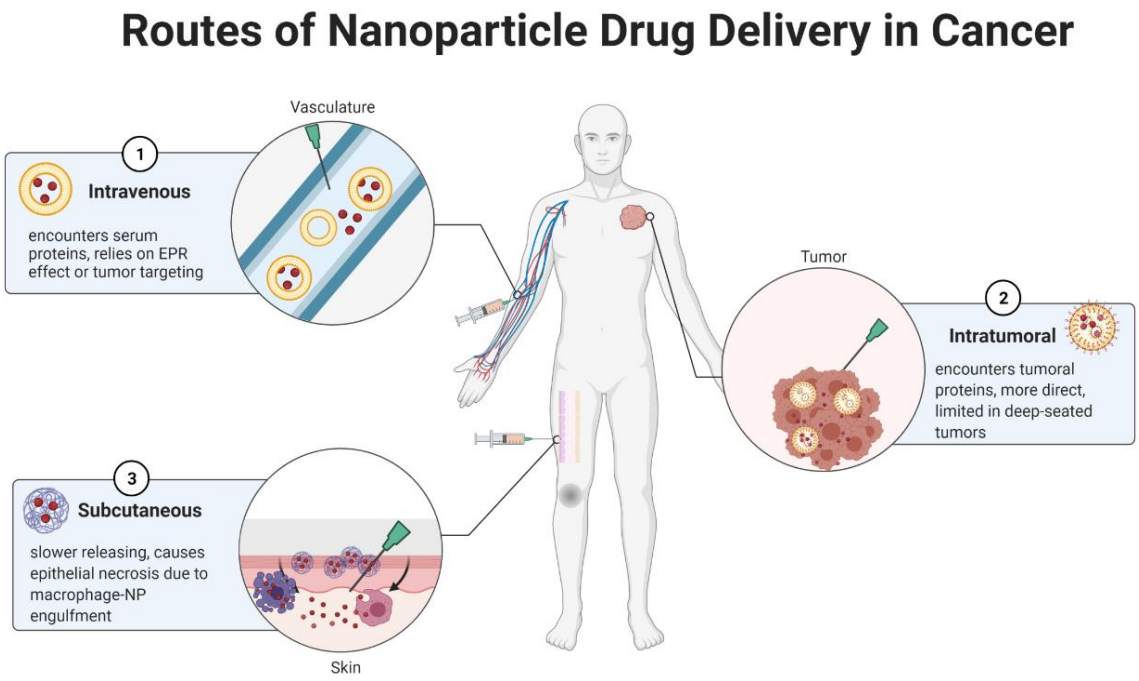

Figure 2. Routes of administration for nanoparticle therapies

NPs have different routes of administration. Each of these have different effects to the surrounding tissue, vasculature, drug delivery capabilities, etc. The most common are intravenous (i.v.) **(1)** and intratumoral (i.t.) **(2)**. Some have shown subcutaneous administration of NPs **(3)**; however, those can lead to macrophage endocytosis and lack of tissue-specific delivery (Created with BioRender.com)

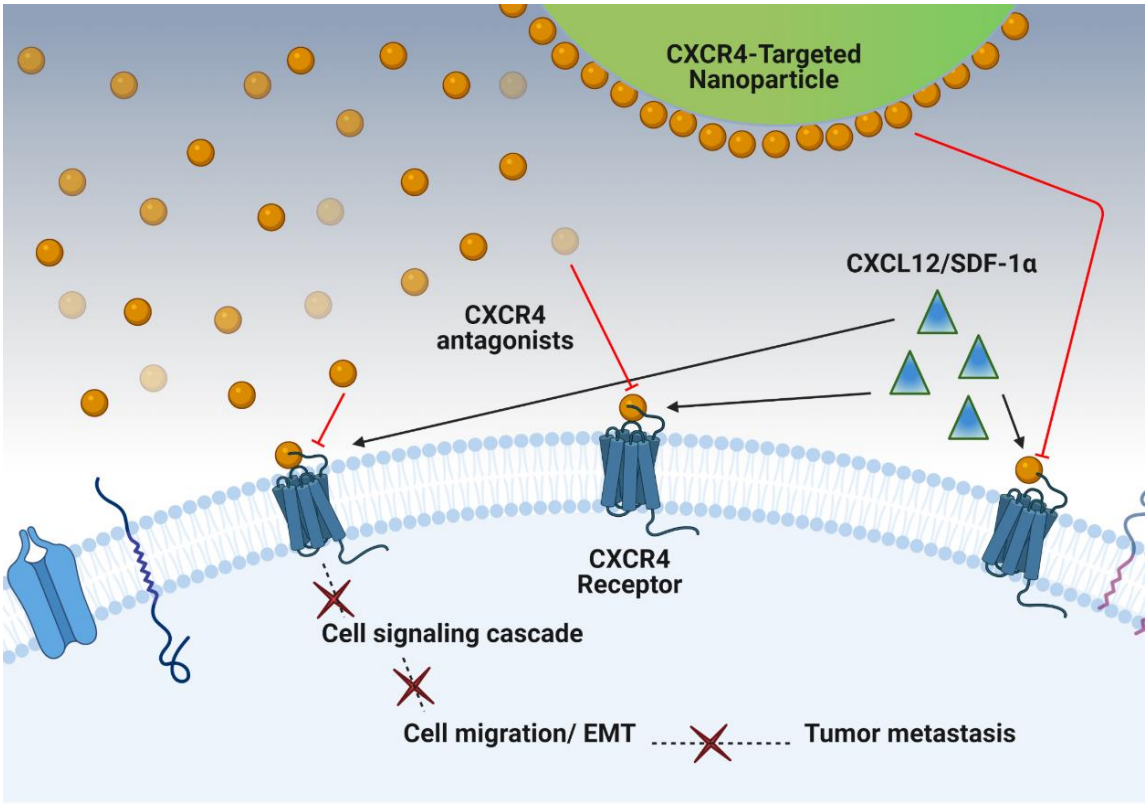

Figure 3. Ligand/Receptor targeting of NPs

Targeting of NPs via ligand/receptor interaction is a viable method of delivery. Receptor-targeting of NPs can use any receptor that is commonly overexpressed in tumor cells. Pictured above is an example of the overexpression of CXCR4. Downstream effects of cancer cell migration, epithelial-mesenchymal transition, and metastasis can be mitigated with CXCR4 inhibition; (Created with BioRender.com)

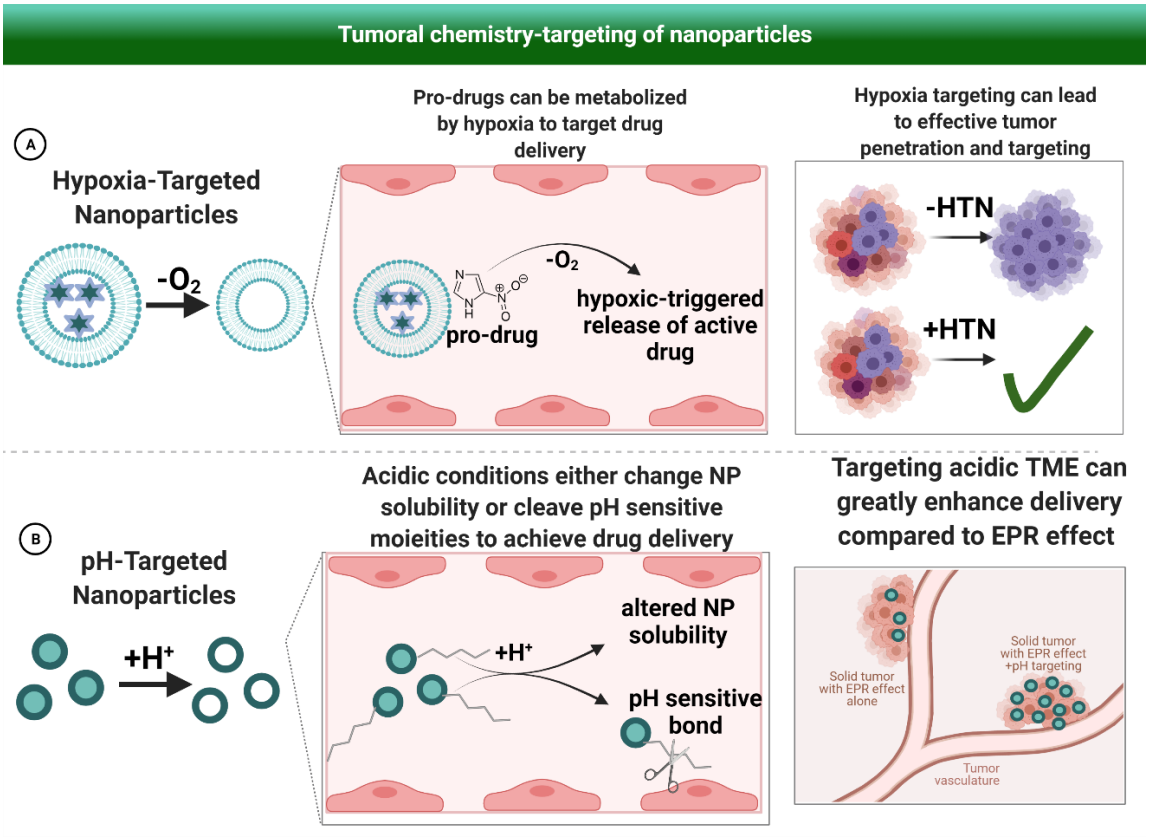

Figure 4. Modifications to enable chemically targeted NPs

NPs can be triggered to release their drug payload by the tumor microenvironment. Two main ways of doing this chemical targeting is hypoxia and pH targeting; Pictured above are examples of, **(A)** nitro-imidazole pro-drug triggered by hypoxia releasing drug, and **(B)** pH targeting the release of drug by altering the stability of NPs; (Created with BioRender.com)

Abbreviations

LTSL-low temperature sensitive liposome

E-LTSL-echogenic LTSL

PBD-PEO- polybutadiene-polyethylene oxide

POLY-polymersome (made of PBD-PEO), E-POLY- echogenic-POLY

DOX- doxorubicin

MTX- mitoxantrone

NP- nanoparticle

ICD- immunogenic cell death

PFP- perfluoropentane

HIFU- high intensity focused ultrasound

HT- histotripsy

CXCR4- C-X-C motif chemokine receptor 4

HT-histotripsy

CENTRAL HYPOTHESIS

The intratumoral combination of echogenic polymersomes loaded with MTX and histotripsy will enhance survival, improve anticancer response, and reduce tumor burden against colon carcinoma in vivo.

Aim 1: Co-encapsulate anthracenedione chemotherapies and perfluoropentane (PFP) in lipid- and polymeric-NPs

a. Determine the biophysical characteristics of polymersomes in comparison to liposomes (size, PDI, zeta, potential, drug loading, thermal release, kinetic assay)
b. Evaluate the effects of echogenicity on biophysical characteristics of polymersomes
c. Investigate focused ultrasound sensitivity of echogenic versus non-echogenic polymersomes in comparison to liposomal constructs

Aim 2: Assess preclinical and clinical application of dual-loaded echogenic polymersomes

a. Compare cytotoxicity of free MTX versus MTX-containing NPs
b. Investigate combination therapeutic potential of high intensity focused ultrasound and MTX (encapsulated and free drug) *in vivo*
c. Administer and monitor canine patient for safety and efficacy of combination

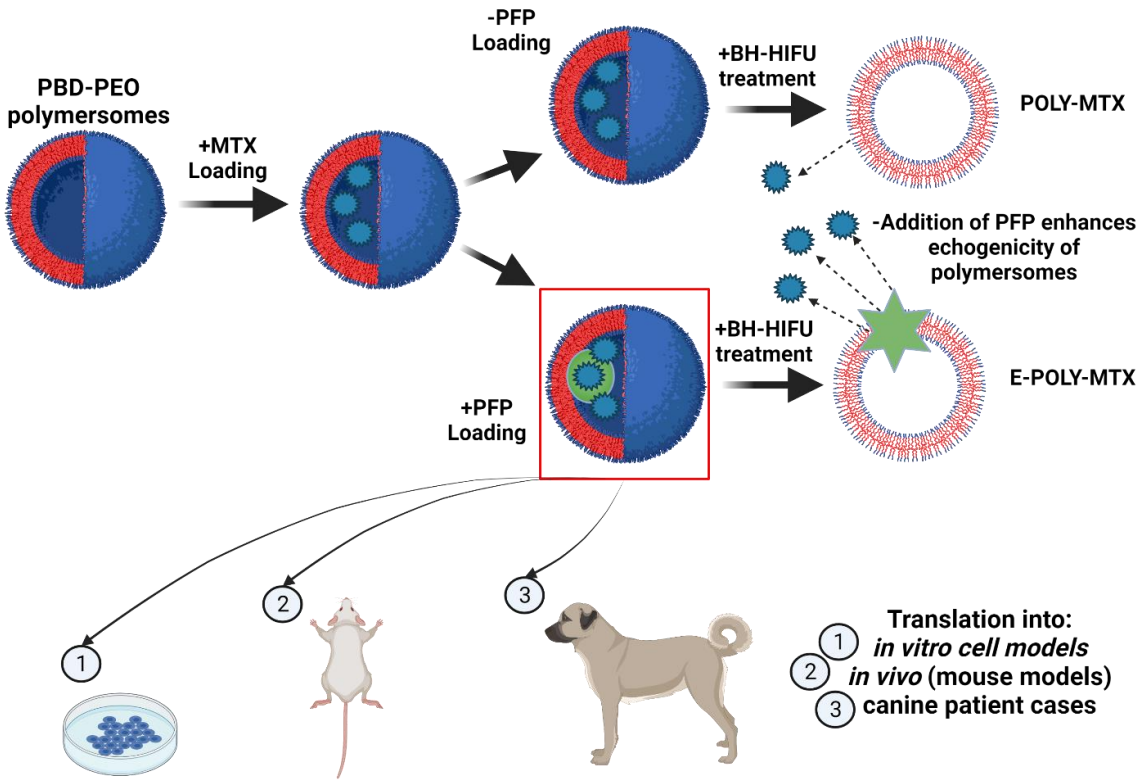

Fig. 5- Central Hypothesis- The intratumoral combination of echogenic polymersomes loaded with MTX and histotripsy will enhance survival, improve anticancer response, and reduce tumor burden against colon carcinoma *in vivo*

Tumor heterogeneity leads to altered drug accumulation. The sub-lethal dosage of drugs tends to lead to the lack of tumor clearance and the development of MDR. Nanoparticles (NPs) can enhance the delivery of drugs to cause more enhanced efficacy, however, first-generation of NPs lacked efficiency and primarily utilized the EPR effect. Newer-generations of NPs utilize stimulus such as HIFU in combination with bubble agents to give highly targeted payload release. We proposed

the inclusion of PFP nanobubbles with polybutadiene polyethylene oxide polymersomes loaded with MTX or DOX to enhance HIFU-sensitivity. This may lead to enhanced drug efficacy and more potent stimulation of immune effects like ICD. The more effective ICD is elicited, the more effective tumor clearance will be achieved in primary and secondary locations. These were tested in safety and efficacy *in vitro, in vivo*, and a single canine case of soft tissue sarcoma.

CHAPTER II

SYNTHESIS AND CHARACTERIZATION OF ULTRASOUND-RESPONSIVE LIPOSOMES AND POLYMERSOMES

Abstract

Low temperature sensitive liposome (LTSL) encapsulation of chemotherapies can enhance tumor accumulation and reduce damage to healthy tissues with high intensity focused ultrasound (HIFU) hyperthermia (40-45ºC). This is promising, but the poor serum stability and rapid clearance of LTSL following systemic administration is a clinical bottleneck. We hypothesized enhanced stability and targeted release with polymersome-based NPs. Briefly, polymersomes were synthesized using polybutadiene-polyethyelene oxide (PBD-PEO) polymers by the thin film and extrusion method, and loaded with anthracenedione chemotherapies (doxorubicin: DOX, & mitoxantrone: MTX). To provide ultrasound-sensitivity, we loaded the polymersomes (POLY) with perfluoropentane (PFP), a fluorocarbon that can assemble into bubbles to display ultrasound sensitivity (E-POLY). These were compared with PFP-loaded LTSL (E-LTSL). LTSL, POLY, E-POLY and E-LTSL were characterized for size and zeta potential using DLS, and drug release in physiological buffers including phosphate buffered saline (PBS) and 10% fetal bovine serum (FBS). Compared to LTSL, POLY demonstrated decreased thermal sensitivity, resulting in reduced release of MTX and DOX compared to LTSL from 37-45ºC. However, in the presence of HIFU-based histotripsy, E-POLY released their contents using two-five minutes of exposure. Our data

suggests the co-loading of PFP and chemotherapeutics in POLY may impart US sensitivity and enhanced thermal stability, potentially resulting in a controlled drug delivery to solid tumors.

Introduction

Conventional chemotherapy achieves low tumor accumulation, induces adverse effects in the non-targeted healthy tissues[228], augments multi-drug resistance by sub-lethal drug exposure [229]; which thereby limit therapeutic efficacy[230]. Tumor targeted approaches with nano-sized vehicles have been heavily researched for localized drug delivery[230]. Several studies have shown that this approach increases intratumoral drug concentration and decreases the needed therapeutic dose and harmful side effects[231]. A variety of intrinsic factors (i.e., pH, hypoxia) or external stimuli (e.g., ultrasound, magnetic field, etc.) can support triggered release of therapeutics from NPs in a tumor (See Chapter 1). We are particularly interested in attaining targeted delivery of mitoxantrone (MTX). MTX induces DNA intercalation, topoisomerase II poisoning, immunogenic cell death (ICD), and interferes with RNA to attain dramatic killing of tumor cells[72,232,233]. It also differs from its anthracycline counterpart, doxorubicin (DOX), in its lowered cardiotoxicity[234]. Despite MTX's benefits in comparison to DOX, systemic toxicity and lack of notable tumor accumulation following parenteral injections are the main clinical challenges[235,236] .

One approach to improve tumor therapy of MTX can be utilizing biocompatible lipid-derived nanoparticles that mimic cellular lipids[237]. Liposomes, such as thermal sensitive formulations (i.e., Thermo-Dox®), can achieve targeted release of encapsulated DOX at >40°C in a site of interest. Unfortunately, the phase III clinical trial employing Thermo-Dox® (OPTIMA, randomized, double-blind, placebo-controlled clinical trial (NCT02112656) was recently halted due to an inability to clinically improve outcomes compared to conventional DOX therapy. This exemplifies a common problem of liposomal drug delivery of lowered stability leading to premature payload release[238].

As an alternative approach, in this study, we encapsulated MTX in LTSL and polymersomes (POLY), and compared their performance in serum to determine effects of polymeric rigidity on stability. The enhanced stability of polymersomes, however, represents an equal and opposite problem with limited release upon stimulus[238] (Fig. 6). Therefore, to provide stimuli-sensitive release by histotripsy via high intensity focused ultrasound (HIFU), we co-loaded LTSL and POLY with PFP nanobubbles. These shortened, mechanical parameters are highly preferred clinically due to the current limitations of thermal ablation (e.g., potential close proximity to a vital organ, bone, nerve sustaining significant damage during long-term heating[239]). We observed a marked enhancement in serum stability of DOX- and MTX-containing POLY and E-POLY in comparison to LTSL derivatives in response to heightened temperature (45-60°C).

To augment release rates, we synthesized echogenic polybutadiene-polyethylene oxide (PBD-PEO) POLY by co-loading them with MTX or DOX and PFP (E-POLY). Results suggested successful synthesis of dual-loaded E-POLY based on size and polydispersity by DLS (dynamic light scattering) analysis, thermal release profiles, and transmission electron microscopy (TEM). Further, data also suggested incorporation of PFP enhanced histotripsy-sensitivity by *in vitro* release.

Materials and Methods

Materials

Perfluoropentane (99%, Exfluor Research, Round Rock, TX) was used as the ultrasound contrast agent. Monostearoyl-2-hydroxy-sn- glycero-3-phosphocholine (MSPC), 1,2-dipalmitoylsn-glycero- 3-phosphocholine (DPPC), and 1,2-distearoyl-sn-glycero-3-phosphoethanolamine-N-(methoxy (polyethylene glycol)2000) (DSPE-PEG-2000) were obtained from Corden (Boulder,

CO). Doxorubicin HCl was obtained from LC Laboratory (Woburn, MA). MTX dihydrochloride, 1,3-propanediol, chloroform, and methanol were purchased from Sigma Aldrich (St. Louis, MO). Poly(1,2-butadiene)-b-poly(ethylene oxide), PBD-PEO, (1.2-b-0.6) was purchased from Polymer Source, Inc. (Quebec, Canada). 1X PBS solutions were purchased from Gibco/Corning. Citrate buffer, 300 mM (pH 4.0), was made in-house from sodium citrate (purchased from VWR) and citric acid (purchased from VWR) and adjusting for pH using an Accumet Fisher Scientific pH probe. Solution of 0.5 M Na_2CO_3 was made from solid Na_2CO_3 (purchased from AMRESCO). PD-10 desalting columns were purchased from GE Healthcare.

Synthesis of echogenic liposomes (E-LTSL) and echogenic polymersomes (E-POLY)

LTSL (DPPC, MSPC, and DSPE-mPEG2000 molar ratio of 85.3:9.7:5.0) and POLY (100% polybutadiene-polyethylene-oxide, PBD-PEO, 1.2-b-0.6) were synthesized as follows. Each lipid or polymer mixture was thoroughly dissolved and mixed in chloroform. MSPC required an additional aliquot of methanol to ensure total dissolution. Chloroform, or the chloroform-methanolic mixture, was removed *in vacuo* using a rotary evaporator (Heidolph) attached to a vacuum pump (ChemGlass) at 45ºC to form a thin film. Residual chloroform was evaporated in a desiccator overnight at RT. LTSL were subsequently hydrated with citrate buffer (2-3 mL of 300mM, pH 4.0 citrate buffer/100g of lipid wt) for 1-3 hours at 55ºC until all solids had become dispersed into solution. The aforementioned solution was then sonicated for 10 minutes and extruded three times through a 200 nm polycarbonate membrane filter at 55ºC under high pressure[240]. Polymersomes were hydrated with a similar 300 mM citrate buffer in a ratio of ~8-9 mL of citrate/100 mg polymer instead. They also required a longer hydration time of 8-9 hours at 50-55ºC to fully disperse into solution relative to LTSL. Faster times or higher temperatures were insufficient in successfully hydrating polymer-based films. Sonication (ten minutes) and three

times high pressure extrusion through a 200 nm polycarbonate membrane filter was followed post-hydration, similar to aforementioned liposomal prep[240].

To make E-LTSL and E-POLY, 0.65 M 1,3-propanediol was included in the hydrating buffer as a surfactant to enhance perfluoropentane(PFP) loading. Echogenic liposomes (E-LTSL) required (1.906 mL buffer+94 µL propanediol/~100 mg lipid, 55ºC, ~1-2h) for hydration, whilst echogenic polymersomes required less volume in comparison to their non-echogenic counterpart (2.64 mL buffer+0.124 mL propanediol/~50 mg polymer, ~55ºC, ~8-9h).

Drug loading in lipid and polymeric NPs

DOX, MTX loading in LTSL, E-LTSL, POLY, E-POLY

Encapsulation of DOX and MTX into LTSL, E-LTSL were carried out using a pH-gradient loading protocol as described by *Mayer et al.*[241]. Briefly, the exterior buffer of the liposomes was adjusted via desalting PD-10 column to ~pH 7.4 using 1X PBS. DOX or MTX was loaded at 2 mg per 100 mg lipid ratio at 37ºC for 1 hour in darkness. Encapsulation of DOX and MTX into POLY and E-POLY were carried in a similar pH-gradient loading protocol with slight modifications. The required time for drug loading was increased to 2.5h. PFP encapsulation was subsequently done for E-LTSL and E-POLY. %EE of DOX and MTX was calculated by fluorescence intensity of drug encapsulated within NPs divided by fluorescence intensity of total drug X 100% as previously published[242].

Size analysis of LTSL, E-LTSL, POLY, E-POLY

LTSL, E-LTSL, POLY, and E-POLY were characterized for size (z-average) using a dynamic light scattering (DLS) instrument (Zetapals, Brookhaven Instruments, Holtsville, NY) by employing a non-negative least squares (NNLS) algorithm. The calibration standard used was a Thermo Scientific 3090A polystyrene nanosphere standard with a particle size of 92 ± 3 nm. Briefly, 1-2 µL of NP solution were added to ~3 mL of water in a cuvette, and DLS measurements were taken at RT. For each liposomal and polymeric formulation an average of three to five measurements was taken, the mean size and standard error of the mean (SEM) were calculated for the LTSL, E-LTSL, POLY, and E-POLY samples.

Drug release from LTSL, E-LTSL and POLY, E-POLY

LTSL-, E-LTSL-, POLY- and E-POLY-MTX and -DOX release were measured using thermoscan release and kinetics assays using a Carey-Eclipse equipped with an inbuilt temperature control system and stirring function ranging from temperatures 25-60°C. HIFU sensitivity was determined using an Alpinion-HIFU system (1.5 MHz transducer frequency, VIFU 2000, Alpinion Medical Systems, Korea).

Thermoscan release assay

Stability was assessed by measuring release of encapsulated drugs from all NP formulations as function of temperature (25–55 or 25-65ºC, for LTSL and POLY constructs, respectively) *in vitro* in PBS and in 10% FBS/90% PBS. For drug release studies, samples (2% drug/lipid wt) were diluted 50-fold in either PBS or 10% FBS, and 3.00 mL of sample was placed in a quartz cuvette

equipped with a stopper and magnetic stirrer. Samples were incubated using a Cary Eclipse Fluorescence Spectrometer (Agilent Technologies, Santa Clara, CA, USA) equipped with an inbuilt temperature control system. DOX release was assessed by excitation at 480 nm and fluorescence emission monitored at 590 nm. MTX was assessed by excitation at 660 nm and emission monitored at 685 nm. Throughout the release assays, every 0.5ºC increment was measured for 25–45 ºC or 25-50ºC for LTSL and POLY constructs, respectively. The solutions were kept under constant stirring to ensure proper heat dispersal and thermal equilibrium. Non-PFP containing NPs (LTSL and POLY) were used under identical conditions as negative controls.

Kinetics assays

To measure drug release as a function of time at a constant temperature, NPs were formulated as described above and held at 25-35°C (for LTSL derivatives) or 40-50°C (for POLY derivatives) for 30-60 minutes for kinetics experiments. For fluorescence measurements, at the same volumes as described previously, the samples were equilibrated to the desired temperature (~25-40°C for LTSL derivatives and ~40-60°C for POLY derivatives for 30-60 min.). Baseline fluorescence measurements for each sample were taken at 25ºC and complete release was calculated by adding 10 µL 1% triton and thorough mixing. Drug release based on fluorescence quantification at a given time (t) under constant temperature exposure was determined using the equation below: where I_o represents the initial fluorescence intensity of E-LTSL, LTSL, E-POLY, and POLY suspensions at 25ºC, and I_t is its intensity at time (t) at a predetermined temperature. I_m represents the fluorescence intensity of completely released drug upon triton release. Data was obtained as percentage release of encapsulated DOX, MTX at a given temperature.

$$\% \text{ DRUG RELEASE} = \left[\frac{I_t - I_o}{I_m - I_o}\right] \times 100$$

Drug Release calculation. where I_o represents the initial fluorescence intensity of NP suspension at 25°C, I_t is fluorescence after treatment, I_m represents the fluorescence intensity of completely released DOX or MTX after addition of 1% triton.
Data was obtained as percentage release of encapsulated DOX or MTX after thermal or histotripsy treatments.

Drug release by HIFU exposures

The effect of PFP on release of encapsulated DOX or MTX from LTSL and POLY (E-LTSL & E-POLY versus LTSL & POLY, respectively) was assessed with HIFU-based histotripsy (HT). The HIFU transducer had a 1.5 MHz central frequency, 45 mm radius, and 64 mm aperture diameter with a central opening of 40 mm in diameter and an automated motion stage to achieve accurate positioning perpendicular to HIFU beam axis. HIFU treatment parameters were as follows: 1% duty cycle, 1-5 Hz pulse repetitive frequency, 450-600 W power. After HIFU, collected samples were analyzed for DOX fluorescence at 480 nm excitation and 590 nm emission, and MTX fluorescence was assessed at 660 nm excitation and 685 emission. Hyperthermia (45°C, DC-50%, PRF-20Hz, P-12 W, 100s per point-3 pts/slice) HIFU parameters were additionally tested similarly.

TEM imaging of LTSL, E-LTSL, POLY, E-POLY

LTSL, E-LTSL, POLY, and E-POLY were imaged using a negative staining technique and a transmission electron microscope (TEM). HIFU-treated E-POLY, E-LTSL, POLY and LTSL were diluted 500–1000x in PBS. A 10 µL drop of diluted NP samples were pipetted onto a carbon grid (Lacey or Holey grid) and left for 1 min so that the NPs adsorbed to the grid, then the liquid was wicked away with a piece of filter paper. The grid was allowed to dry for 30s. For negative staining,

a 9 mL drop of 2% phosphotungstic acid (PTA) was pipetted onto the grid and left for 30s, then it was wicked away with a piece of filter paper. Again, the grid was briefly dried before imaging. The imaging was conducted at 200 kV using a JEOL JEM-2100 TEM (JEOL, Peabody, MA) by Lisa Whitworth from the Oklahoma State Microscopy Laboratory.

Results

Characterization of Nanoparticles

Drug-loaded nanoparticles (NPs) were synthesized using an active loading technique of transmembrane pH gradient. The NPs thus produced yielded an encapsulation efficiency of DOX-loading ~90-95% in LTSL. Similarly, encapsulation of MTX was ~90-93% for LTSL.

To characterize LTSL properties, hydrodynamic sizes of LTSL were measured. Size by DLS of LTSL measured 187.23 ± 1.28 nm (Table 1). Loading LTSL NPs with DOX (LTSL-DOX) in a discrete replicate showed a similar c.a. 200 nm size at 213.97 ± 1.86 nm (Table 1). Similarly, loading LTSL with our other anti-cancer drug, MTX, showed a size of 259.33 ± 3.78 nm (Table 1). To confirm size measurements obtained by DLS, we analyzed NPs by TEM. We observed c.a. 200 nm spheroid structures in TEM for LTSL-MTX constructs (Fig. 15). To determine uniformity of LTSL, polydispersity (PDI) was determined by DLS. LTSL (±DOX or MTX) had a PDI ranging from 0.126-0.171, indicating a high degree of uniformity in population size. LTSL-MTX were also supported to be similar sizes qualitatively by TEM observation (Fig .15). Zeta potential yields insight to both potential biophysical interactions and NP long-term stability. Thus, zeta potential was measured by phase analysis scattering (PALS). Zeta potential readings of LTSL gave readings ranging from -48.88 to -32.09 mV. These negative values are consistent with previous models of -48.0 mV[132]. The anionic nature is expected due to DSPE-PEG being a phospholipid.

Liposomal drug delivery has limitations in premature drug payload release. Therefore, polymersomes with enhanced stability are desired. Thus, we synthesized polymersomes (POLY) made of an inert polymer, polybutadiene-polyethylene oxide (PBD-PEO). To compare drug-loading capabilities, POLY were also actively loaded by transmembrane pH gradient similar to LTSL. POLY produced similar encapsulation efficiencies of DOX relative to LTSL (90-92% vs. 90-95%, respectively). Similarly, loading of MTX was comparative in POLY (84-85%) to LTSL (90-93%). While a higher amount of total drug was encapsulated at a higher 8% wt/wt (0.52 mg MTX/ 10 mg POLY), the encapsulation efficiency dropped to c.a. 65%. Thus, 2% wt/wt was decided as an optimized approach.

To compare POLY properties to LTSL, hydrodynamic sizes of POLY were measured similarly. These POLY NPs were comparable in size to LTSL (approx. 200 nm POLY relative to 200 nm LTSL, Table 1). To confirm size measurements obtained by DLS, we analyzed POLY-MTX by TEM. Similar to LTSL, c.a. 200 nm spherical particles were observed in POLY-MTX (Fig. 15). Relative size uniformity was confirmed with PDI readings based on similar values (0.151-0.194) to LTSL (Table 1). To compare differences of zeta potential of POLY to LTSL, zeta potential measurements were recorded. Zeta potential readings of POLY were relatively more positive in comparison to LTSL. POLY with and without drug range from -29.21 to -20.66 mV relative to the average of -38.39 mV for LTSL NPs. These POLY zeta potential values are comparatively more negative than previous models of PBD-PEO polymersomes that show zeta potential values of c.a. -5 mV[243].

Our long-term goals were to create NPs that could be triggered to release their drug payload locally. Toward this goal, we synthesized both previously published LTSL[242] and our novel POLY NPs that included the echogenic agent, perfluoropentane (PFP). To determine the impacts that this agent had on NP properties, we characterized E-LTSL and E-POLY in similar techniques aforementioned. We compared their properties to the non-echogenic LTSL and POLY NPs, respectively. Results

showed a slight reduction in most cases of drug-loading efficiency. DOX encapsulation efficiency was decreased from 90-95% to 60% (LTSL-DOX vs. E-LTSL-DOX). Similarly, MTX loading dropped from 90-93% (LTSL-MTX) to 68% (E-LTSL-MTX). These values are similar to previous reports (c.a. 70-80%)[242]. These reductions can be potentially explained with the sonication loading step of PFP releasing of some encapsulated drug.

To analyze any size differences caused by PFP, sizes of E-LTSL and LTSL were compared. Comparing E-LTSL hydrodynamic size to LTSL, results showed E-LTSL size was slightly decreased in comparison to LTSL (171.88 ± 1.38 vs. 187.23±1.28) (Table 1). Drug-containing E-LTSL derivatives measured in similar sizes to E-LTSL (174.01 ± 1.87 nm (E-LTSL-DOX) and 171.43 ± 5.02 nm (E-LTSL-MTX) (Table 1)). These values were correspondent to E-LTSL values in previous reports (171.6±0.5) nm[132]. To compare size distribution of E-LTSL relative to LTSL, PDI measurements were analyzed against each other also. In comparison to LTSL (0.126-0.171, Table 1), E-LTSL derivatives were maintained in uniformity in a similar fashion (0.171-0.222). E-LTSL and its drug containing E-LTSL (DOX & MTX) showed a decrease in zeta potential relative to LTSL. These E-LTSL NPs ranged from -54.33 to -49.64 mV, whereas LTSL zeta potentials ranged from -48.88 to -32.09 mV (Table 1). Thus, anionic nature of LTSL was maintained with addition of PFP.

To determine physicochemical changes to POLY upon addition of PFP, biophysical characterizations were performed post addition of PFP. Drug loading of DOX was similar between POLY to E-POLY (90-92% compared to 93%). In contrast, in discrete replicates, POLY-MTX showed encapsulation efficiencies of 84-85% while PFP-loaded E-POLY-MTX showed 95-100%. Hydrodynamic size measurements showed alike values of c.a. 200 nm for echogenic and non-echogenic polymersomes (E-POLY 244.80 ± 7.64 nm, POLY-236.90±2.77 nm, Table 1). E-POLY loaded with DOX and MTX similarly showed 200-nm sized NPs (Table 1). Size distribution was

confirmed as monodisperse with measured PDI values that were comparable to POLY (0.171-0.222 vs. 0.151-0.194) (Table 1). In contrast, there was a larger variety of zeta potential readings of E-POLY and drug-containing E-POLY (DOX & MTX) relative to POLY (-46.26 to -19.30 mV vs. -29.21 to -20.66 mV). These values were divergent from previous models of PBD-PEO, which showed neutral/slight negative charge. Our POLY and E-POLY showed relatively consistent negative zeta potential when averaging POLY and E-POLY groups with drug. Average values were -25.39 (POLY) and -30.80 (E-POLY).

Comparing release profiles of LTSL and POLY derivatives

Temperature release profile of NPs

Our primary goal of creating locally-triggered NPs demands NP stability when stimulus is not present. Thus, determining temperature stability in biologically relevant temperatures was a necessity. Relative temperature stability can be determined by thermal scan. To determine temperature stability of LTSL, drug release was characterized in a thermal scan approach. Results showed maintenance of drug payload (DOX) until c.a. 40°C, followed by rapid DOX release (Fig. 9, orange line). Similarly, our other chemotherapy, MTX, showed to be contained within LTSL-MTX until reaching 40°C. This was then followed with a rapid release of MTX (Fig. 9 light blue line). This observation was consistent with past findings that LTSL from *Maples et al.* released cargo payload (DOX) at c.a. 40°C with the same formulation of NP[132].

More precise, temperature release profiles can be determined by kinetic assays. To determine temperature release profiles of LTSL, we analyzed drug release via kinetic assays. Results showed DOX release was at 21% upon reaching temperature (39°C) at time 0. Within 5 minutes, 36% of DOX had been released. Within 20 minutes, c.a. 65% of DOX had been released. At time point 60

minutes, 88% of DOX had been released (Fig. 10, orange line, closed triangles). In comparison, lower temperatures did not release DOX payload to the same extent. In contrast, enhanced temperatures beyond 39°C led to rapid release of DOX. For instance, 40°C led to rapid release of DOX payload immediately upon experiment initiation. This led to 99% DOX release within 21 minutes (Fig. 10, red line, closed triangles).

DOX is used clinically, but has limitations due to its dose-limiting cardiotoxicity. In reply, the related compound mitoxantrone (MTX) was synthesized to have similar therapeutic benefits with less cardiotoxic effects. Thus, we proposed the loading of MTX into NPs could further benefit its therapeutic profile. To compare temperature release profiles of MTX to DOX in LTSL, we characterized kinetic drug release of LTSL-MTX. Data showed required increases of temperature to cause release of LTSL-MTX (41°C, Fig. 10, indigo line, closed triangles) relative to LTSL-DOX (39°C, Fig. 10, orange line, closed triangles). Within the first 20 minutes, there was a steady increase of MTX release (41°C). In contrast, temperatures below did not indicate the same level of steep drug release throughout 60-minute incubation time (35, 37, 39°C, Fig. 10, black, gray, turquoise lines, closed triangles).

NPs composed of lipids (liposomes), are destabilized by serum. Thus, it is important to measure thermal stability in serum-containing solutions. To establish the serum-sensitivity of drug-loaded LTSL, thermal experiments were repeated in 90%PBS/10%Fetal Bovine Serum (FBS) solutions. Data showed LTSL-DOX started releasing DOX c.a. 35°C (Fig. 9, orange line, closed diamonds). Thus, demonstrating lowered stability in comparison to LTSL-DOX in PBS (c.a. 40°C, Fig. 9, orange line). Similarly, LTSL-MTX in serum media showed a reduction in stability relative to LTSL-MTX in saline. This was characterized by a drop in temperature required for MTX release in FBS (c.a. 35°C, Fig. 9, light blue line, closed diamonds) relative to LTSL-MTX in saline solutions (41°C, Fig. 9, light blue line).

To further establish serum sensitivity of LTSL, drug release by kinetic assays were conducted in serum-containing saline. Results showed LTSL-DOX showed a marked, early release (c.a. 50%) immediately upon reaching 37°C (Fig. 11, left graph, gray line, closed triangles) relative to 37°C inducing 50% release in LTSL-DOX over 60-minute incubation instead. Similarly, 39°C sparks a steep release of DOX from LTSL-DOX immediately in FBS instead of inducing slow and steady release without serum (Fig. 11, orange lines, closed diamonds vs. Fig. 10, orange line, closed diamonds). Similarly, LTSL-MTX displayed an increased thermal sensitivity in serum saline versus saline alone (37°C, Fig. 11, right graph, gray line, closed triangles vs. 41°C, Fig. 11, right graph, gray line, closed triangles, respectively).

Polymersomes have thicker membranes in comparison to lipid NPs. This thicker membrane generally leads to enhanced stability relative to liposomal formulations. Thus, to compare temperature sensitivity of POLY to LTSL, drug release was characterized in an extended 25-50°C in a thermal scan approach. Results showed enhanced thermal stability of POLY-DOX (Fig. 8, orange line) compared to LTSL-DOX (Fig. 9, orange line) at similar temperatures (40°C). Upon reaching 45-50°C, POLY-DOX released c.a. 40% DOX (Fig. 8, orange line). Equivalently, POLY-MTX only released 8% of its MTX payload upon reaching 50°C (Fig. 8, light blue line). Thus, POLY-MTX (Fig. 8, light blue line) also displayed an enhanced thermal stability relative to LTSL-MTX (Fig. 9, light blue line).

To compare more precise thermal release profiles of POLY to LTSL, kinetic assays were analyzed up to 50°C in phosphate-buffered saline. Results showed release of POLY-DOX required the full 60 minutes for 100% DOX release at 40°C (Fig. 12, left graph, black line, closed triangles). At 45°C, c.a. 25 minutes were required for 100% DOX release (Fig. 12, left graph, burgundy line, closed triangles) versus 50°C causing full DOX release prior to 20 minutes (Fig. 12, left graph, pink line, closed triangles). Thus, POLY released DOX much slower in comparison to LTSL. Alike, POLY-MTX demonstrated enhanced thermal stability relative to LTSL-MTX. POLY-MTX

released 48% MTX at the end of 60-minute incubation at 40°C (Fig. 11, right graph, black line, closed triangles) and 65% release after a similar 60-minute incubation time at 45℃ (Fig. 11, right graph, light blue line, closed triangles). At 50°C, 100% MTX was achieved at approximately 39 minutes (Fig. 11, right graph, blue line, closed triangles). These values were much lower in release in comparison to LTSL-MTX (99% MTX release within 21 minutes at 41°C, Fig. 10, indigo line, closed triangles). Thus, both POLY derivatives (DOX & MTX) results showed higher temperature are required for notable drug release in comparison to their liposomal counterparts (LTSL-DOX and LTSL-MTX, respectively).

The most important aspect of the application of polymeric NPs (POLY) is their ability to not be degraded in serum in contrast to liposomes (LTSL). To compare the serum-sensitivity of previously published LTSL to our novel POLY, we conducted thermal scan tracking of drug release in similar temperatures. Results showed reduction of DOX release from POLY-DOX (45-50°C, 36% release) in saline relative to DOX release in FBS (11% release, 50°C, Fig. 9, orange line, closed diamonds). Similarly, MTX thermal scan noted reductions from 8% MTX in PBS to 3% in serum-containing saline for POLY-MTX NPs.

To compare serum-modified thermal release profiles of POLY to LTSL, release of DOX and MTX were characterized in a kinetics approach. Results showed POLY-DOX displayed notably less DOX release at 45, 50°C (Fig. 13 burgundy, pink lines, 21% and 50% release at 60-minutes, respectively) relative to LTSL's steady release at 37°C (Fig. 11, left figure, gray line). Higher temperatures were required (55-60°C) to release notable amounts of DOX from POLY-DOX (50%+). Moreover, DOX release was measured at the end of 60 minutes to yield 21%, 50%, 80%, 95% release for 45°C, 50°C, 55°C and 60°C, respectively. POLY-MTX showed similar MTX release reductions relative to POLY-MTX in saline. This was characterized by a marked reduction of MTX release that was not similar to the steep release of POLY-MTX after reaching 50°C in PBS (Fig. 12, blue line, closed triangles). Instead, POLY-MTX in serum displayed less release over 60

minutes comparatively (c.a. 20% over 60 minutes, Fig. 13, blue line, closed triangles). POLY-DOX and POLY-MTX results in serum thus suggested a flipped effect of serum on POLY in comparison to LTSL.

Upon addition of echogenic agent, PFP, thermal release profiles could be altered. This is due to the boiling point of PFP being c.a. 29°C. Thus, if NP release is within range of the boiling point of PFP, any differences to thermal release profiles must be considered. To compare any marked changes to thermal stability of LTSL or POLY post addition of PFP, thermal characterizations were repeated in similar fashion. Thermal scans of E-LTSL and E-POLY were done and compared to their non-echogenic counterparts. E-LTSL-DOX showed a slight slower release of DOX in comparison to LTSL-DOX (Fig. 9 red vs. orange lines). E-LTSL-MTX showed comparably similar temperature stability to LTSL-MTX (Fig. 9 blue vs. light blue lines). On a similar note, E-POLY-DOX showed a slight reduction in release compared to POLY-DOX (Fig. 8, red vs. orange lines). Similarly, E-POLY-MTX showed almost identical release profiles as POLY-MTX (Fig. 8 blue vs. light blue lines).

To compare thermal release profile differences in echogenic NPs, kinetic drug release was measured and compared to non-echogenic controls. Results showed no large differences in DOX cargo release in echogenic LTSL. There were small deviations, however, the tested 39°C and 40°C showed release that were within 15-20% relative to LTSL-DOX (Fig. 10, left graph, lines vs. lines with diamonds). MTX cargo release showed a similar agreement with non-echogenic and echogenic LTSL by showing release within 5-10% after 60-minute incubation (Fig. 10, right graph, lines vs. lines with diamonds). Comparing polymeric cargo release showed slightly different results when adding PFP. Addition of PFP seemed to slow the release of DOX at each temperature tested relative to non-echogenic POLY (Fig. 12, left fig., lines vs. lines with diamonds). The most prominent example was at 40°C, which showed almost half the DOX release at 30 minutes and 60 minutes relative to POLY-DOX (Fig. 12, left fig, black line vs. black line with diamonds). MTX

release showed a similar trend of E-POLY having a lessened release over time in comparison to POLY at the same temperature. Specifically, 50°C showed half the release at 30 minutes. In contrast to DOX release that maintained half release over the full 60 minutes, however, E-POLY-MTX and POLY-MTX both released MTX at c.a. 100% over 60 minutes (Fig. 12, right fig blue line vs. blue line with diamonds).

To compare thermal stability of E-LTSL and LTSL in solutions more representative of biological conditions, thermal scans and kinetic assays were repeated in 10% FBS/ 90% PBS solutions. Results showed DOX release of E-LTSL DOX in thermal scans were slightly more prone to early release relative to LTSL-DOX (Fig. 9, red line with diamonds vs. orange line with diamonds). E-LTSL-MTX showed very similar MTX release profiles compared to non-echogenic LTSL-MTX in serum (Fig. 9 blue line with diamonds vs. light blue line with diamonds). Therefore, DOX and MTX release of E-POLY showed little (DOX) to no (MTX) enhancement of drug release in comparison to POLY-DOX, and POLY-MTX, respectively.

Kinetic assay drug release of E-POLY NPs was also measured in FBS. Results of echogenic polymeric NPs (E-POLY) were compared to non-echogenic POLY NPs. This data showed almost identical MTX release throughout the entirety of the 60-minute incubation at 45°C, 50°C, 55°C, and 60°C at the end of 60-minutes of MTX release between POLY-MTX and E-POLY-MTX in FBS (Fig. 13, right fig. lines vs. lines with diamonds, respectively). Addition of PFP to POLY-DOX similarly did not cause notable differences in release in FBS relative to POLY-DOX at tested temperatures (45°C, 50°C, 55°C, 60°C; lines vs. lines with diamonds).

Comparison of drug release of NPs in response to HIFU exposure

Specific heating within tumors without causing surrounding tissue damage is highly challenging. Therefore, a main focus of our research has been to utilize high intensity focused ultrasound

(HIFU). HIFU has two parameters that can be tested for its NP release capabilities. These include thermal- and mechanical-based parameters. To understand the thermal ultrasound-sensitivity of LTSL, we monitored drug release after hyperthermia treatment by HIFU. Results showed c.a. 100% release of LTSL-MTX release upon hyperthermia (Fig. 14A, checkered blue bar). Thus, LTSL hyperthermia-sensitivity that was HIFU-induced was established.

To compare POLY hyperthermia-sensitivity to LTSL, we measured MTX release. In contrast to LTSL release, results showed POLY had little to no MTX release (1.82 ± 1.18%) (Fig. 14A, black bar).

To compare MTX release of echogenic NPs to non-echogenic NPs, similar hyperthermia experiments were conducted to determine effects of PFP. Results showed E-LTSL MTX release (94.55±2.01%, Fig. 14A, gray checkered bar) were similar relative to LTSL MTX release (93.43±3.31%, Fig. 14A, blue checkered bar). Similarly, POLY and E-POLY showed similar MTX releases comparatively. POLY and E-POLY released MTX at rates of 1.82±1.18% and 0.19±1.15%, respectively (Fig. 14A, black bar vs. gray bar). Therefore, LTSL and POLY maintained their respective responsiveness and non-responsiveness to hyperthermia despite PFP addition, respectively.

Another methodology of HIFU is mechanical-based histotripsy (HT). HT has been shown to interact with bubbles in solution. Thus, we introduced PFP nanobubbles to hypothetically maximize NP interaction with HT. To understand the mechanical ultrasound-responsiveness of LTSL, histotripsy treatments were conducted and drug release was measured. Results showed 45.35% release of DOX post HT treatment (Fig. 14B, red bar, vertical lines). Similarly, MTX release was measured in LTSL-MTX to yield 54.40% release (Fig. 14B, blue bar, vertical lines).

To compare the HT-triggered release of POLY to LTSL, drug release was analyzed post HT treatment. Data showed reduction of DOX release of POLY-DOX (0.4%, Fig. 14B, red bar) in comparison to LTSL-DOX (45.4%, Fig. 14B, red bar, vertical lines). Similarly, HT treatment released MTX from MTX-loaded POLY less relative to its LTSL counterpart (0.48% vs. 54.40%, respectively, Fig. 14B blue bar vs. blue bar, vertical lines). Thus suggested LTSL had HT-sensitivity while POLY did not.

To measure the effect of PFP on NP stability, HT treatments were similarly given to echogenic NPs. We compared echogenic and non-echogenic drug release differences from HT exposure. Results showed increased DOX release of E-LTSL relative to LTSL (45.35% to 68.99%, respectively, Fig. 14B, red graph, vertical lines vs. red graph, horizontal lines). Similarly, MTX showed enhancement of release in E-LTSL (66.79%, Fig. 14B, blue bar, horizontal lines) in comparison to LTSL (54.40%, Fig. 14B, blue bar, vertical lines).

To determine the effects of PFP on POLY HT stability, E-POLY drug release was compared to POLY post HT treatment. Results showed in increase in DOX release from POLY (0.4%) to E-POLY (5.57%) (Fig. 14B, red checkered bar vs. red bar, respectively). Similarly, MTX showed enhanced release based on PFP loading (E-POLY-13.64%, blue checkered bar vs. POLY-0.48%, blue bar, Fig. 14B).

To compare drug release from enhanced HT exposure, we repeated HT release studies. We also included a longer duration five-minute HT treatment (Fig. 14C). Results showed increased release of POLY from two-minute treatment to five-minute treatment. Similarly, E-POLY showed enhanced release from increased HT exposures of five minutes relative to two minutes. Meanwhile, we also compared efficiency of release of echogenic to non-echogenic POLY NPs. Results showed enhancement of release from echogenic (E-POLY) to non-echogenic (POLY) post two-minute

treatment (p=0.0043, Fig. 14C). Release was also enhanced E-POLY in comparison to POLY at five-minute treatments (p=0.0008, Fig. 14C).

Microscopy supports E-POLY HT-sensitivity

To compare release data and visual representations, transmission electron microscopy (TEM) images were taken before and after HT treatments. Observations showed LTSL and E-LTSL rupture post HT treatment (Fig. 15). This, along with release data, suggest LTSL and E-LTSL HT-sensitivity.

To compare POLY HT-sensitivity qualitatively to E-POLY, TEM experiments were used to visually inspect NP samples. While visually, LTSL and E-LTSL showed complete rupture and no intact NPs, POLY demonstrated intact NPs (Fig. 15 rows 1 and 2 vs. 3 respectively.) In contrast, POLY agreed with its release data by showing intact NPs (Fig 15, row 3). Despite E-POLY not showing full drug release via fluorescence readings, TEM visually showed little to no intact NPs (Fig. 15, row 4). This lack of 3-dimensional structures supports PFP increasing POLY HT-sensitivity by making them echogenic.

Discussion

My lipid-based nanoparticles (LTSL) would be predicted to perform poorly in a living organism. This conclusion is based upon *in vitro* properties of my LTSL. (1) Immediate and long-term stability of LTSL-DOX were decreased by serum media (Fig. 9, 11, left graphs). (2) Similar drug retention limitations were observed in MTX-containing LTSL (Fig. 9, 11, right graphs). My conclusion that LTSL are poor choices for bio-therapeutic NP is consistent with recent findings. Recent findings show a predominant model lipid NP, Thermo-DOX®, failed to clinically achieve

progression-free survival[244]. Our reported LTSL NPs showed lowered stability in serum similar to our previously reported *Maples et al.* lipid NP with the same composition[242].

In reply to the challenges presented by lipid-based NP, we attempted to synthesize polymeric NPs containing a chemotherapeutic. This combination of polybutadiene-polyethylene oxide (PBD-PEO) POLY NPs with MTX has not yet been reported. In the current study, evidence of synthesis of our novel PBD-PEO POLY NPs is presented by five biophysical analyses of NP properties. (1) 200 nm-sized NPs were verified by DLS (Table 1) and TEM (Fig. 15). This was consistent with our goal since we used 200 nm-sized pores during extrusion in NP synthesis. (2) Uniformity of polymeric NPs was confirmed to be monodisperse with similar literature values[245] as in Table 1. In addition, observations by electron microscopy of images showed POLY-MTX (Fig. 15) representative of a uniform size of c.a. 200 nm. (3) In contrast to the good agreement between observed vs. predicted NP radii, we noted that the observed zeta potential of our NPs were lower than we predicted (-29.21 mV vs. -5.0 mV, resp.; Table 1 vs reported zeta potential[243]). Speculatively, this discrepancy might have resulted from adsorption of negative phosphate ions (PO_4^{3-}) from PBS to NP surface. 4) Drug loading capability of POLY NPs was confirmed through pH gradient-active loading and separation of free drug by column. 5) Purified, drug-loaded NPs were confirmed to contain drug cargo by release via detergent lysis. There have been many previous reports using polymersomes as a drug delivery platform[246]. While there is one recent report of polymeric encapsulation of MTX with a different polymer[247], we report the first using PBD-PEO. Our polymeric NP encapsulation of chemotherapies thus could be utilized as a targeted therapeutic to avoid deleterious effects from premature drug release seen in liposomal formulations[116].

Echogenic NPs were synthesized to enhance drug release with histotripsy (HT). Physicochemical properties of echogenic polymersomes (E-POLY) confirmed that we successfully synthesized

PFP-loaded polymeric NPs. (1) The echogenic NP demonstrated radii, polydispersity, and zeta potentials comparable to their non-echogenic equivalents (Table 1). (2) POLY lacking the echogenic PFP component did not release drug when exposed to HT (Fig 14). (3) In contrast, including the echogenic agent, PFP, in the NP formulations resulted in 200-nm NPs (Fig. 15, Table 1) that released their DOX cargo in response to HT (Fig. 14). (4) Similar PFP-specific echogenic release was observed when using MTX cargo (Fig. 14). (5) Polymeric NPs demonstrated a lack of cargo release upon hyperthermic conditions by HIFU (Fig. 14A). (6) Visual confirmation of destruction of E-POLY through transmission electron microscopy (TEM) (Fig. 15). (7) More MTX cargo was released from longer duration HT treatment relative to shorter treatment times thus supporting that release is HT-triggered (Fig. 14C). While the use of echogenic polymersomes has been previously reported in different polymer types[248-250], this was the first report using a PBD-PEO polymer or of echogenic polymersomes containing MTX. Echogenicity was imparted into NPs by PFP-loading. This was proposed due to PFP nanobubbles potentially interacting with HT similar to gas bubbles/bubble clouds[251]. Our *in vitro* data suggests the application of our dual drug- and PFP-containing E-POLY can aid in effectively treating solid tumors with HT.

Although lipid NPs have been used clinically in many applications[252], we conclude our PBD-PEO POLY NPs are potentially superior in biological application relative to LTSL. (1) POLY can be loaded with hydrophilic chemotherapies (e.g., DOX and MTX) similar to LTSL. (2) POLY-based NPs do not degrade upon addition of serum in contrast to LTSL (c.f. Fig. 9 vs. Fig 8, respectively). (3) POLY can be loaded with PFP to give HT-triggered drug release (Fig. 14).

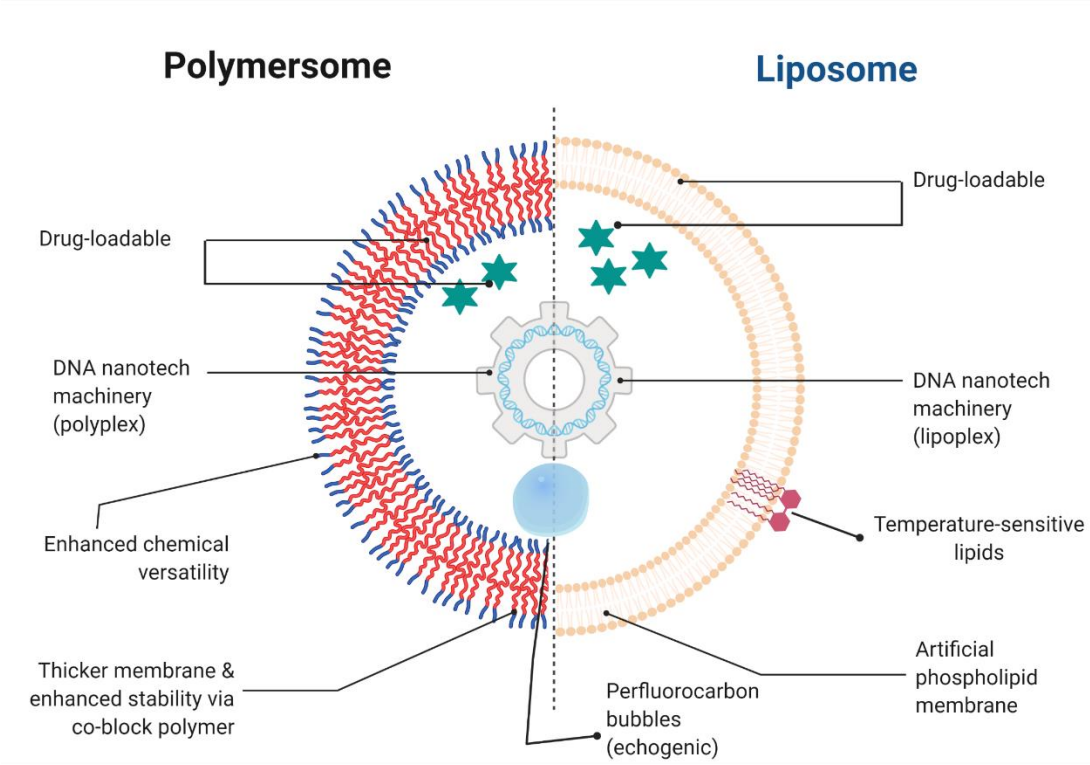

Figure 6. Structural differences between polymersomes and liposomes

Polymersomes have a thicker membrane that provides improve stability relative to liposomes. Chemical versatility is enhanced in polymersomes, whereas both lipid and polymer NPs have the ability of drug loading, complexing with polynucleotides, and loading with fluorocarbon bubbles[116]; (Created with BioRender.com)

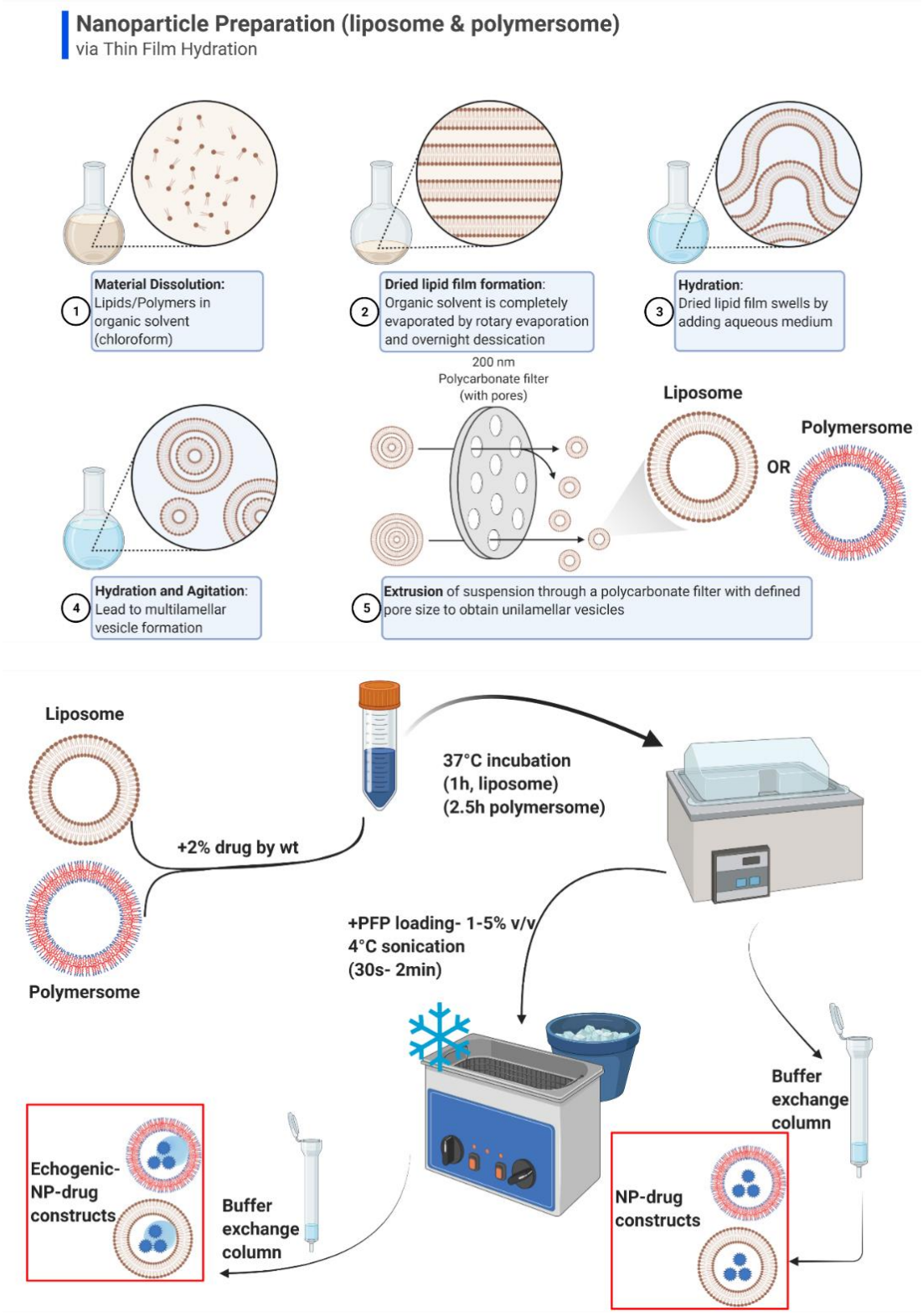

Fig 7. Schematic of PFP and drug loading in LTSL and POLY

NPs were synthesized via a thin film hydration procedure. Both liposomes and polymersomes were drug-loaded by active, pH gradient at 37°C by incubation for 1 hour and 2.5 hours, respectively. PFP was loaded into LTSL and POLY by made by sonication at 4°C. Purification by PD-10 buffer exchange column and concentration via centrifugation (as needed) was done to obtain a pure final product; (Created with BioRender.com)

Nanoparticle Construct	*Size (nm)*		*Polydispersity*		*Zeta Potential (mV)*	
	mean	**SD**	**mean**	**SD**	**mean**	**SD**
LTSL	187.23	1.28	0.137	0.019	-48.88	3.82
LTSL-DOX	213.97	1.86	0.126	0.016	-32.09	1.11
LTSL-MTX	259.33	3.78	0.171	0.010	-34.200	1.67
E-LTSL (1,3-PD-LTSL)	171.88	1.38	0.098	0.03	-52.47	2.44
E-LTSL-DOX	174.01	1.87	0.146	0.029	-49.64	2.62
E-LTSL-MTX	171.43	5.02	0.188	0.04	-54.33	0.50
POLY	236.90	2.77	0.194	0.019	-29.21	1.71
POLY-DOX	222.03	3.37	0.151	0.023	-26.30	2.46
POLY-MTX	224.77	4.16	0.161	0.019	-20.66	1.99
E-POLY (1,3-PD POLY)	244.80	7.64	0.171	0.026	-46.26	3.21
E-POLY-DOX	214.08	0.95	0.222	0.010	-26.84	3.60
E-POLY-MTX	231.31	2.28	0.220	0.015	-19.30	1.13

Table 1. Physicochemical properties of E-POLY, POLY, E-LTSL and LTSL.

NPs were synthesized via thin film hydration and drug loaded by pH gradient. Characterizations of size, polydispersity, and zeta potential were performed at room temperature. Stable hydrodynamic size (~200 nm) with no particle aggregation upon addition of drugs or PFP was noted for LTSL, POLY, E-LTSL and E-POLY. The polydispersity index and zeta-potential were in similar ranges for LTSL and POLY. Each size and polydispersity reading of NP represents n=180 repeated measurements of a single discrete NP preparation.

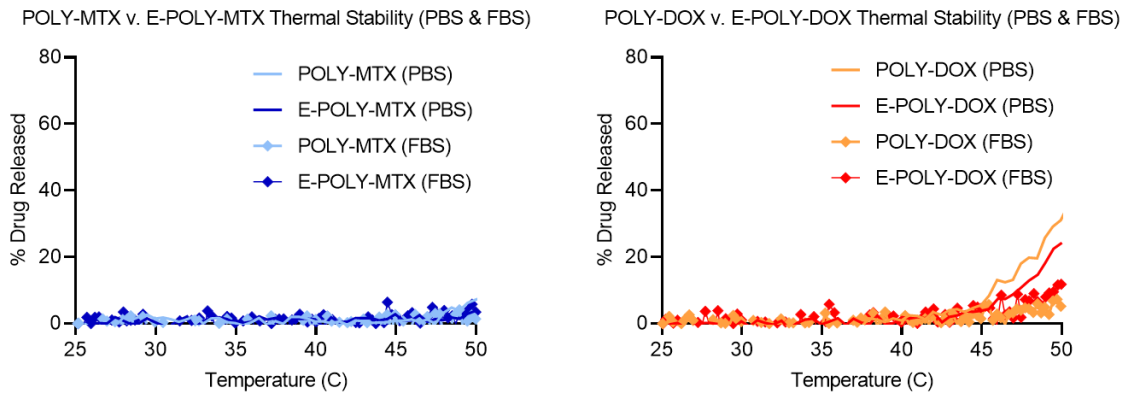

Figure 8. POLY and E-POLY displayed thermal stability

To determine temperature-sensitivity of POLY NPs containing drug cargo, POLY and E-POLY drug release was measured in a thermal scan approach (Lines). To compare differences of drug release of POLY NPs in response to serum-containing media, experiments were repeated in 10% FBS (Lines with diamonds).

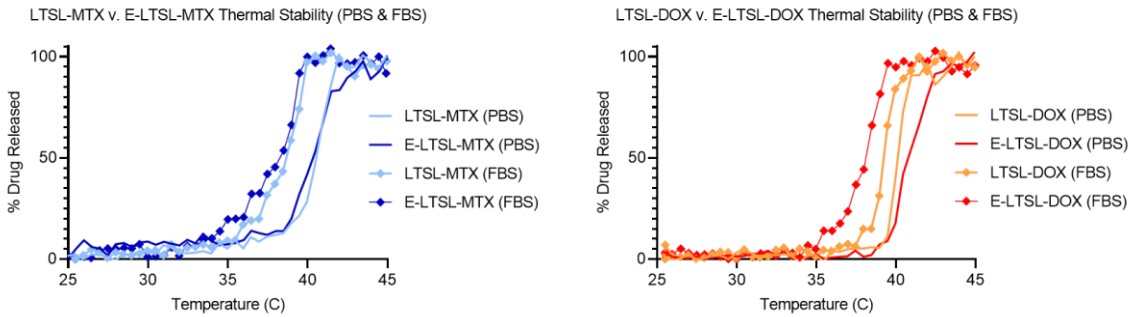

Figure 9. Serum exposure lowered the stability of LTSL

LTSL drug release was measured in a similar fashion to Fig. 8 to determine temperature sensitivity with (lines with diamonds) and without serum (lines).

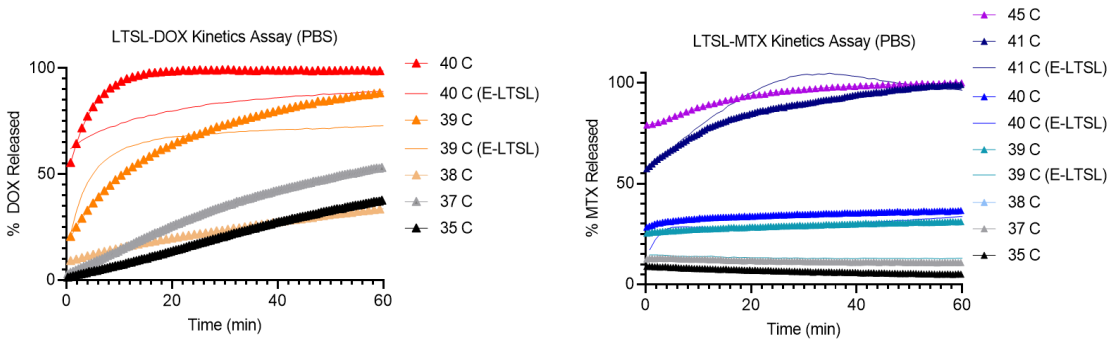

Figure 10. Controlled release via temperature of LTSL and E-LTSL in PBS

To determine drug release profiles, LTSL containing drug payload (DOX, MTX) were incubated for 60 minutes at various temperatures. To compare the release of echogenic to non-echogenic LTSL, key temperatures were chosen and repeated for comparison (lines vs. lines with diamonds, respectively).

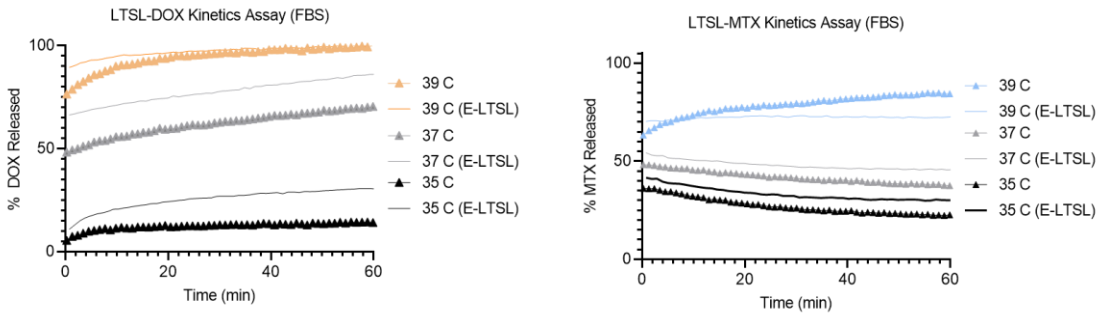

Figure 11. FBS decreased thermal stability of LTSL that contain DOX or MTX regardless of PFP content

To determine serum alterations of thermal release profiles of LTSL NPs, similar experiments to Fig. 10 were conducted in serum-containing saline (10% FBS).

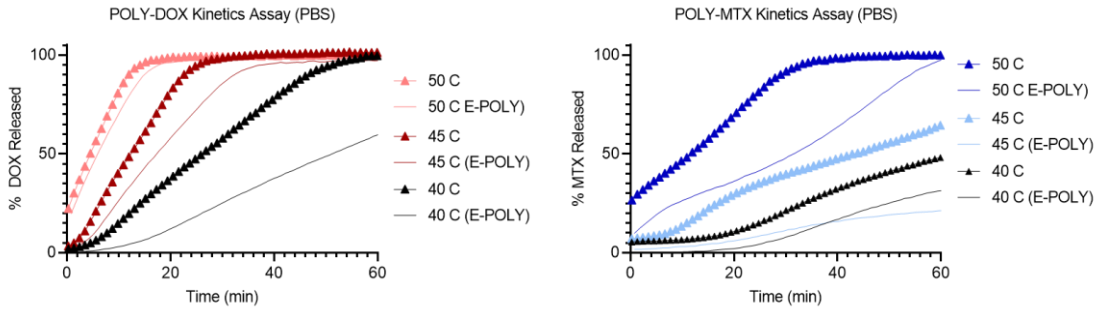

Figure 12. PFP encapsulation does not cause premature payload release of POLY

To determine drug release profiles of POLY, POLY containing drug payload (DOX, MTX) were incubated for 60 minutes at heightened temperatures. To compare the release of echogenic to non-echogenic POLY (E-POLY), incubations were repeated and drug release was measured (lines vs. lines with diamonds, respectively).

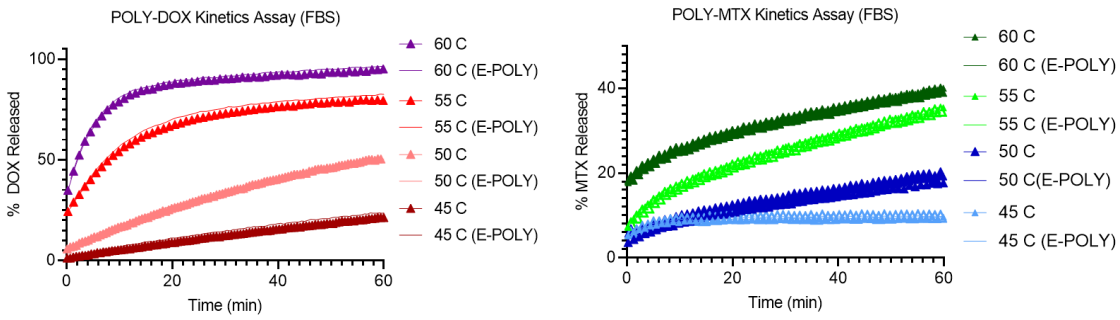

Figure 13. POLY demonstrated enhanced stability in FBS

To compare release profiles of POLY NPs post serum incubation, similar experiments to Fig. 12 were conducted in serum-containing saline (10% FBS).

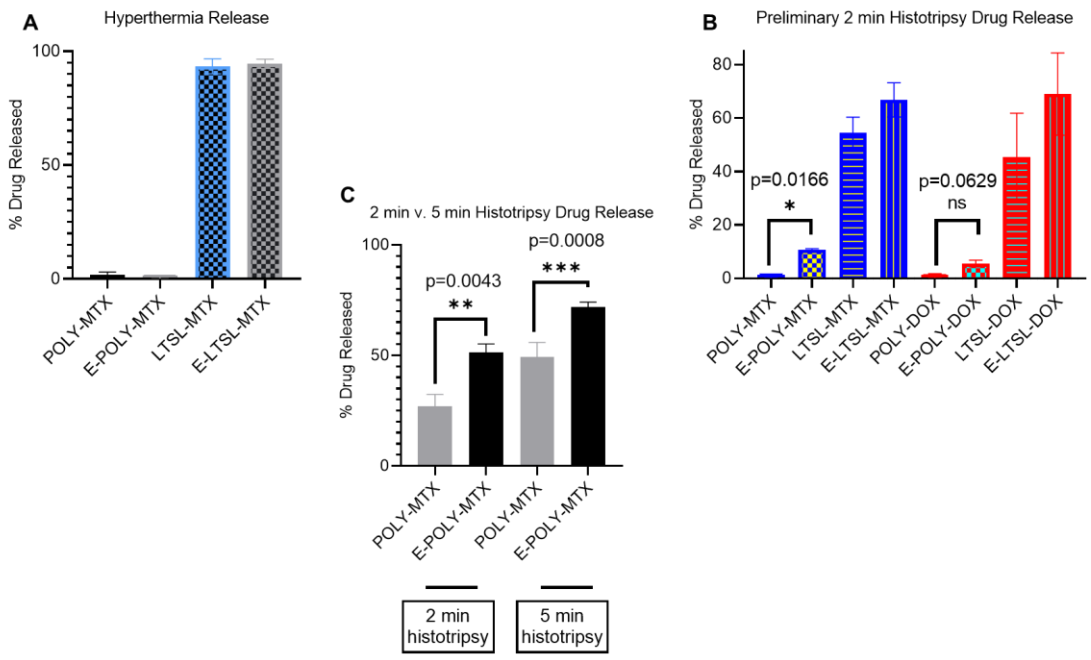

Figure 14. Histotripsy-triggered release of DOX and MTX E-POLY NPs

To determine the HIFU sensitivity of NPs, hyperthermia and histotripsy (HT) parameters were tested with NPs. **(A)** Comparison of MTX release from POLY-MTX, E-POLY-MTX, LTSL-MTX and E-LTSL-MTX in response to hyperthermia (n=3 for each group, replicates of same NP preparation); **(B)** comparison of MTX and DOX release in response to two-minute histotripsy (n=2 for each group, replicates of same NP preparation; **(C)** comparison of MTX release in MTX-containing polymersomes (POLY and E-POLY) in response to two- (n=3 for each group, replicates of same NP preparation) and five-minute histotripsy treatments (n=5 for each group, replicates of same NP preparation). Values were represented as mean ± standard deviation (SD) of the mean. Statistical comparisons were performed with unpaired t test with Welch's correction.

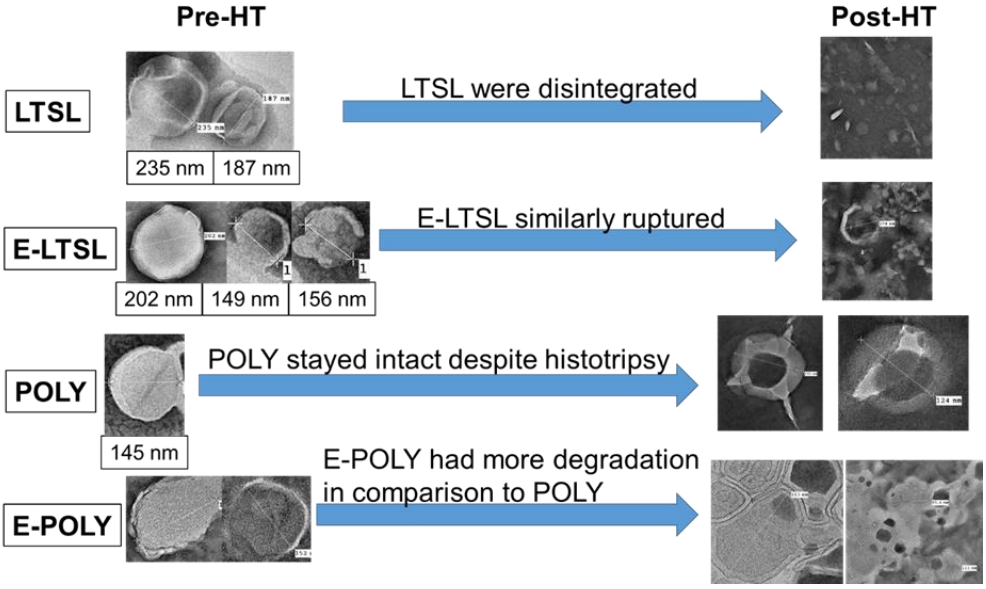

Figure 15. E-POLY demonstrated visual confirmation of MTX release upon histotripsy

To visualize NPs post HT treatment, transmission electron microscopy (TEM) was utilized to image NPs. NPs treated with two-minute HT parameters were fixed and visualized. Left column- pre HT treatment, right column- post HT treatment.

CHAPTER III

ANTI-TUMOR EFFECTS OF ECHOGENIC-POLYMERSOME (E-POLY) IN A MURINE COLON CARCINOMA MODEL

Abstract

Systemically injected NPs have been utilized to achieve a local triggered release of drug payload non-invasively with HIFU. While this approach can sensitize tumor cells for better therapeutic responses through tumor micro-environment (TME) alteration, the significant off-target effects of these nanoparticles limit therapeutic efficacies. In this study, we tested whether local tumor injection and combination with NPs can improve efficacy of treatments with echogenic-polymersomes (E-POLY) *in vitro* and *in vivo*. Briefly, a bilateral murine model of colon cancer was treated with E-POLY containing mitoxantrone (MTX) or free MTX intratumorally on days 10, 19, 25, 31. HIFU was applied concurrently for treatment of ~80-90% of initial tumor volume under ultrasound (US) guidance initially and followed with ~30% subsequent treatments. Mice were followed for >40 days to monitor growth of treated and untreated tumors. To translate this approach for clinical treatment, a canine patient was similarly treated with POLY-DOX (polymersome-doxorubicin) + HIFU. Data suggested that DOX-loaded POLY induced tumor reduction in a canine case of soft tissue sarcoma. In a murine colon cancer model, reduced primary and secondary tumor volumes were observed post treatment when treated with POLY-MTX, E-POLY-MTX, and free MTX. Moreover, extended survival was observed when HIFU was combined with MTX modalities in comparison to untreated control. Upon H&E staining and pathologist analysis, it was confirmed that E-POLY-MTX+HIFU achieved a higher level of necrosis (65-70%) in comparison to other treatment groups (5-40%). Further studies to understand these findings are currently underway.

Introduction

In-situ vaccination (ISV) of solid tumors is an immunotherapy approach that is aimed to enhance anti-tumor immunity via local treatments regardless of presence of signature tumor markers[253] and stage of cancer or comorbidities[254]. In this approach, a patient's own tumor cell lysate acts as an 'antigen depot' of tumor specific or tumor-associated antigens[255,256]. This phenomenon is especially amplified when the tumor cells undergo immunogenic cell death (ICD) that is characterized by the expression of damage-associated molecular patterns (DAMPs) that triggers dendritic cell and T-cell infiltration[257,258]. The dendritic cells can pick the antigens and present them to the closest draining lymph node, potentiating anti-cancerous immune response against patient's treated and untreated tumors (abscopal effect)[256]. Enhancement of ICD via drugs that have therapeutic and immunomodulatory functions (i.e., MTX or DOX) has been shown, or via HIFU-mediated sonic stress of tumor cells[259-262].

Conventional chemotherapy with MTX or DOX can cause deleterious, cardiotoxic effects. NP loading of chemotherapeutics to reduce adverse effects has been widely explored, however, relying on enhanced permeability and retention (EPR) effect alone by intravenous injection often results in insufficient chemotherapy accumulation (<5% of injected dose)[57,261-263]. One approach to overcome this barrier can be by an NP-ISV approach that induces stimuli-sensitive release during HIFU and induces anti-tumor immunity[132,261,264]. With modern image-guidance, directly injecting into tumor at any location is possible. This coupled with HIFU could induce ICD without harming surrounding tissue[265,266]. HIFU has been shown to enhance targeted delivery with NPs containing temperature-sensitive lipids or polymers[132], enhance *in vitro* gene transfer via NPs by disrupting the cell membrane[267], and increase cellular uptake[268]. This combination of NP-HIFU treatment expands the utility of therapeutic ultrasound, since many current HIFU monotherapies have yet to

show significant results in moderate or high risk patients (e.g., prostate cancer patients[269]). Thereby, the proposed NP-ISV approach has a potential clinical basis.

To investigate our hypothesis, we employed a bilateral CT26 colon cancer model. Murine CT26 colon carcinoma cancers demonstrate immunogenic features, suitable for ISV trials especially in combination with immunogenic cell death inducers, such as MTX[78,79]. We investigated whether the local treatment of CT26 with POLY and E-POLY can improve outcomes since this approach bypasses the serum proteins and need for delivery, thereby giving a much higher pool of injected dose in the targeted tissue, and also a direct interaction with tumoral proteins and antigens.

To optimize the NP effects with HIFU, we encapsulated perfluoropentane (PFP) in POLY to create E-POLY. Our *in vitro* studies (Chapter 2) showed that the presence of PFP decreased NP stability and improved the release of encapsulated content with HIFU likely through acoustic droplet vaporization and acoustic bubble cavitation[270]. It may be noted that previously DOX-loaded liposomal microbubbles increased ER stress, HMGB1 and ATP release to improve control of CT26 tumors[271]. Thus, we hypothesized that E-POLY loaded with nanobubbles would synergize with HIFU to improve local efficacy and distant regression of untreated tumors.

Many types of HIFU parameters (ablation, hyperthermia, or histotripsy etc.) can induce immune effects. In particular, histotripsy (HT) has been shown to enhance immune effects, such as the stimulation of TNF-α by macrophages, to a greater extent than thermal ablative conditions[178]. The lack of extensive thermal degradation can lead to reductions in denaturing of release proteins[178]. Thus, we wanted to investigate whether a HT protocol with E-POLY could induce an immune mediated killing of colon tumors and the feasibility of clinical translation for clinical trials via a preliminary evaluation in a canine sarcoma patient. Canine cancers demonstrate similar incidence rate, pathological signs, mutations, and gene fusions to humans[272]. Canine soft tissue sarcoma has

been shown to not meet beneficial outcomes when treated with DOX monotherapy[273], but HIFU was shown to be effective against sarcoma, eliciting a 47.3 response rate and a 80.6% disease control rate[274]. Soft tissue sarcomas also respond better to MTX, and it has even been tested in clinicals as early as the mid-1980s[275,276]. Thus, a demonstration of feasibility can have a high translational significance for the proposed study.

Materials and Methods

POLY and E-POLY Synthesis

POLY and E-POLY encapsulating MTX were synthesized via thin film hydration and extrusion methodology. Briefly, polymersomes films rehydrated in sterile 300 mM citrate buffer, pH 4.0 (echogenic contained 0.65 M 1,3-propanediol) at 55ºC under high pressure[240] (ratio of ~8-9 mL/100 mg polymer) were sonicated for 10 minutes, extruded through 200 nm polycarbonate filters three times, and run through a column exchange buffer with 1X PBS solution. Loading of MTX was accomplished by adding 2% w/w (2 mg MTX/100 mg polymer film) at 37°C incubation for 2.5h. PFP-loaded POLY and POLY alone were purified using PD-10 column to generate purified NPs.

Cell Culture

Murine colon carcinoma CT26 were obtained from ATCC® and cultured in DMEM medium supplemented with 10% FBS and 1% pen/strep in a 5% CO_2 environment unless otherwise mentioned.

Cytotoxicity Assays (MTS)

Cytotoxicity of MTX alone was compared with POLY-MTX and E-POLY-MTX at multiple time points (24, 48, 72h) using a CellTiter 96® AQueous Non-Radioactive Cell Proliferation assay at 1.25, 2.5, 5, 10 µM MTX concentrations. Similar corresponding concentrations of POLY and E-POLY were used based on %EE as normalization to test the safety of blank, non-drug containing NPs. CellTiter colorimetric method determines the number of viable cells using tetrazolium compound [3-(4,5-dimethylthiazol-2-yl)-5-(3-carboxymethoxyphenyl)-2-(4-sulfophenyl)-2H-tetrazolium, inner salt; MTS]. ~5-10 x 10^4 CT26 cells suspended in 100 µL of DMEM supplemented with 10% FBS, 1% penicillin-streptomycin were treated with MTX, POLY-MTX, and E-POLY-MTX in the presence of untreated controls for 24, 48 and 72 hours. Following this, the culture media was discarded, and 20 µL of CellTiter 96®AQueous reagent solution was pipetted into each well, and the plates were incubated for 4h at 37°C in a humidified 5% CO2 atmosphere. The absorbance at 490 nm was recorded using a 96-well plate reader.

Mice tumor study design and protocols

All animal studies were approved by the Institutional Animal Care and Use Committee (IACUC). Female BALB/c mice (6-8 weeks old) were purchased from Charles River Laboratories. Mice were housed within the Lab Animal Resources at the College of Veterinary Medicine with the relevant guidelines and regulations. Female mice were engrafted with CT-26 colon carcinoma cells on the right flank region by subcutaneously injecting 1×10^6 cells dispersed in 100 µL PBS. 2 days later, 1×10^6 CT-26 colon cells in 100 µL PBS were injected on the left flank. Tumors were measured with digital caliper, and tumor volume was calculated using the formula: volume = (length × width^2) × ½. Treatments were initiated when tumors reached a volume of 20-50 mm^3. For *in vivo* treatments, mice were randomly divided into six groups (n=5) [free MTX±HIFU, E-POLY-

MTX±HIFU, Untreated control ± HIFU]. Each mouse received 4 ISV treatments of MTX or E-POLY-MTXs on day (d)10, d19, d25, and d31 days. HIFU treatment was given immediately post tumor injection.

HIFU (histotripsy) methodology for in vivo tumor treatments

An US-guided HIFU system (Alpinion medical systems, Bothell, WA, USA) was used for tumor exposures. The system consisted of a HIFU transducer with a 1.5 MHz central frequency, 45 mm radius, and 64 mm aperture diameter with a central opening of 40 mm in diameter and an automated motion stage to achieve accurate positioning perpendicular to HIFU beam axis. HIFU treatment parameters used were as follows: 1% duty cycle, 5 Hz pulse repetitive frequency, and 600 W power (equivalent to 233 W acoustic power). Mice anesthetized with 2-3% isoflurane were restrained in custom-built mouse holders, mounted on a 3-D positioning stage, and lowered into a 37ºC degassed water bath for coupling. The primary flank tumor was aligned to HIFU beam axis using real-time US-guidance. An integrated VIFU-2000 software was used to define target boundary and slice distance in x, y, and z directions for automatic rastering. Each focal point (1 × 1 × 10 on the x, y and z axes, respectively) within the raster treatment pattern was heated for 20 seconds, and for the first HIFU treatment, ~80-90% of tumor volume was exposed to HT. Tumors >100 mm^3 were re-treated with HT for up to 4 exposures to maintain immune-rich environment (~30% or 1/3rdof total tumor volume). Following treatment, tumors were harvested and assessed histopathologically by a board-certified pathologist (OADDL).

Treatment methodology for canine soft tissue sarcoma case

For canine sarcoma treatment, treatment condition was similar to mice studies: 1% duty cycle, 5 Hz pulse repetitive frequency, and 600 W power (equivalent to 233 W acoustic power). Two

POLY-DOX ISV was administered (Dose: 0.68 mg DOX, and 1.94 mg DOX for the first treatment and second treatment). Each focal point (1 × 1 × 10 on the x, y and z axes, respectively) was treated for 20 seconds using HT parameters covering ~10-20% of tumor volume for the first and second treatments. US images were obtained to verify hyperechoic lesions in the tumor at the site of treatment focal point.

Statistical analysis

Treatment groups were compared for differences in tumor volumes using Tukey's multiple comparisons or survival statistics using GraphPad Prism 9.2.0 (GraphPad Software Inc, La Jolla, CA, USA). Significance was denoted as $p<0.05$, unless otherwise noted. Cytotoxicity data sets were represented as mean ± standard error of the mean (SEM) unless otherwise indicated (n=6 per group unless otherwise indicated). For analysis of these groups, two-way ANOVA was performed followed by Dunnett's multiple comparison's test. Tumor volumes were represented as mean ± standard error of the mean (SEM) unless otherwise indicated (mice n=5 per group). For analysis, two-way ANOVA was performed followed by Tukey's multiple comparison's test unless otherwise specified. Survival was analyzed by curve comparison via Log-rank (Mantel-Cox) test.

Results

POLY-MTX and E-POLY-MTX induced CT26 cell killing responses compared to POLY and E-POLY

To determine the toxicity of empty, unloaded polymersomes (POLY and E-POLY) without MTX, we tested toxicity via MTS assays. Data showed all unloaded POLY and E-POLY showed cell

viability of >85% at 24h, >94% at 48h, and >92% at 72h (Fig. 17). Thus, POLY had no notable toxicity from 24-72h incubation. Similarly, E-POLY did not show toxicity at similar time points. All POLY or E-POLY derivatives were tested at concentrations that equaled to relative 1.25-10 μM MTX in POLY NPs containing MTX.

To compare toxicity of polymer-derived NPs containing MTX to free MTX, we determined viability differences of free MTX, POLY-MTX, and E-POLY-MTX. Experiments were done in serial dilution (10 μM to 1.25 μM MTX) for 24-72 hours. Results showed free MTX alone (53% viability) was significantly more effective than E-POLY-MTX (70%) at 24h. Free MTX also was significantly better than POLY-MTX (76%) ($p<0.05$) at 24h (Fig. 18). In contrast, increasing the exposure time to 48h and 72 hours nullified these differences. MTX vs E-POLY-MTX vs POLY-MTX were comparable with each other with cell viabilities of 40%, 39% and 37% at 48h, and 20%, 22% and 26% at 72h respectively ($p<0.05$) (Fig. 18).

Combination of free MTX and HIFU potentiated an enhanced anti-tumor effect

To gain knowledge on the potential of MTX and HIFU as a combination therapy, we used the two as a combination regimen against CT26 tumors in a preliminary bilateral model. Results showed E-POLY-MTX significantly reduced tumor burden of treated tumors (orange line, Fig. 19, left graph). E-POLY-MTX similarly showed reduction of untreated secondary tumors compared to untreated controls (orange line, Fig. 19, right graph). Data suggested local and abscopal effects. In contrast, the addition of HT negated effectiveness of E-POLY-MTX in both local and distant sites relative to E-POLY-MTX alone. (Fig. 19, black lines- E-POLY-MTX+HT vs. orange lines E-POLY-MTX alone, both graphs). Thus, E-POLY-MTX+HT demonstrated contrary results to our hypothesis.

To compare free mitoxantrone effectiveness to E-POLY-MTX, tumor volumes were analyzed and compared. Free MTX did not produce a significant tumor regression in the primary tumor (1.74-

fold decrease, Fig. 19, left graph, light green line). In contrast, it did produce a significant tumor reduction at the secondary tumor site (3.8-fold decrease, Fig. 19, right graph, light green line). With the addition of HT, MTX effects were enhanced to give the greatest degree of tumor regression in both primary (~8-fold reduction, Fig. 19, left graph, purple line) and secondary tumors (Fig. 19, right graph, purple line) relative to all given treatments. Thus, a preliminary, novel finding of HT and MTX displaying enhancement was observed.

Free MTX+HIFU and E-POLY-MTX alone increased murine survival rates

To determine the survival of mice, mice were kept post treatment and observed for prolonged drug treatment efficacy. Results showed similar trends to tumor volume data. MTX+HIFU ($p=0.0089$, $n=5$, purple line, Fig 20) significantly enhanced survival to the greatest degree. The only other group that extended survival significantly was E-POLY-MTX alone ($p=0.015$, $n=5$, orange line, Fig. 20). On day 40, the mice that survived (~20%) treatments were MTX+HT, MTX, and E-POLY-MTX. Therefore, survival data supports that the best responding treatment groups in this preliminary study were E-POLY-MTX alone and free MTX+HT.

E-POLY-MTX improves tumor imaging and enhances necrotic area

To visualize echogenicity of tumors during treatments, high-resolution two-dimensional B-mode US images were taken of *in vivo* treatment groups. Results showed E-POLY-MTX displayed notable hyperechoic regions post injection (Fig. 22, C, labeled on left panel). These regions were absent in non-NP groups (Fig. 22, A, B). To demonstrate enhanced echogenicity response during treatment, ultrasound images were also taken during treatment. Our observations showed cavitation bubbles within the tumor. These bubbles were produced from E-POLY-MTX injection (Fig. 22, C, right panel).

To determine differing necrotic profiles of E-POLY-MTX with and without HT, tumors were harvested, fixed and submitted for analysis by Hematoxylin and Eosin (H&E) staining. Reported results showed a preliminary result of HT and E-POLY-MTX monotherapies causing between 30-40% necrosis (n=1 for each group, Fig. 23). In contrast, the combination of HT and E-POLY-MTX as a combination therapy caused enhanced necrosis (65-70%, Fig. 23) relative to monotherapy groups. This value was reported by a board-certified pathologist blinded.

POLY-DOX NPs with HT demonstrated safety in canine patient

To determine safety and efficacy of DOX in a polymeric NP delivery format with HT, POLY-DOX+HT was administered to a canine patient. The canine patient presented with an oral soft tissue sarcoma. RECIST (Response Evaluation Criteria in Solid Tumors) evaluation of patient showed stable disease despite a reduction from 14,638 mm^3 to 11,540 mm^3 in 21 days (Fig. 24). Unfortunately, this canine patient dropped out of this treatment protocol before completion, precluding further treatments and evaluations. RECIST requires a 30% reduction for report of partial response, and in the shortened 21 days' time period, this threshold was not achieved.

Discussion

We hypothesized that putting MTX inside POLY NPs would generate stable MTX NPs. These NPs would hypothetically be less toxic relative to free MTX if drug was maintained within NPs when administered to cells. Contrary to this prediction, POLY-MTX displayed a similar cytotoxicity profile relative to free MTX in MTS assays (Fig. 18). Our observations that empty, unloaded POLY showed minimal toxicity supports the idea that MTX-loaded polymeric NP have toxicity derived from MTX rather than from the NP formulae themselves (Fig. 17). Consistent with this interpretation, our POLY NPs are made of biocompatible materials. Thus, their lack of

baseline toxicity without drug is expected. Based on the similar toxicities, we conclude that the encapsulation of MTX within NPs did not negatively impact MTX efficacy (Fig. 18A vs. C).

The loading of PFP into polymeric NPs containing MTX did not alter their toxicity profiles relative to POLY-MTX that lacked PFP. (1) Basal, unloaded E-POLY showed minimal toxicity similar to unloaded POLY (Fig. 17). (2) E-POLY loaded with MTX cargo displayed a similar toxicity profile relative to POLY-MTX and free MTX (Fig. 18). Thus, echogenic polymersomes loaded with MTX (E-POLY-MTX) showed similar toxicities in CT26 colon carcinoma MTS viability assays.

One reason for this toxicity of MTX-loaded NPs might be endocytosis, transport, and nuclear localization of MTX of MTX-loaded NPs. Polymer-derived NPs are known to be preferentially endocytosed through caveolae-mediated endocytosis[277,278]. Free MTX demonstrated enhanced toxicity at 24h, however, this difference was not observed at 48h and 72h. Therefore, a potential explanation could be that caveloae-mediated endocytosis is a slow mode of entry into the cell[279]. This could explain the disparity seen between free MTX and MTX-NPs at 24h versus not seen at 48h, 72h. This proposed endocytic explanation would also explain why toxicity was observed despite NP drug release not being triggered prior to cytotoxicity assay (i.e., via detergent lysis or HT exposure). The cells were simply incubated with intact NPs containing MTX or free MTX and compared following incubation. The endocytic process would then give intracellular concentrations of MTX.

Following these *in vitro* tests, we included HT in a preliminary *in vivo* study to determine the efficacy of combination of MTX+HT. The combination of free MTX and HT produced potent tumor responses *in vivo*. **(**1) Primary tumor volumes were decreased significantly in comparison to untreated controls (Fig. 19). (2) Secondary tumors showed a potent response to free MTX-HT treatments (Fig. 20). **(**3) Free MTX+HT also extended mouse survival (p=0.0089) (Fig. 20). There

have been *in vitro* investigations of the combination of MTX and HIFU to determine heat response differences[280]. They showed MTX increased the amount of apoptotic cells with HIFU in its thermal parameter in the referenced study[280]. Our novel combination of MTX+HT, however, extended to show *in vivo* application and further shows the enhanced effectiveness of mechanical-based HT (Fig. 19, 20, 21). Thus, the application of MTX with thermal and mechanical HIFU parameters have been established and broadened to include *in vivo* application.

Echogenic polymer NP delivery of MTX, however, produced conflicting results when used in combination with HT *in vivo*. Polymeric delivery of MTX enhanced effectiveness relative to free MTX in primary tumors (Fig. 19). In support of HT enhancing MTX effectiveness when used as E-POLY-MTX+HT relative to E-POLY-MTX alone, we observed a few key findings. (1) E-POLY-MTX+HT produced enhanced necrosis relative to monotherapy groups (Fig. 22). (2) confirmation of echogenicity of NPs by ultrasound (Fig. 21). In contrast, we also observed results indicating a reversal of effectiveness of E-POLY-MTX from inclusion of HT. (1) Primary tumor growth rates of E-POLY-MTX+HT were increased relative to E-POLY-MTX alone (Fig. 19). (2) Secondary E-POLY-MTX+HT tumors showed no regression vs. E-POLY-MTX showing significant tumor regression compared to untreated control (Fig. 20). (3) Survival rates of E-POLY-MTX alone were not enhanced with HT treatments (Fig. 21). Recently, there have been reports of the synthesis of a similar ultrasound-targeted MTX-NP. However, in contrast to our approach, they used a liposomal delivery system with PLGA NPs within to create ultrasound-sensitivity[281]. *Xin et al*. tested this formulation as an intravenous delivery system divergent to our current intratumoral approach. Therefore, NP delivery of MTX is a currently applicable goal. Our preliminary experimentation, however, failed to show significant enhancement of NP effectiveness when adding HT in an intratumoral approach.

Our E-POLY-NPs showed *in vivo* tolerance and safety. (1) Intratumoral injections of E-POLY-MTX were well-tolerated. (2) Multiple injections of E-POLY-MTX showed no negative or allergic reactions in mice. (3) Multiple injections were well tolerated in a canine patient.

Canine tumors offer a similar homology with human cancers[80]. Beyond murine cancer models, one of the best cancer models that mimics the spontaneity and pathological signs of human cancers is canine cancer[80,272]. Preliminary results showed safety and tolerance to lower dose DOX in form of polymeric NP loaded with DOX cargo (POLY-DOX). Additionally, reduction of tumor was observed in the first 21 days. This reduction, however, did not meet the RECIST 30% reduction threshold to be reported as partial response. We hoped for more treatments to determine effects of treatments over a full treatment regimen, however, our patient dropped out. We anticipate additional *in vivo* studies to optimize co-treatment efficacy of polymeric NPs and HT. Our lab has had recent success in treating canine sarcomas with liposomal-DOX+HT. Others have also showed DOX is more effective than surgery in hemangiosarcoma[282], but there are inherent cardiotoxicity problems with DOX. Thus, a polymeric NP that retains drug cargo until HT is administered is highly applicable.

While much of the presented data investigates novelty of NP or combination of MTX+HT, we do understand that some data is preliminary in finding to-date. Further studies are required to determine necessary information: 1) Optimization of MTX, MTX-NP, and HT treatments are required to fully investigate efficacy of combination treatment. 2) Differences of drug delivery potential of free MTX relative to E-POLY-MTX can be compared *in vivo* in an intravenous administration plan. The current study used an intratumoral delivery, therefore, the only differences that could have been seen would have been from i) NPs retained within the tumor versus free drug, or ii) PFP-enhancement of HT treatment relative to free drug. A follow-up study could utilize the delivery aspect of NPs to determine differences of toxicity and tumor reduction from free drug to

NP-MTX. 3) Inclusion of non-echogenic polymersomes (POLY-MTX) would be an ideal NP control in a follow-up study. 4) A larger follow-up study with more than five mice per group would ideally help strengthen previous results. This would be especially valuable due to our conflicting *in vivo* results. 5) Mechanistic studies investigating the role of HT with MTX could also help explain current data. Markers such as calreticulin (CRT), binding immunoglobulin protein (BiP), and eukaryotic translation initiation factor 2A (eIF2α) are ER-stress indicators. These can be used to help determine the amount of immunogenic cell death (ICD) that is induced from treatments. These have similarly been monitored in combination protocols using MTX with radiation instead of HIFU previously[283].

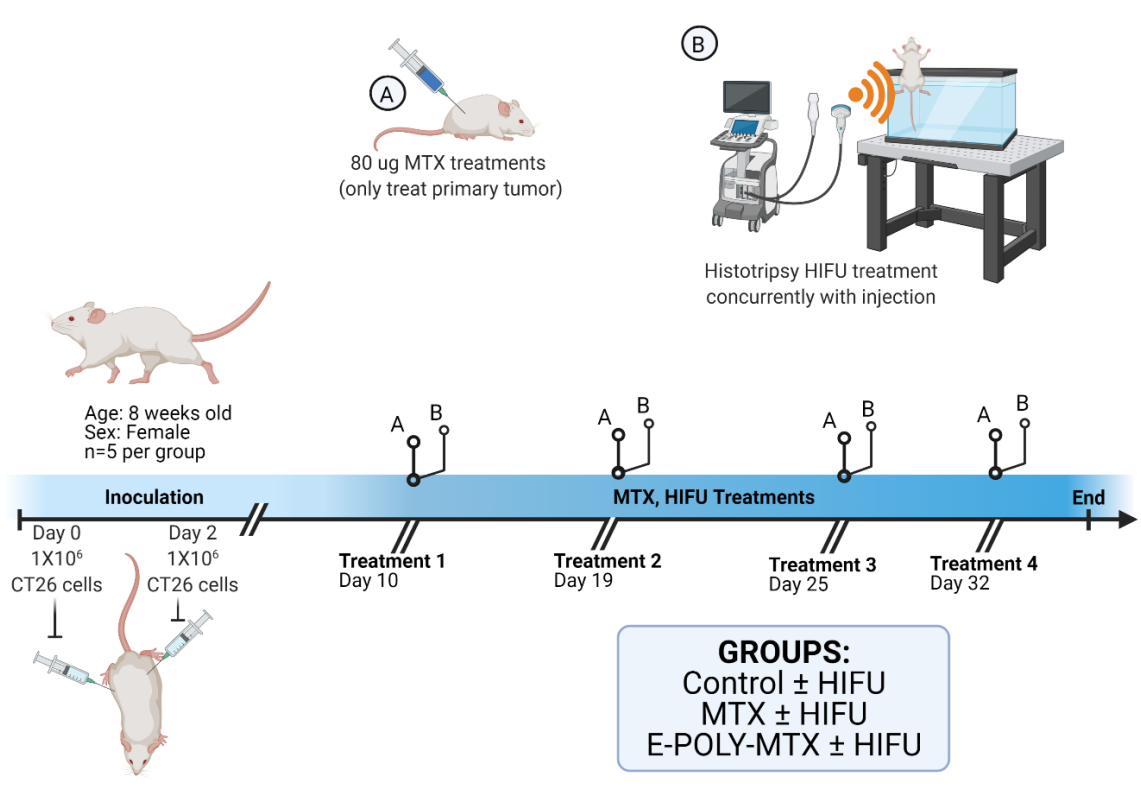

Figure 16. Graphical abstract of *in vivo* treatment plan

Female, 8 weeks old, BALB/c mice were inoculated with $1x10^6$ CT-26 tumor cells in their right flank on day 0 and $1x10^6$ left flank on day 2. Right flank tumors were treated on days 10, 19, 25 and 32 with 80 µg MTX intratumoral injection (A) followed by histotripsy (HT) treatment via HIFU (B). Mice tumor volume was measured daily and were sacrificed when tumor volumes reached $\geqslant$ 2000 mm^3. Groups included untreated control, HT, free MTX, MTX+HT, E-POLY-MTX, E-POLY-MTX+HT.

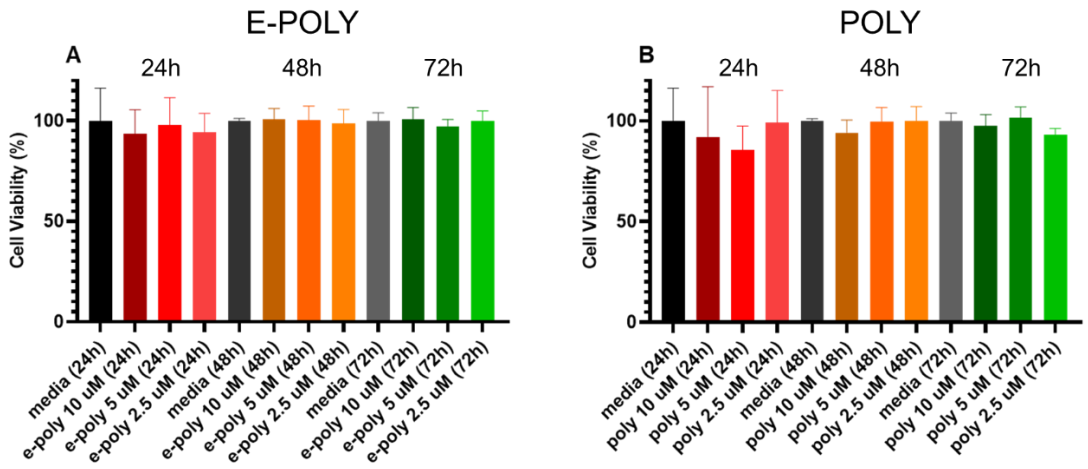

Figure 17. POLY and E-POLY demonstrate no notable toxicity as unloaded NPs *in vitro*

To determine the safety of basal, unloaded polymeric NPs, POLY and E-POLY without drug payload were tested for toxicity. CT26 murine colon carcinoma cells plated in 96 well plates were treated with polymer concentrations that corresponded to 10, 5, 2.5, 1.25 μM MTX in MTX-loaded POLY and E-POLY for 24, 48, or 72h. **(A)** Mean cell viability were averaged for all groups (n=6, well replicates of a single NP preparation and a single passage of cells). E-POLY concentrations were normalized for each group corresponding to loaded NPs that contained 10, 5, 2.5, 1.25 μM MTX. **(B)** Mean cell viability in media control (n=6, well replicates of a single NP preparation). POLY concentrations were normalized for each group corresponding to loaded NPs that contained 10, 5, 2.5, 1.25 μM MTX. Data presented as mean ± SD.

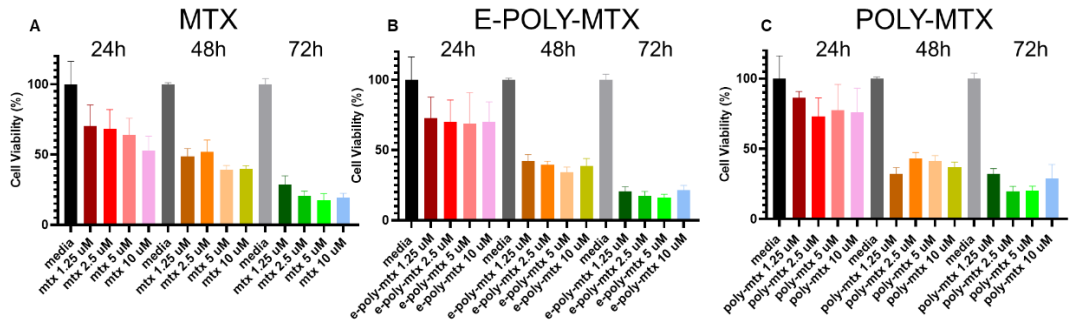

Significant comparisons	10 uM	5 uM	2.5 uM	1.25 uM
MTX vs. POLY-MTX				
24 h	***	*	ns	**
48 h	ns	ns	*	****
72 h	ns	ns	ns	ns
MTX vs. E-POLY-MTX				
24 h	**	ns	ns	ns
48 h	ns	ns	**	*
72 h	ns	ns	*	*

Figure 18. Efficacy of POLY loaded with MTX (POLY-MTX and E-POLY-MTX) were comparable with free MTX after 24 hours *in vitro*

To measure cytotoxicity profiles of NPs containing MTX cargo to free MTX, MTS assays of CT26 murine colon carcinoma cells were treated with serial dilutions of MTX (10, 5, 2.5, 1.25 µM) for 24, 48, and 72h. **(A)** Mean cell viability were averaged for all. MTX concentrations were calibrated to 10, 5, 2.5, 1.25 µM MTX. **(B)** Mean cell viability were averaged for all groups. E-POLY-MTX concentrations were calibrated to E-POLY-MTX containing 10, 5, 2.5, 1.25 µM MTX. **(C)** Mean cell viability were averaged for all groups. POLY-MTX concentrations were calibrated to POLY-MTX containing 10, 5, 2.5, 1.25 µM MTX. Data are presented as mean ± SD. Statistical comparisons were performed with two-way ANOVA with Tukey's multiple comparisons test. (n=6 for each MTS, well replicates of a drug suspension and a single passage of cells).

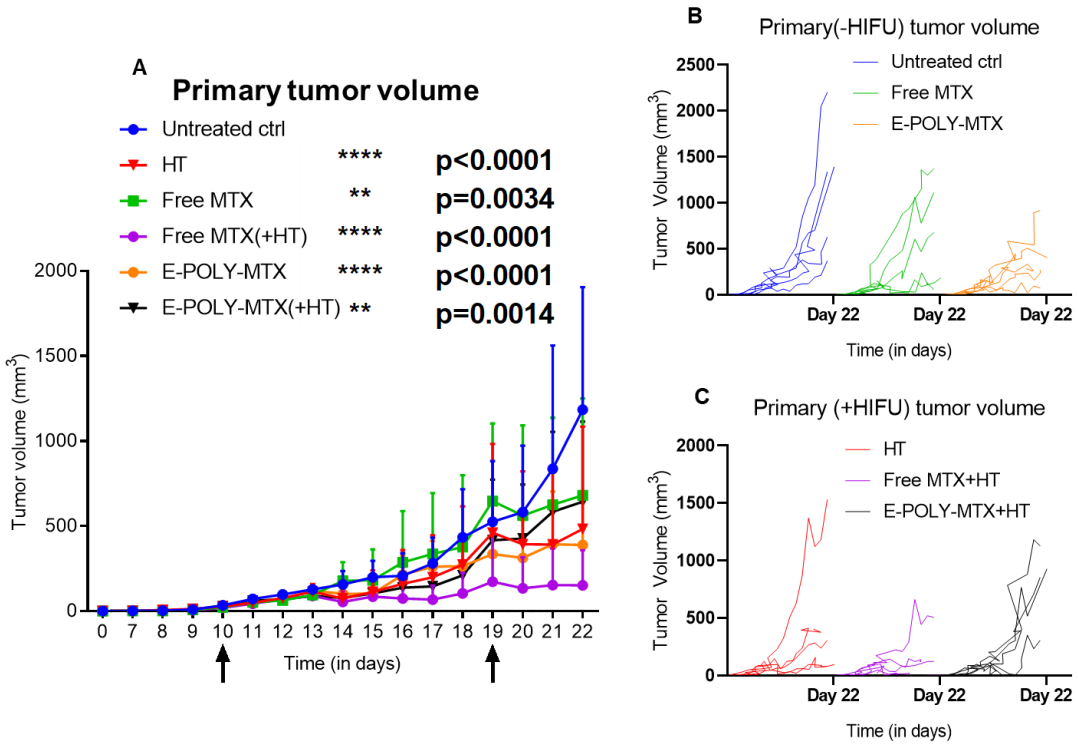

Figure 19. MTX groups were effective at producing primary tumor regression compared to untreated control

To compare the efficacy of MTX-treatment regimens, mice were inoculated (day 0, primary; day 2, secondary) and treated on days 10, 19. Tumor volumes were measured daily. **(A)** Average primary tumor volumes of MTX-treated mice over 22 days (n=5) were presented and analyzed on day 22. **(B)** Individual groups of untreated control, MTX alone, E-POLY-MTX presented as individual mice tumor values. **(C)** HT was added in groups HT, MTX+HT, E-POLY-MTX+HT and individual mice primary tumor volumes presented instead of averages. Averages (A) were presented as mean ± SD. Statistical comparisons were performed with two-way ANOVA in comparison to untreated control.

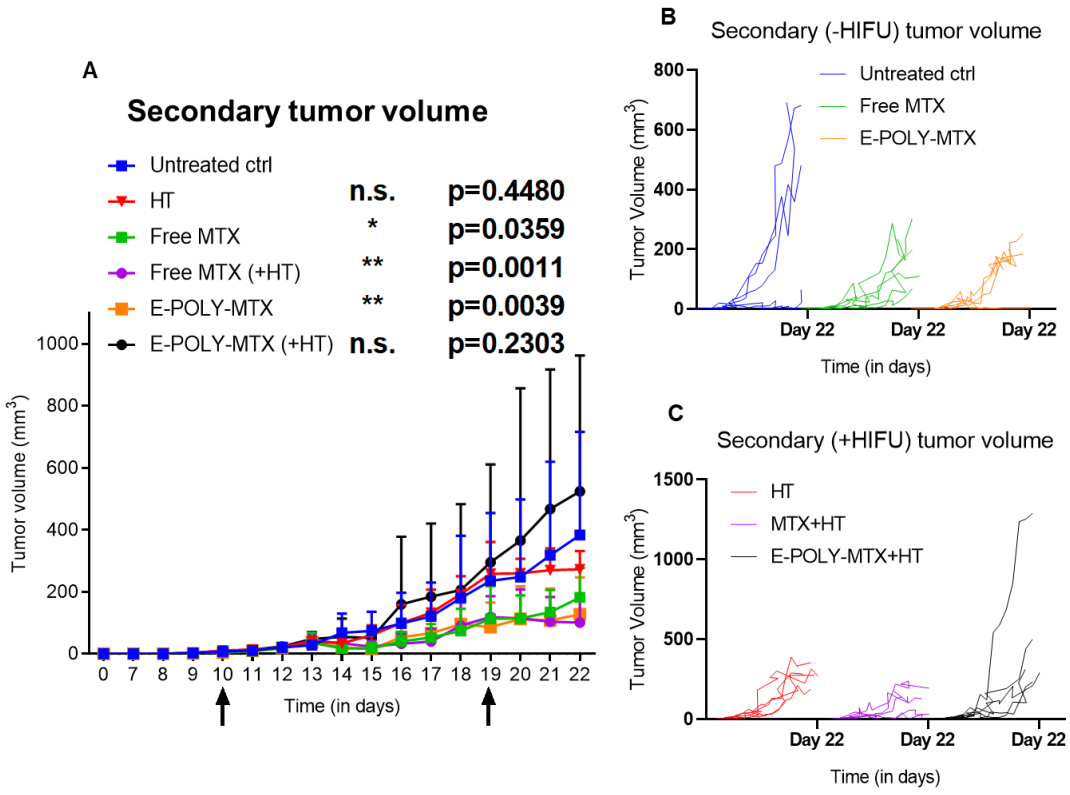

Figure 20. HT enhances free MTX, whereas E-POLY-MTX elicits better effects without HT

To determine the abscopal effects of MTX and MTX-NPs ±HT, mice were similarly inoculated and measured for secondary tumor growth as was done for primary tumor growth in Fig. 19. Arrows indicate treatment days. **(A)** represents average secondary tumor volumes of mice over 22 days (n=5). **(B)** shows individual tumor growth of untreated control, MTX alone, E-POLY-MTX presented as individual mice tumor values. **(C)** similarly shows individual mouse secondary tumor values over 22 days that used HT in treatment plan (HT, MTX+HT, E-POLY-MTX+HT). Averages (A) were presented as mean ± SD. Statistical comparisons were performed with two-way ANOVA relative to untreated control.

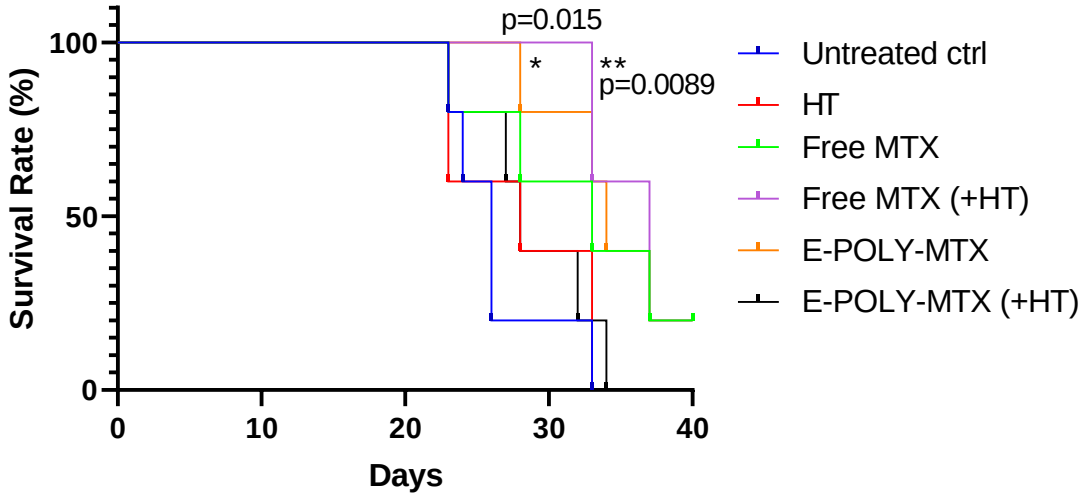

Figure 21. Free MTX enhanced survival in combination with HT relative to untreated control

To compare survival rates, female BALB/c mice with bilateral CT26 tumors were treated on days 10, 19, 25, 32 with MTX or E-POLY-MTX (±HT) based on tumor size (≤100 mm^3). Survival was defined when mice reached day 40 post inoculation of when tumors reached 2000 mm^3. Data was presented as % survival rate (n=5). Survival curve comparison with log-rank (Mantel-Cox) test was performed to determine significance.

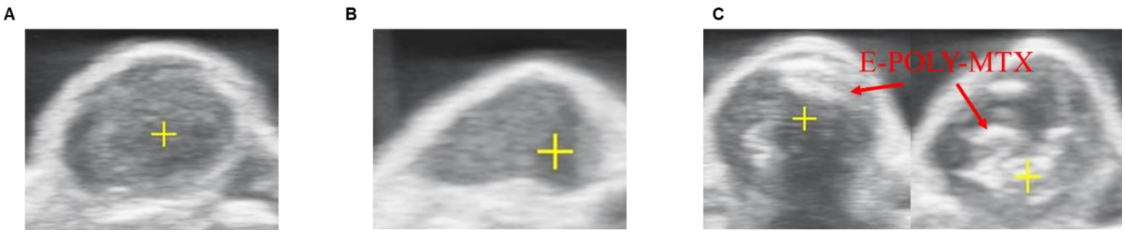

Figure 22. Ultrasound imaging confirms echogenicity of E-POLY-MTX during HT of CT26 tumors

To visualize echogenicity of NPs, HT treatments groups were imaged by ultrasound. Ultrasound images of groups: **(A)** HT, **(B)** MTX+HT, **(C)** E-POLY-MTX+HT are provided. Hyperechoic regions (white) are labeled in (C). Left panel of (C) is before HT treatment, whereas right panel during treatment. No hyperechoic regions were visualized in (A) and (B).

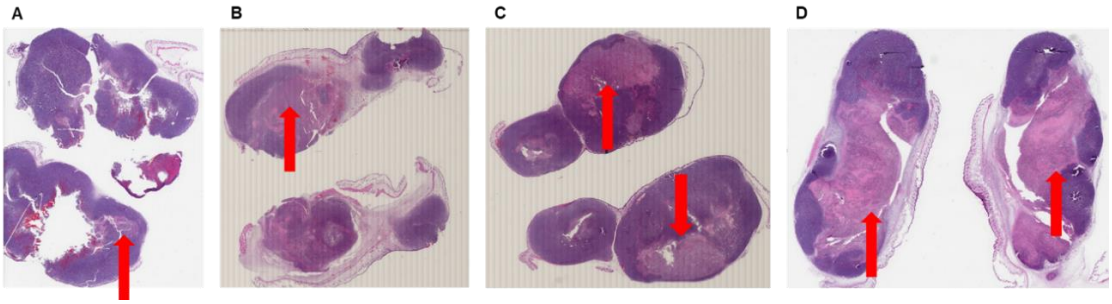

Figure 23. HT+E-POLY showed higher necrotic areas compared to monotherapy and untreated groups

To determine levels of necrosis from combination echogenic polymersomes containing mitoxantrone (E-POLY-MTX) and histotripsy (HT), mouse tumors were harvested, fixed and analyzed for necrosis by hematoxylin and eosin (H&E) staining. **(A)** Untreated control (n=1) showed 5-10% necrosis, **(B)** HT (n=1) alone treatment induced 35-40% necrosis, **(C)** E-POLY-MTX (n=1) showed 30-40% necrosis, **(D)** E-POLY-MTX+HT (n=1) showed 65-70% necrosis. Arrows indicate regions of necrosis read by a board-certified pathologist.

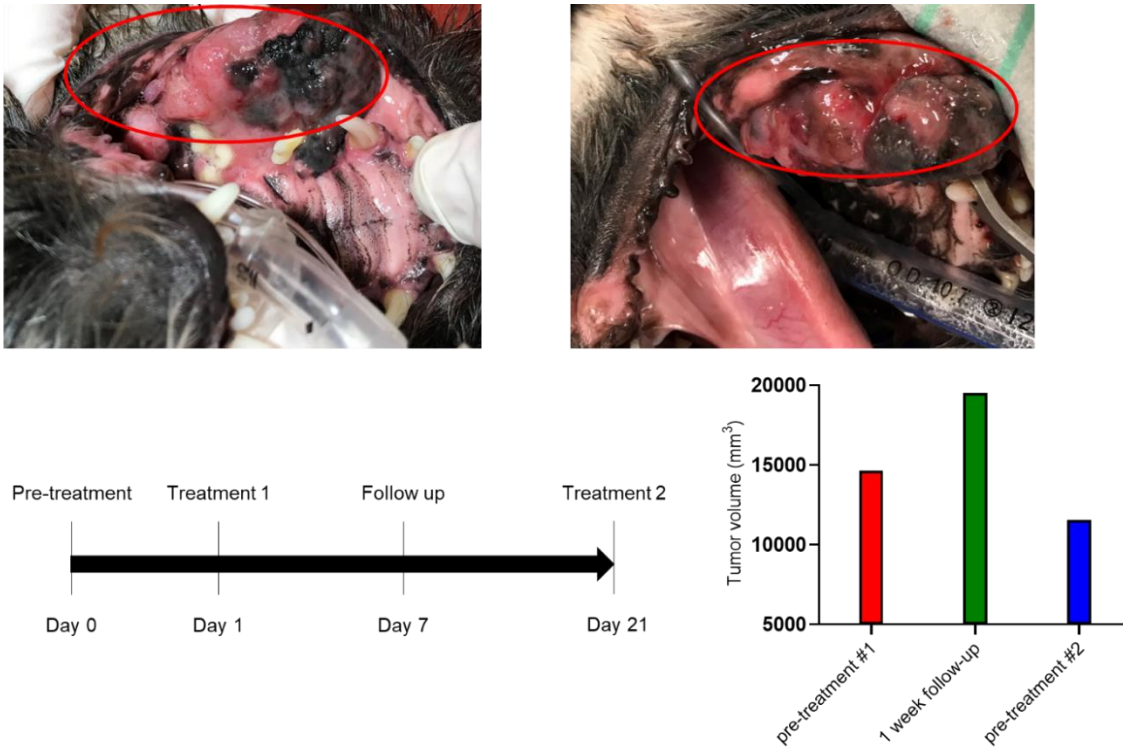

Figure 24. POLY loaded with DOX demonstrated safety and initial reduction in a canine patient

To determine safety and efficacy in canines, a canine patient presenting with soft tissue sarcoma was treated with POLY containing DOX. Two treatments with POLY containing 0.68 mg and 1.94 mg DOX (PD-POLY-DOX) were administered.

CHAPTER IV

CXCR4 BLOCKADE SENSITIZES MURINE AND HUMAN CANCER CELLS TO ANTHRACENEDIONE-BASED CHEMOTHERAPIES

Abstract

Activation of SDF1-α(CXCL12)/CXCR4 pathway is associated with cancer metastasis, drug resistance, and overall poor prognostic outcomes in patients. The objective of this study was to understand the role of CXCR4 signaling inhibition with small molecules in improving anthracenedione (doxorubicin, DOX, mitoxantrone, MTX, and pixantrone, PIX) cytotoxicity against cancer cells. We selected commercially available AMD-3100 and a recently reported antagonist (TJH06) for *in vitro* cytotoxicity assessment with chemotherapies. To ease clinical translation, low-temperature sensitive liposome-based nanoparticle (LTSL-NP) delivery system was developed by covalently linking the thiol pendant-armed antagonist to LTSL. Results showed that CXCR4 antagonism improved chemotherapy efficacy, and a successful synthesis of CXCR4-LTSL for potential targeting of tumor cells. Studies are currently underway to assess the CXCR4-LTSL efficacy in an *in vivo* tumor model.

Introduction

Multi-drug resistance (MDR) is a major challenge in treating solid tumors[284]. It is characterized by resistance to many compounds that are structurally different and target different cellular pathways[285]. MDR can be acquired through genetic changes (e.g., *mdr-1* gene), hypoxia, nitric oxide imbalances[285-287]. Alternatively, cells can simply be more resistant to a certain chemotherapy (i.e., primary resistance)[21] through many intracellular factors such as the CXCR4/CXCL12 (SDF-1α) axis, CCL2, VEGF, CXCL8, angiogenin etc.[288]. In particular, CXCR4 signaling is enhanced by hypoxia and HIF-1α[289,290], resulting in tumorigenesis and metastasis. CXCR4 overexpression is known to occur in over 20 human tumor types including breast, ovarian, prostate, esophageal, melanoma, lung, and neuroblastoma[291], and correlates with tumor aggressiveness and poor prognosis[292]. CXCR4 expressing tumor cells migrate to distant sites like lung, liver, and bone marrow that constitutively express high levels of CXCL12, leading to metastatic spread and poor survival[293,294]. While the baseline expression of CXCR4 is variable within tumor types, the treatment with various anti-cancer therapies (DOX) can lead to the upregulation of CXCR4[295]. The expression of CXCR4, whether induced by treatment or intrinsically expressed, leads to the dysregulation of various pathways, (e.g., the VEGF-mediated promotion of angiogenesis through Akt phosphorylation via the PI3K/Akt pathway of MDA-MB-231 breast cancer). Therefore, CXCR4 antagonism can be a logical addition to current cancer treatment regimens to improve outcomes.

Targeting of CXC receptor 4 (CXCR4)/CXCL12) axis has been shown to sensitize for tumor cells to therapies[296,297], reduce or prevent metastasis[298], and enhance tumor imaging[299]. To understand the potential therapeutic benefits of commercial CXCR4 antagonist AMD-3100 (Plerixafor) and synthesized CXCR4 antagonists, SJA05 and TJH06, we utilized them in combination with chemotherapies doxorubicin (DOX), mitoxantrone (MTX), and pixantrone (PIX). To maximize the potential of CXCR4 antagonism in therapy, we chose to include the topologically-constrained[300-

[303] copper-tetraazamacrocycle complexes as alternatives to AMD-3100 since they have been shown to have enhanced CXCR4 binding and higher residence time[304-307]. To address this, *Hubin et al.* reported copper-tetraazamacrocycle CXCR4 antagonist complexes as alternatives to AMD-3100 for enhanced CXCR4 binding and tumor residence time[304-307]. Results showed enhanced therapeutic efficacy against tumor cell lines in a dose-dependent manner. Herein, we first utilized CXCR4 antagonists in combination with DOX, MTX, PIX to investigate potential synergisms of CXCR4 antagonism and reverse MDR[300-303]. Next, we developed covalently linked tetraazamacrocycle and electrostatically attached CXCR4 antagnosits decorated LTSL co-loaded with anticancer agents. We propose that our approaches can block MDR pathways, improve the net-chemotherapy delivery to cancer cells, thereby overcoming the drug efflux mechanisms and chemotherapy barriers such as systemic toxicity[308], low intratumoral drug accumulation[309], and development of MDR[310]. Further, its combination with thermal therapies using LTSL will maximize efficacy[311,312], and improve enhanced permeability and retention (EPR) effects[57].

Materials & Methods

Cellular Experiments

Cell Lines and cell culture

Cells of human (astrocytoma) glioblastoma U87 (U87.CD4 and U87.CD4.CXCR4) were received from the NIH AIDS program and cultured in DMEM medium supplemented with 15% FBS, 1ug/mL puromycin (CXCR4+ only), 300ug/mL G418, glutamine and pen/strep. Cells of murine breast cancer (4T1) were received from ATCC CRL-2539 and cultured in RPMI media supplemented with 10% FBS. Cells of murine skin cancer (B16F10) were received from ATCC CRL-6475 and cultured in DMEM media supplemented with 10% FBS. Cells of murine ovarian cancer (ID8) were received from ATCC and cultured in RPMI media supplemented with 10% FBS. All cells were incubated in a 5% CO_2 environment, unless otherwise mentioned.

Expression of CXCR4 in U87.CD4.CXCR4, & U87.CD4cells

Baseline expression of CXCR4 of received glioblastoma cell lines was quantified via flow cytometry. U87.CD4.CXCR4 was used a positive-CXCR4 cell line, while U87.CD4 was not transfected for CXCR4 expression. Antibodies against CXCR4 (PE-conjugated, rat anti-mouse CXCR4 IgG_{2B}); were purchased from R&D. For staining, cells were harvested, washed, and adjusted to a cell suspension of 1 x 10^6 cells/mL in ice-cold PBS, 2% FBS. After washing 1X and resuspending in 100 µL staining buffer containing primary antibodies, 1 µL of conjugated primary antibody (PE-anti-mouse CXCR4) was added in 100 µL staining buffer per sample. Cells were then incubated for 1h in the dark, on ice, then washed 3X by centrifugation and resuspended in 1 mL of ice-cold PBS, 2% FBS. After the third wash, resuspension of cells in 200 µL 1% PFA (paraformaldehyde) and incubation for 15 min in dark, on ice was performed. Following two washings, cells were resuspended in 200 µL staining buffer until flow cytometer readings.

CXCR4 inhibition by AMD-3100, TJH06

For flow cytometry and cytotoxicity assays, the antagonistic effects of both AMD-3100 and TJH06, [Cu(**2**)], were tested at concentrations of 50 µM and 100 µM in cell lines, U87.CD4.CXCR4 and U87.CD4.

In vitro cytotoxicity of combinatorial regimen anthracenedione (DOX, MTX, PIX) and CXCR4 antagonist (AMD-3100, TJH06)

Cytotoxicity of each chemotherapy as a monotherapy (10 µM) and in combination with both CXCR4 antagonists (AMD-3100 and TJH06, [Cu(**2**)], See *Fig. 27-28*). at concentrations 50, 100 µM were evaluated using an in-vitro homogeneous, colorimetric method for determining the number of viable cells using (3-(4,5-Dimethylthiazol-2-yl)-2,5-Diphenyltetrazolium Bromide) (MTT). This assay was used to determine any cytotoxic effects of the corresponding drugs of DOX,

MTX or PIX and the addition of CXCR4 inhibition. Briefly, ~5-20 x 10^3 cells were suspended in 100 µL of DMEM supplemented with 10% FBS, 1% penicillin-streptomycin for B16F10 cell model or RPMI supplemented with 10% FBS, 1% penicillin-streptomycin for 4T1 cell model and seeded in 96-well plates and incubated for 24 hours at 37 °C in a 5% CO2 atmosphere. Later, the adhered cells were treated with 10 µM of DOX, MTX or PIX (+/- 50, 100 µM CXCR4 antagonists) with untreated control for 24 hours. Following this, the culture media was discarded, cells were washed with PBS and fresh media was given. Then, 10 µL of MTT was pipetted into each well and incubated for 4 hours at 37 °C in a 5% CO_2 atmosphere. The measured absorbance at 540 nm was used to calculate % cell viability.

Chemical Synthesis

Synthesis of ligands bis-cross bridged- cyclam, cyclen and their corresponding metal complexes, SJA05and TJH00 respectively

Bis-cross bridged cyclam and its copper complex (SJA05) was synthesized and characterized as published previously[313]. Briefly, the synthetic preparation involved the addition of glyoxal, and iodomethane, then the subsequent borohydride reduction and purifications listed in Scheme 1, below.

Bis-cross bridged cyclen and its corresponding copper complex (TJH06) was synthesized from the published linked tetraazamacrocycle-glyoxal condensate bromide salts[314] following the same synthetic steps as for the published cyclam analogue[315]. Yields and analytical data are presented individually below for the two synthetic steps following Handel's linked precursors.

Methylated Linked Salt: 30 equivalents of CH_3I were used. The reaction was stoppered and stirred for 14 days. The product was a white solid. Yield = 89%. Electrospray mass spectra in 50% methanol–50% H_2O (Agilent 6490 EMS): m/z 647 [M-3I]+. Elemental analysis calculated for

$C_{30}H_{50}N_8I_3Br$: C 36.64, H 5.13, N 11.40; Found: C 36.42, H 5.16, N 11.63. $^{13}C^{316}$ NMR (75 MHz, DMSO) 40.91 (N-α-CH_2), 41.33 (N-α-CH_2), 45.04 (N-α-CH_2), 45.18 (N-α-CH_2), 53.73 (N-α-CH_2), 57.03 (N-α-CH_3), 57.88 (N-α-CH_2), 59.11 (N-α-CH_2), 59.25 (N-α-CH_2), 63.07 (N-α-CH_2), 75.64 (C_{aminal}), 75.72 (C_{aminal}), 127.07 ($C_{aromatic}$), 129.16($C_{aromatic}$), 133.49 ($C_{aromatic}$), 134.57($C_{aromatic}$).

*meta-linked Cross-bridged bis-cyclen (**2**)*: 30 equivalents of $NaBH_4$ were used. The reaction was stirred under N_2 for 5 days. The product was a yellow oil. Yield = 86%. MS (ES) *m/z* 527 [MH]+. $^{13}C^{316}$ NMR (75 MHz, C_6D_6) 44.39 (N-α-CH_3), 57.03 (N-α-CH_2), 57.34 (N-α-CH_2), 57.99 (N-α-CH_2), 58.86 (N-α-CH_2), 60.53 (N-α-CH_2), 61.57 (N-α-CH_2), 128.27 ($C_{aromatic}$), 129.79 ($C_{aromatic}$), 140.68 ($C_{aromatic}$), 140.75 ($C_{aromatic}$). The ligand HCl salt was made by bubbling HCl gas through an ethanol solution, filtering the yellow solid that formed and washing with ethanol and ether before drying under vacuum. Elemental analysis calculated for $C_{30}H_{54}N_8 \cdot 8HCl \cdot 4H_2O$: C 40.46, H 7.92, N 12.58; Found: C 40.81, H 8.22, N 12.44.

$[Cu_2(\mathbf{2})(OAc)_{1.3}](PF_6)_{2.7}$

In an inert atmosphere glove box, 0.250g (0.0005 mol) of **2** was added to 20 mL of anhydrous CH_3CN in a 50 mL Erlenmeyer flask. 0.182g (0.001 mol) of anhydrous $Cu(OAc)_2$ was added to this solution, which was then stirred on a stir/heating plate at 50-60°C using a small glass funnel as a condenser for a 24-hour period. The solution immediately turned dark blue. After this period, the flask was removed from the glove box and a small amount of brown precipitate was filtered off with a fine grade filter frit. The dark blue filtrate was evaporated to dryness by rotary evaporation. The resulting blue oil was dried on a vacuum line. The dry oil was dissolved in a minimal amount of CH_3OH. 0.815 g of NH_4PF_6 (0.005 mol) was added to a separate beaker containing 5 mL of CH_3OH. This NH_4PF_6 solution was then slowly added to the metal solution, which was allowed to stir for 5 minutes. The solution was placed in the freezer overnight to complete the precipitation. The blue powder product was collected on a filter frit, and the precipitate was rinsed with 5 mL of

cold CH_3OH and 5 mL of ether. Yield: 0.156 g, 28%. Electrospray mass spectra in 50% methanol–50% H_2O (Agilent 6490 EMS): *m/z* 386 $[Cu_2L(OAc)_2^{2+}]$. Elemental Analysis calculated for $[Cu_2(C_{30}H_{54}N_8)(C_2H_3O_2)_{1.3}](PF_6)_{2.7}$: C 34.90, H 5.20, N 9.99; Found: C 35.10, H 5.39, N 9.94.

Synthesis of thioacetyl-methyl-cyclam ligand and copper complex

IPTA, made from iodo-chloro replacement of 3-chloropropyl thioacetate, was used in 1.5 equivalents to one equivalent of Me1H1Bcyclam ratio to synthesize a thioacetyl-methyl-cross bridged cyclam ligand. In summary, 1.83 g (0.0075 mol) was added to 1.32 g (0.0050 mol) of H_1Me_1-cb-cyclam (provided by Dr. Hubin) in 13 mL DMF in the presence of 2 equivalents (1.52 g) K_2CO_3. The reaction was left to stir 5 days. The reaction was worked up by addition of 100 mL water, extraction with dichloromethane, washing with saturated sodium chloride, drying organic layer with sodium sulfate, and evaporating to oily product. The product was 0.89g. Yield- 50%.

The copper complex was synthesized by co-mixing equivalent molar concentrations of ligand and $CuCl_2$ in 5-10 mL anhydrous methanol in an inert N_2 glovebox. Metal complex solution was left stirring for 1-7 days in an inert atmosphere. The resultant blue solution was filtered, and minimal solid residue discarded. Precipitation via ammonium hexafluorophosphate ion exchange was in 5 molar excess was followed by adding ammonium hexafluorophosphate directly to the filtrate and placing in a freezer to maximize precipitation.

Electrospray mass spectra in 50% methanol–50% H_2O (Agilent 6490 EMS): m/z = 357 ($C_{18}H_{37}N_4OS+$); m/z = 454 $[Cu(C_{18}H_{36}N_4OS)Cl]$; m/z = 436 $[Cu(C_{18}H_{36}N_4OS)H_2O]$. Elemental analysis for $[Cu(C_{18}H_{36}N_4OS)Cl]PF_6 \cdot 5H_2O$: Calculated: C, 32.14; H, 6.59; N, 8.33. Found: C, 31.40; H, 6.09; N, 8.63.

Syntheses of thiol-methyl-cyclam and cyclen ligands and their copper complexes

IPTA was similarly synthesized from 3-chloropropyl thioacetate to previous section. Tetracyclam and tetracyclen was synthesized via previously published protocols[314]. Tetracycles were then added with IPTA in a 2:1 mol ratio in minimal acetonitrile. The reaction was left stirring for 7 days. The reaction mixture was worked up via filtration of the solid product followed by washing with additional acetonitrile and ether, then vacuum drying. Yield- 40-50%.

Thioacetyl-tetracycles were then methylated via iodomethane in as 10:1 mol ratio in acetonitrile. The reaction mixture was left stirring for 21 days. Reaction mixture was worked up via filtration of the solid product followed by washing with additional acetonitrile and ether, then vacuum drying. Yield-55-65%.

Thioacetyl-methyl-tetracycles were reduced via borohydride reductions. Excess molar equivalences (15:1) were added in 80 mL of solvent per gram of reactant in 95% ethanol/5% water. The reaction was stirred at RT for 7 days under nitrogen. The reaction mixture was worked up by addition of HCl. Then, removal of solvent, dissolving in 30% KOH, and extracting product into chloroform, drying over sodium sulfate, filtration, and solvent removal to give the final product. Yield- 90-95%.

The copper complex was synthesized by co-mixing equivalent molar concentrations of ligand and $CuCl_2$ or $Cu(OAc)_2$ in 5-10 mL anhydrous methanol in an inert N_2 glovebox. Metal complex solution was left stirring for 1-7 days in an inert atmosphere. The resultant blue solution was filtered and minimal solid residue discarded. Precipitation via ammonium hexafluorophosphate ion exchange was in 5 molar excess was followed after by adding ammonium hexafluorophosphate directly to the filtrate and placing in a freezer to maximize precipitation.

($C_{17}H_{31}IN_4OS$)·0.5H_2O: C, 42.95; H, 6.78; N, 11.78. Found: C, 42.61; H, 6.66; N, 11.74; thioacetyl-methyl-tetracyclam- m/z = 236 ($C_{18}H_{34}IN_4OS2+$), 353 ($C_{18}H_{34}N_4OS+$), 481 ($C_{18}H_{34}IN_4OS+$), elemental analysis- calculated ($C_{18}H_{34}I_2N_4OS$)·2H_2O: C, 33.55; H, 5.94; N, 8.69. Found: C, 33.66; H, 5.77; N, 8.55; thiol-methyl-cb-cylam- m/z = 315 ($C_{16}H_{35}N_4S+$), elemental analysis- calculated (C16H34N4S . 0.6$CHCl_3$. 1.3H2O): C, 48.68; H, 9.15; N, 13.68. Found: C, 48.72; H, 9.05; N, 13.32; copper-thiol-methyl-cb-cyclam- m/z = 376 (CuL+), elemental analysis- calculated [$CuC_{16}H_{34}N_4S(PF_6)_2$] ·0.8$H_2O$: C, 27.44; H, 5.41; N, 8.00. Found: C, 27.68; H, 5.32; N, 7.70.

Cyclen compounds- thioacetyl-tetracyclen- m/z = 311 ($C_{15}H_{27}IN_4OS$), elemental analysis- calculated ($C_{15}H_{27}IN_4OS$)·0.2H_2O: C, 40.76; H, 6.25; N, 12.68. Found: C, 40.65; H, 6.31; N, 12.58; thioacetyl-methyl-tetracyclen- m/z = 453 (C16H30IN4OS+), elemental analysis- calculated ($C_{16}H_{30}I_2N_4OS$)·0.7H_2O: C, 32.41; H, 5.34; N, 9.45. Found: C, 32.44; H, 5.17; N, 9.29; thiol-methyl-cb-cylen- m/z = 286 (C14H31N4S+), elemental analysis- calculated ($C_{14}H_{30}N_4S$)·0.95$CHCl_3$: C, 43.89; H, 7.60; N, 13.60. Found: C, 43.78; H, 7.85; N, 13.36; copper-thiol-methyl-cb-cyclen- m/z = 348 (CuC14H30N4S+), elemental analysis- calculated [$CuC_{14}H_{30}N_4S$ ($PF_6)_2$]: C, 26.28; H, 4.73; N, 8.75. Found: C, 26.03; H, 4.40; N, 8.64.

Model maleimide crosslinking reaction

Thiol-methyl-cb-cyclam (0.165 g, 1eq) was mixed with phenyl maleimide (0.0906 g, 1 eq) in minimal chloroform and methanol with 0.15 g potassium carbonate. Reaction was left stirring for 10 days. Work up was filtration of carbonate followed by evaporation of solid. Yield 0.364 g. (Visualized in *Scheme 5*). Electrospray mass spectra in 50% methanol–50% H_2O (Agilent 6490 EMS): m/z = 488 (C26H42N5O2S+). NMR peaks of the alkene-phenyl maleimide were analyzed and tracked for the decrease/disappearance to indicate crosslinking reaction (δ = 6.77ppm).

CXCR4-LTSL Synthesis

Covalent CXCR4-LTSL procedure

Preparation of covalently modified LTSL via thiol pendant-armed cyclam was done by dissolving complex from previous method in minimal dimethyl sulfoxide (5mg/~50 µL). This mixture was then added into the chloroform suspension containing slightly modified LTSL lipid ratios of DPPC- 85.3%, MSPC- 9.7%, PEG- 4.5%. Addition of 0.5 mol% of Cu-L-Mal-PEG (copper-ligand-maleimide-PEG) was used for covalent CXCR4-NPs and labeled C-CXCR4-LTSL. Nanoparticles (NPs) were then dried *in vacuo* as previously published (See Chapter 2). In brief, NPs were dried overnight in desiccator. Following drying, they were hydrated in a 300 mM citrate buffer, pH 4.0. After external buffer exchange via PD-10 column with 1X PBS, 2% wt/wt drug loading was done by incubating liposomes at 37°C for one hour. LTSL were used in their normal ratios of DPPC- 85.3%, MSPC- 9.7%, PEG- 5% as a control.

Electrostatic CXCR4-LTSL procedure

LTSL (DPPC- 85.3%, MSPC- 9.7%, PEG- 5%) were synthesized as previously described. Following synthesis, LTSL (2mg/100 µL) were incubated with various amounts of AMD-3100 or SJA05 (10-1000 µg, 2mg/mL stock solution) for electrostatic coordination to the surface of NPs. Solutions were thoroughly mixed, vortexed, and incubated for ~30 minutes.

Size analysis of CXCR4-LTSL

Both covalently attached and electrostatically linked versions of CXCR4-NPs were characterized for size (z-average) using a dynamic light scattering (DLS) instrument (Zetapals, Brookhaven Instruments, Holtsville, NY) by employing a non-negative least squares algorithm. The calibration standard used was a Thermo Scientific 3090A polystyrene nanosphere standard with a particle size of 92 ± 3 nm. During measurements, the filter wheel attenuation for sample optimization was set to between 500–750 kcps for the detectors avalanche photo diode and photo multiplier tube

respectively. Briefly, 1-2 µL of LTSL solution were added to 3 mL of water in a cuvette, and DLS measurements were taken at RT.

Statistical Analysis

Treatment groups were compared for differences using 2-way ANOVA multiple comparisons with Tukey's multiple comparisons test using GraphPad Prism 9.2.0.

Results

CXCR4 expression in cancer cell lines

To determine the CXCR4 expression of glioblastoma cells, we measured the baseline expression of CXCR4 using flow cytometry. U87.CD4.CXCR4 demonstrated ~60% CXCR4 expression. U87.CD4 showed negligible expression of CXCR4 (<0.2%; Fig. 26). Thus, verification of CXCR4 cell lines was shown.

CXCR4 inhibition of AMD-3100 versus TJH06 *antagonist*

To determine the CXCR4 antagonistic activity of commercial vs synthesized agents, we measured the free CXCR4 receptors by flow cytometry after pre-treatment with CXCR4 antagonists. Results showed decrease of unblocked CXCR4 receptors available for fluorescent antibody binding. Inhibition of CXCR4 was successful at 100 µM for both AMD-3100. AMD-3100 decreased measurable expression from ~60% to ~19% in U87.CD4.CXCR4 (Fig 27, pink bars, left vs. right). Similarly, inhibition of CXCR4 was successful with TJH06. TJH06 blocked CXCR4 receptor expression from ~60% to ~1% (Fig 27, turquoise bars, left vs. right).

Antagonism of CXCR4 augments chemotherapy efficacy in various cancer cell lines

To determine the efficacy of the combinatorial drug regimen of anthracenedione-based chemotherapies and CXCR4 antagonism, we measured the co-treatment efficacy via cytotoxicity assays. We used 2 different concentrations (50, 100 μM) of the commercial (AMD-3100) and synthesized (TJH06) CXCR4 antagonists for 24h treatments. Results showed both AMD-3100 and TJH06 improved cytotoxicity of therapies (Fig. 28-29). Moreover, TJH06 induced increased killing responses compared to AMD-3100. Specifically, a significant enhancement in DOX toxicity in all murine cancer cell lines was observed in the presence of TJH06 (100μM) except ID8 ovarian cancer cells. MTX also displayed significant increases in cell cytotoxicity in combination with TJH06. Likewise, PIX's effects were enhanced by TJH06 in all cell lines except ID8 ovarian cancer cells. Overall, significant cancer cell killings were achieved in 3/15 cases with AMD at 50 μM. Meanwhile, 6/15 cases were significant with TJH06 at 50 μM. When the treatment concentration was increased to 100 μM, significance rose to 7/15 cases in AMD and 12/15 cases in TJH06. This indicated TJH06 produces a relatively higher enhancement in drug efficacy. It also demonstrates concentration dependence.

To determine the chemotherapy that had the most enhancement upon CXCR4 addition, we analyzed differences of co-treatments to free drug controls. When these free drugs are compared with co-treatments including CXCR4 antagonists (AMD, TJH), it was shown that DOX is enhanced in 10/20 cases of significance, MTX 12/20 and PIX 7/20. Therefore, MTX received the most benefits from addition of CXCR4 co-treatment.

Chemical synthesis

To determine the feasibility of attaching a cross-bridged cyclam derivative to NPs, we chemically modified a previous ligand to display a pendant thiol arm for maleimide-thiol crosslinking. Results showed support of successful chemical modification by LC-MS, NMR, and elemental analysis. After synthesizing thiol-pendant armed ligand/metal complex, a preliminary result of crosslinking

was shown by model compound (phenyl maleimide). Results showed the decrease of the alkene proton (δ = 6.77ppm) of our model compound over time. This was indicative of crosslinking.

Synthesis and characterization of covalently attached CXCR4 antagonists loaded with DOX

To determine preliminary ways of covalently attaching CXCR4 antagonists to LTSL, CXCR4-NPs were synthesized by thiol-maleimide crosslinking. Our data suggests successful NP synthesis with no significant deviation of properties relative to LTSL (Table 2). During NP synthesis and drug loading, there was a significantly lowered encapsulation efficiency of DOX. Values decreased from >90% to 52% drug loading for covalent-CXCR4-LTSL.

Synthesis and characterization of electrostatically linked CXCR4 low temperature-sensitive liposomes (LTSL) co-loaded with chemotherapies (DOX, MTX, PIX)

To determine the ability of CXCR4 antagonists to electrostatically attach to the surface of anionic LTSL, we mixed both drugs with our LTSL solutions and characterized the results. Results indicated no significant changes in size or polydispersity. However, zeta potential changes were directly correlated to the increase of CXCR4 antagonist used (Fig. 30). Similarly, results from SJA05 addition showed increases in zeta potential. The increases were more enhanced in comparison to AMD-3100. This is most likely due to the molecular structure of SJA05 containing Cu^{2+} ions. This would contribute to the cationic nature of the molecule.

Discussion

CXCR4 antagonism improved anthracenedione-based chemotherapy (DOX, MTX, PIX) effectiveness. (1) Addition of AMD-3100 showed decreased viability relative to free drug controls (Fig. 28, 29). (2) Co-treatments with TJH06 similarly showed increased toxicity relative to free drug controls (Fig 28, 29) (3) The cases of enhancement were increased when concentration of

CXCR4 antagonists was doubled from 50 to 100 μM (Fig. 28, 29). Thus, concentration-dependence of effect was demonstrated. To the best of our knowledge, this is the first report of CXCR4 blockade used in combination with DOX, MTX and PIX in glioblastoma. Others have reported that DOX blockade sensitized osteosarcoma to doxorubicin[317]. We also report the use of TJH06, a synthesized CXCR4 compound, in use as a co-therapy with chemotherapies, whereas many only report commercially available CXCR4 antagonists (AMD-3100).

In this study, a novel thiol-armed macrocycle was reported. (1) Electrospray mass spectrometry peaks were indicative of ligand synthesis and copper isotope splitting. (2) Elemental analysis values showed carbon, hydrogen, and nitrogen in the acceptable range for our calculated compounds. (3) NMR peaks show peaks suggesting compound synthesis and preliminary reaction by decrease in phenyl-maleimide peak.

We report preliminary evidence of LTSL NPs containing CXCR4 through two methods. Covalent CXCR4 NPs evidence includes: (1) The model reaction phenyl maleimide and thiol-ligand produced a reduction in phenyl-maleimide proton NMR peak, indicating reaction. (2) Size and polydispersity of NPs stayed similar relative to LTSL not containing thiol ligand (Table 2). (3) Zeta potential was slightly more positive due to the small amount of cationic CXCR4 antagonist moiety added (0.5 mol%) (Table 2). Others have reported different a similar maleimide conjugation with a biomolecule instead that utilized amines rather than thiols[318].

A different method of crosslinking moieties onto NPs can occur through simple attraction/repulsion mechanisms and binding. Previously published CXCR4 antagonist, SJA05, and commercially available, AMD-3100, were compared in this study for their ability to attach to anionic LTSL. Electrostatic attachment showed similar evidence of initial success of synthesis. (1) Addition of AMD-3100 increased zeta potential (Fig. 30) like previous reports[204]. This demonstrates the anionic character of LTSL becoming more cationic in nature due to small molecules being added. (2)

Incubation of LTSL with SJA05 further enhanced the cationic nature (Fig. 30). This fits expected observations since copper-containing complexes would be more cationic (Fig. 30, left panel) relative to AMD-3100. (3) The increase of AMD-3100 and SJA05 concentrations increased the cationic nature of NPs (Fig. 30). Others have reported a similar procedure of attaching AMD-3100 onto anionic lipid-coated nanoparticles[204]. Another similar charge-based formulation used polynucleotides (siRNA) within NP formulation[319]. This is the first report of using the synthesized SJA05 CXCR4 antagonist in this electrostatic NP prep. Therefore, in application, the surface coating of CXCR4 antagonists could ensure that all CXCR4 antagonists are on the surface to interact with CXCR4 receptors. In contrast, the interactions with serum proteins would need to be anticipated and tested to ensure loss of antagonist did not occur. Hence, the potential application of CXCR4 within NPs has been utilized in various applications. CXCR4 blockade can be used as a targeting mechanism[320] or sensitization/therapeutic enhancement[317].

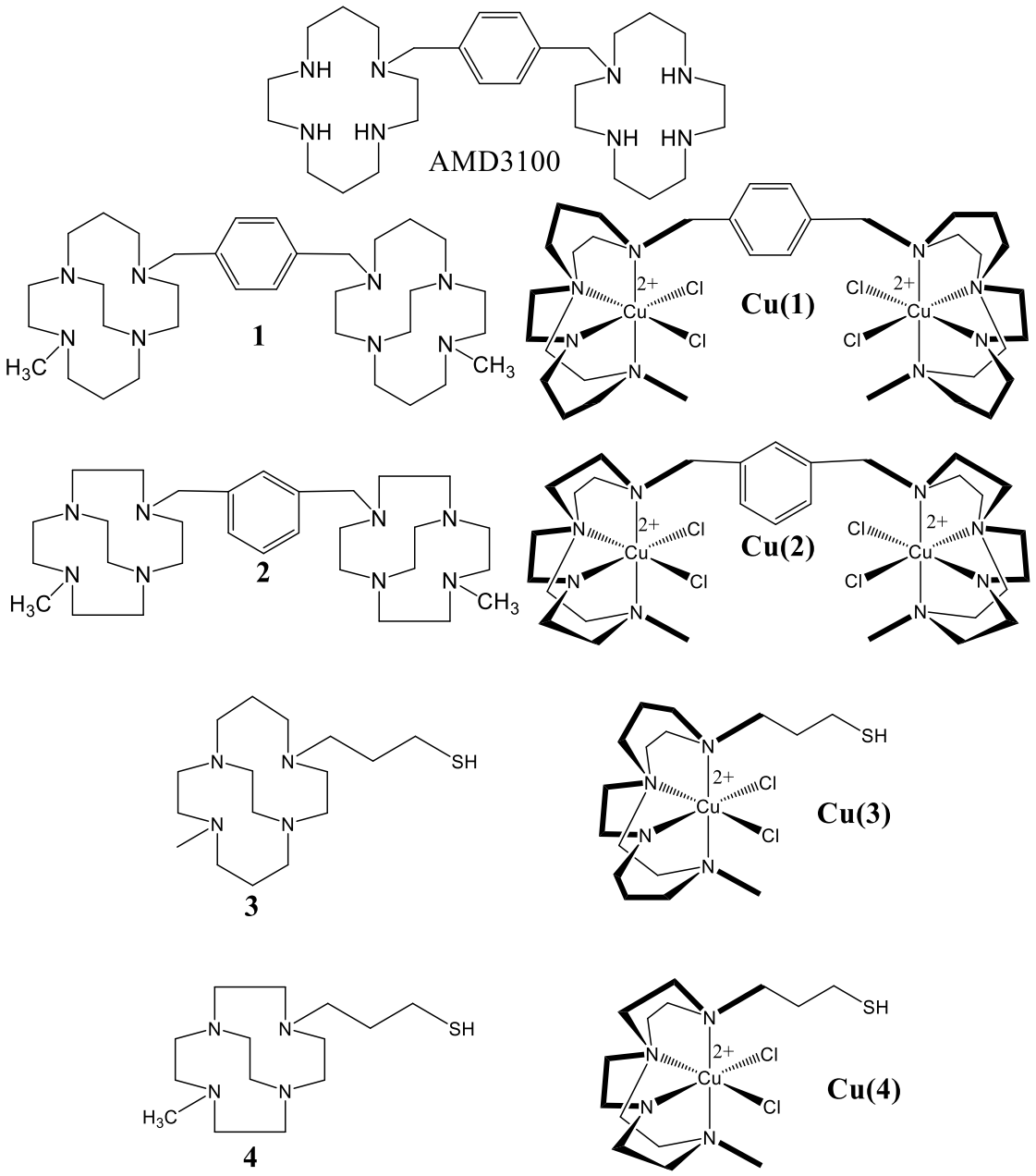

Figure 25. CXCR4 antagonists used throughout manuscript

AMD-3100 (Plerixafor) was purchased from AdooQ; Ligands 1-4 and their corresponding metal complexes were synthesized at Southwestern Oklahoma State University (SWOSU) in the lab of Dr. Timothy Hubin; (**1**) p-linked-cb-cyclams and its copper complex Cu(**1**) TJH06 (**2**), m-cb-cyclens m-linked-cb-cyclens and its copper complex Cu(**2**); TJH00 (**3**), thiol-methyl-cb-cyclam and its copper complex Cu(**3)**; TJH02 (4), thiol-methyl-cb-cyclen and its copper complex Cu(**4)**

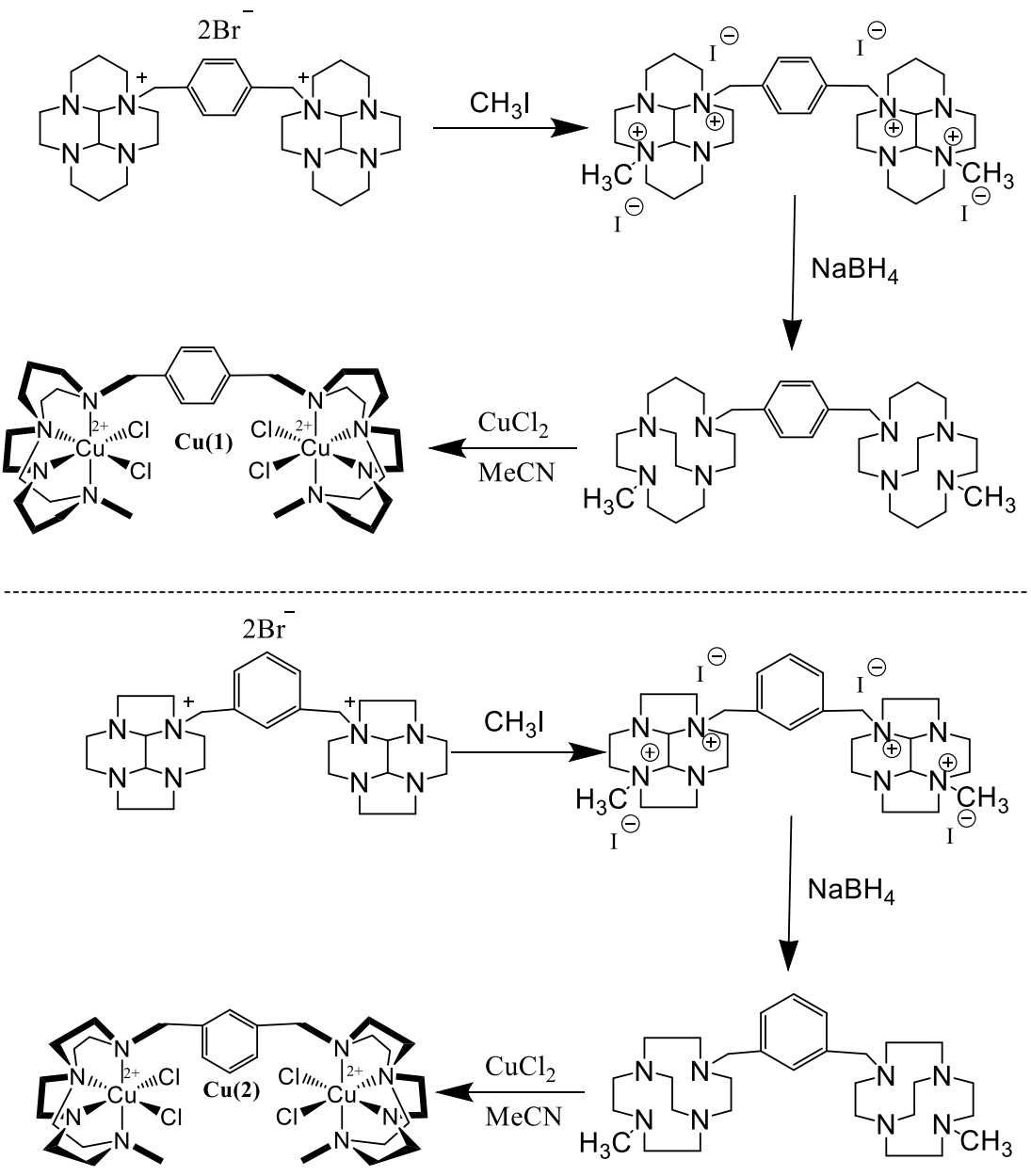

Schemes 1, 2. Synthetic routes of bis-cyclam (SJA05) and cyclen ligands (TJH06)

Previous step of glyoxal addition is not pictured. Iodomethane is added to macrocycles to give bis-methylated macrocycles. These are reduced by sodium borohydride and complexed with $CuCl_2$ to yield bis-copper complexes. (1, Top, cyclam synthesis; 2, Bottom, cyclen synthesis)

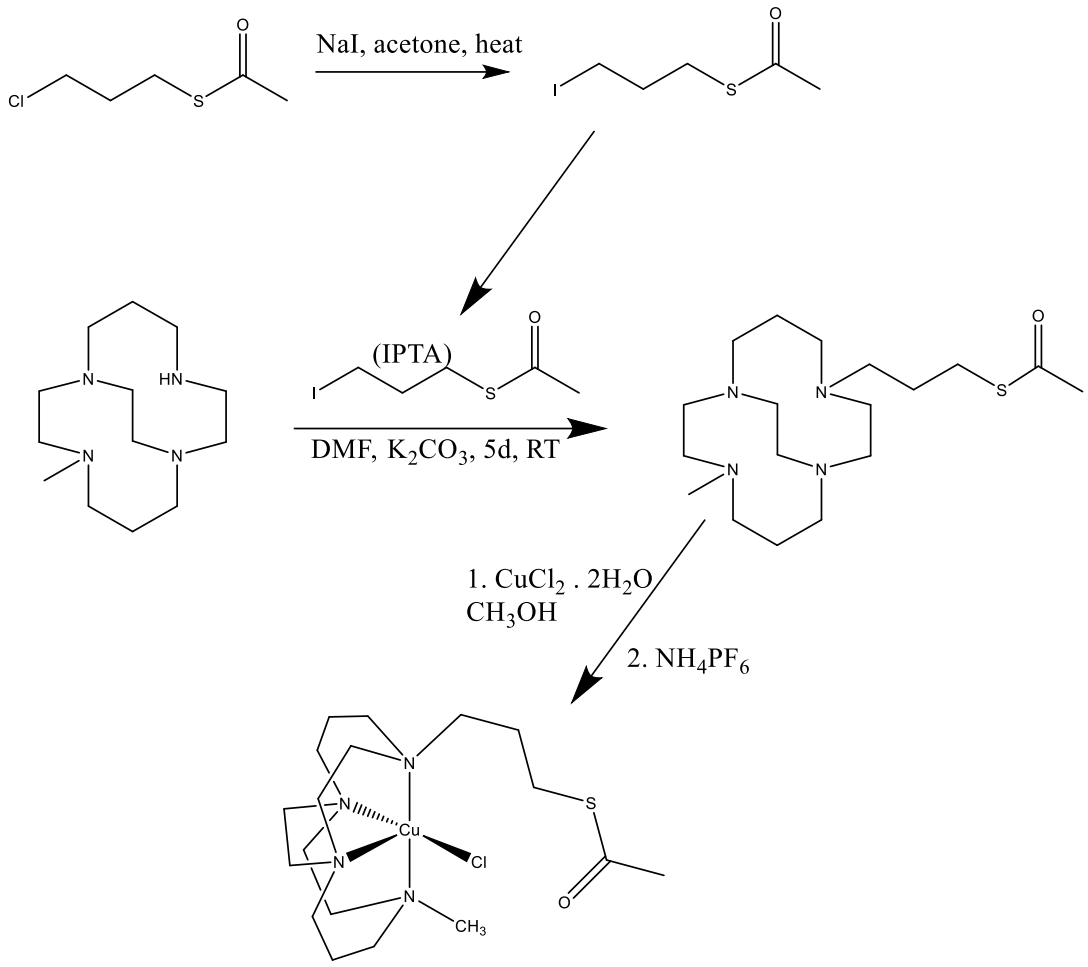

Scheme 3. Synthetic route of synthesis for novel thiol ligands via glyoxal-bridge, thiol arm addition and deprotection.

To determine if addition of thiol pendant arm was possible, we did a pilot reaction with a protected thiol arm. Chloro-propyl thioacetate was replaced with iodine via published procedure to make it more amenable to attachment to macrocycle (named IPTA). Attachment of IPTA was followed to a H_1Me_1-cb-cyclam in dimethylformamide (DMF). Subsequent copper complexation in methanol was conducted.

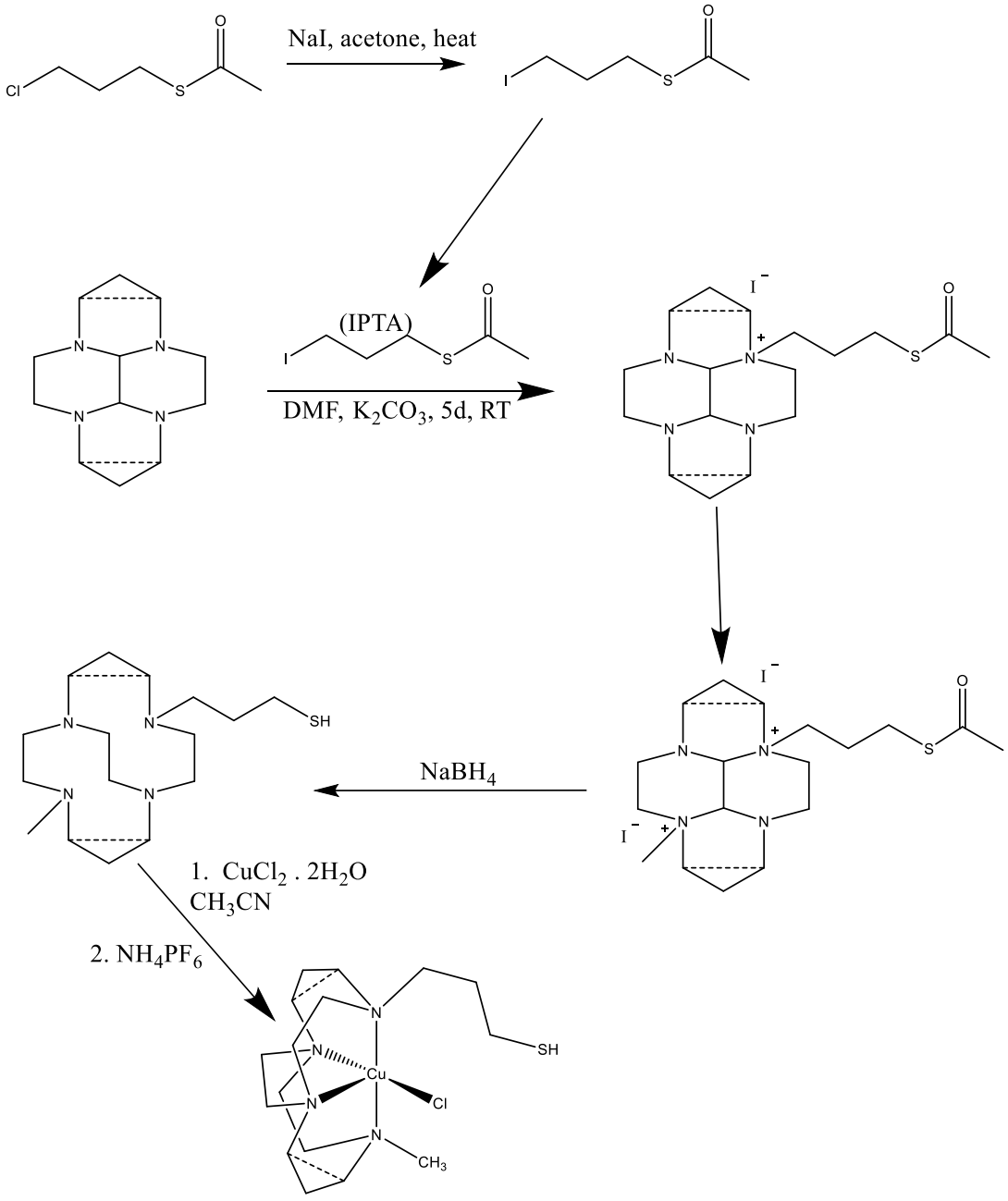

Scheme 4. Metal complexation of thiol cyclam and cyclen thiol ligands.

For a larger scale production, a similar technique was used with a simpler macrocycle. Steps included 1) arm attachment, 2) methylation, 3) borohydride reduction, 4) copper complexation.

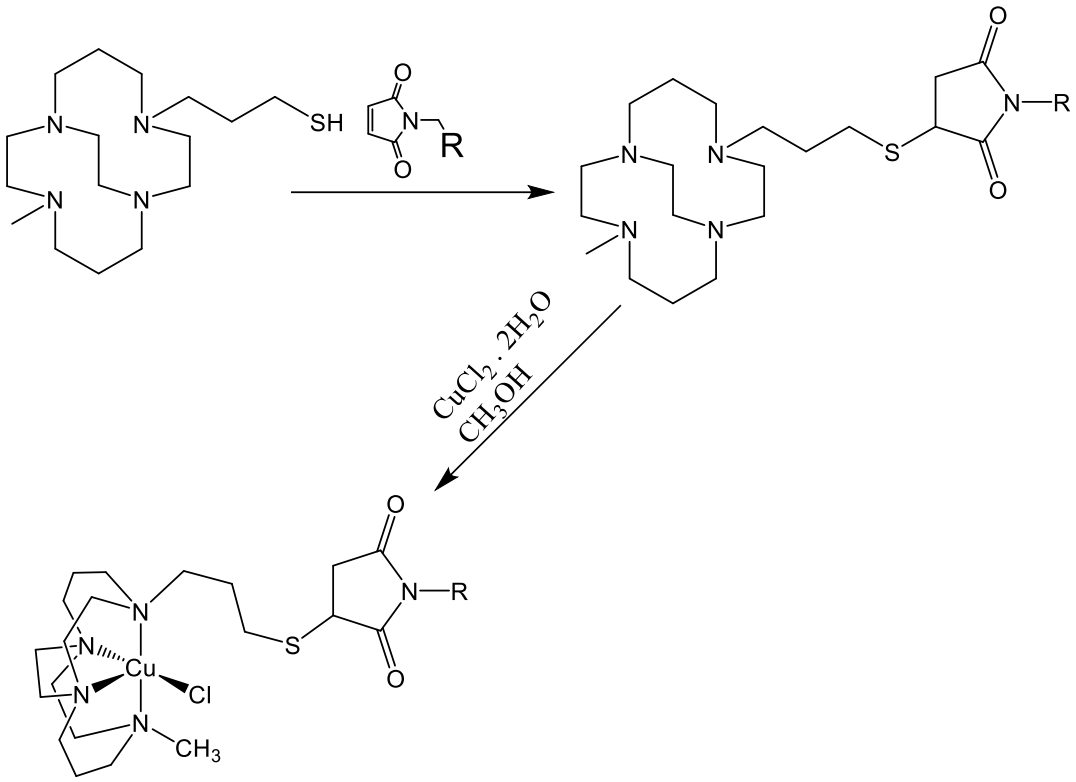

Scheme 5. Model phenyl thiol-maleimide complexation reaction.

To determine the potential of thiol-maleimide crosslinking, a model phenyl maleimide was used to observe crosslinking potential. R- Phenyl; Thiol-methyl-cb-cyclam was reacted with phenyl maleimide to yield a crosslinked product as illustrated above. This reaction occurs through thiol-maleimide crosslinking reaction to yield a thiosuccinimide product.

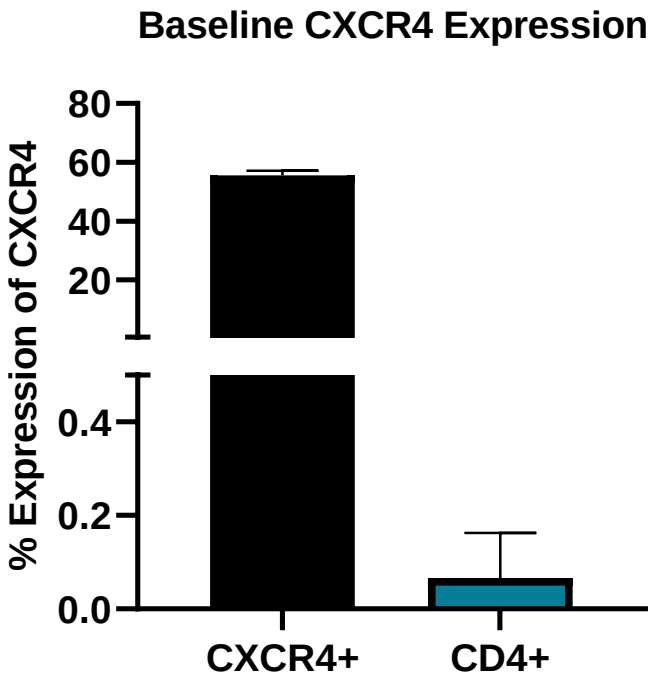

Figure 26. Glioblastoma variably expressed CXCR4 depending on specific cell line

To determine baseline expression of CXCR4 in glioblastoma cell lines, surface expression of CXCR4 was quantified through flow cytometry by PE-CXCR4 antibody (R&D).

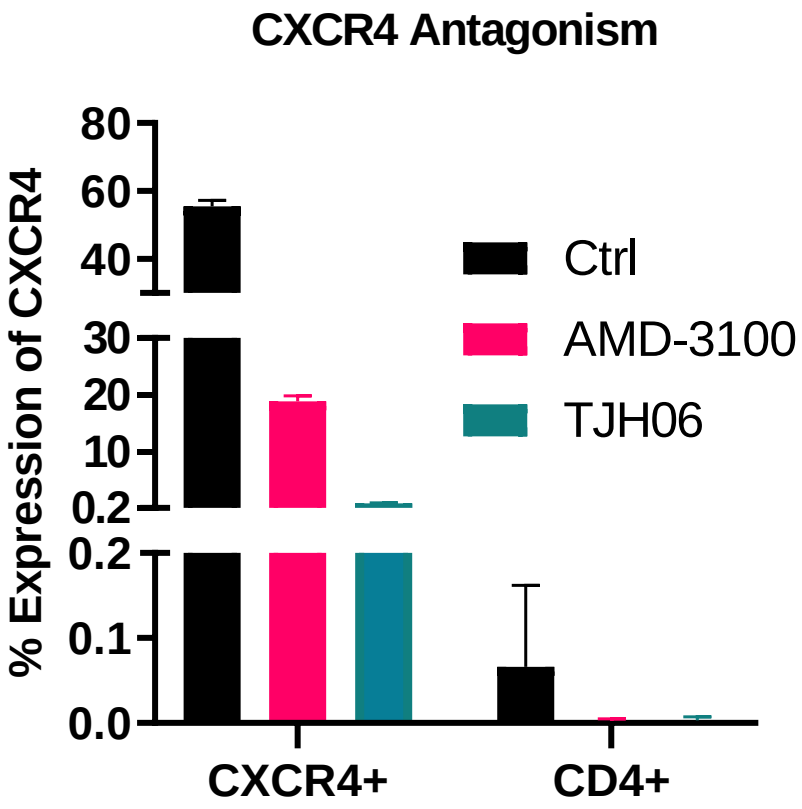

Figure 27. CXCR4 inhibition with TJH06 was greater compared to AMD-3100 in glioblastoma U87.CD4.CXCR4 and U87.CD4 cell lines

U87.CD4 and U87.CD4.CXCR4 cells were seeded, then pre-treated with CXCR4 antagonists (100 µM (AMD-3100 and TJH06)). Cells were then similarly stained as Fig. 26 with PE-CXCR4 antibody (R&D) and fixable viability stain 450 (BD Horizon) after several washings.

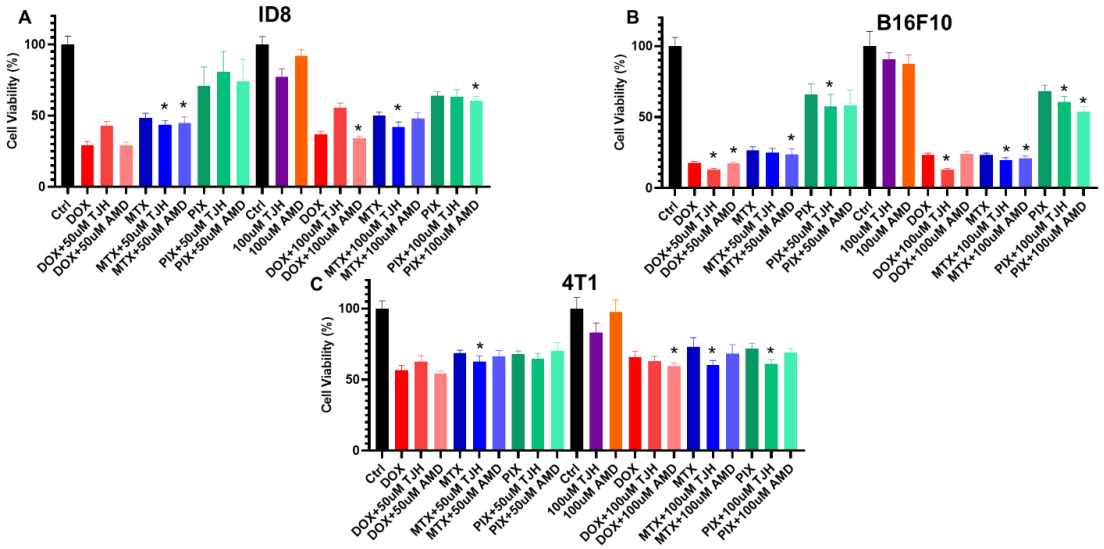

Figure 28. CXCR4 antagonism enhanced DOX, MTX, and PIX in murine cancer cells *in vitro*

To determine co-treatment efficacy of chemotherapies + CXCR4 antagonists in murine cancer cells, B16F10, 4T1, and ID8 were co-treated with CXCR4 antagonists TJH06 or AMD-3100 (50, 100 μM) and chemotherapies for 24h. Cell viability was measured by MTT assay. Cytotoxicity data sets were represented as mean ± SD unless otherwise indicated (n=6-12 per group unless otherwise indicated, well replicates of a single passage of cells). For analysis of these groups, two-way ANOVA was performed followed by Dunnett's multiple comparison's test ($p < 0.05$ is considered significant). **(A)** ID8, **(B)** B16F10, **(C)** 4T1. All comparisons are relative to free drug control.

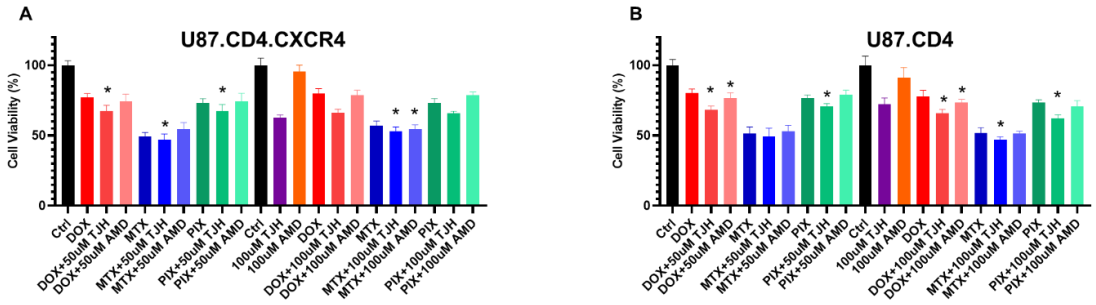

Figure 29. CXCR4 antagonism enhanced DOX, MTX, and PIX against human glioblastoma cells *in vitro*

To determine co-treatment efficacy of chemotherapies + CXCR4 antagonists in human glioblastoma cancer cells, U87 (CD4.CXCR4 and CD4) cells were co-treated with CXCR4 antagonists TJH06 or AMD-3100 (50, 100 µM) and chemotherapies for 24h. Cell viability was measured by MTT assay. Cytotoxicity data sets were represented as mean ± SD unless otherwise indicated (n=6-12 per group unless otherwise indicated, well replicates of a single passage of cells). For analysis of these groups, two-way ANOVA was performed followed by Dunnett's multiple comparison's test ($p < 0.05$ is considered significant). **(A)** U87.CD4.CXCR4, **(B)** U87.CD4. All comparisons are relative to free drug control.

Covalent CXCR4-NPs	Size (nm)		Polydispersity (PDI)		Zeta Potential	
	mean	SD	mean	SD	mean	SD
LTSL	194.61	1.42	0.126	0.018	-40.05	1.35
L-Cu-LTSL	191.97	0.45	0.124	0.012	-38.24	3.45

Table 2. Covalent-CXCR4-LTSL showed similar physicochemical profile as LTSL

To determine biophysical characteristics of LTSL when adding 0.5 mol% of thiol-maleimide crosslink reaction, comparative batches of LTSL were synthesized. LTSL lipid ratio- DPPC- 85.3%, MSPC- 9.7%, PEG- 5%, covalent-CXCR4-LTSL lipid ratio- DPPC- 85.3%, MSPC- 9.7%, PEG-4.5%, Copper-thiol ligand-maleimide-PEG-0.5% (L-Cu-LTSL).

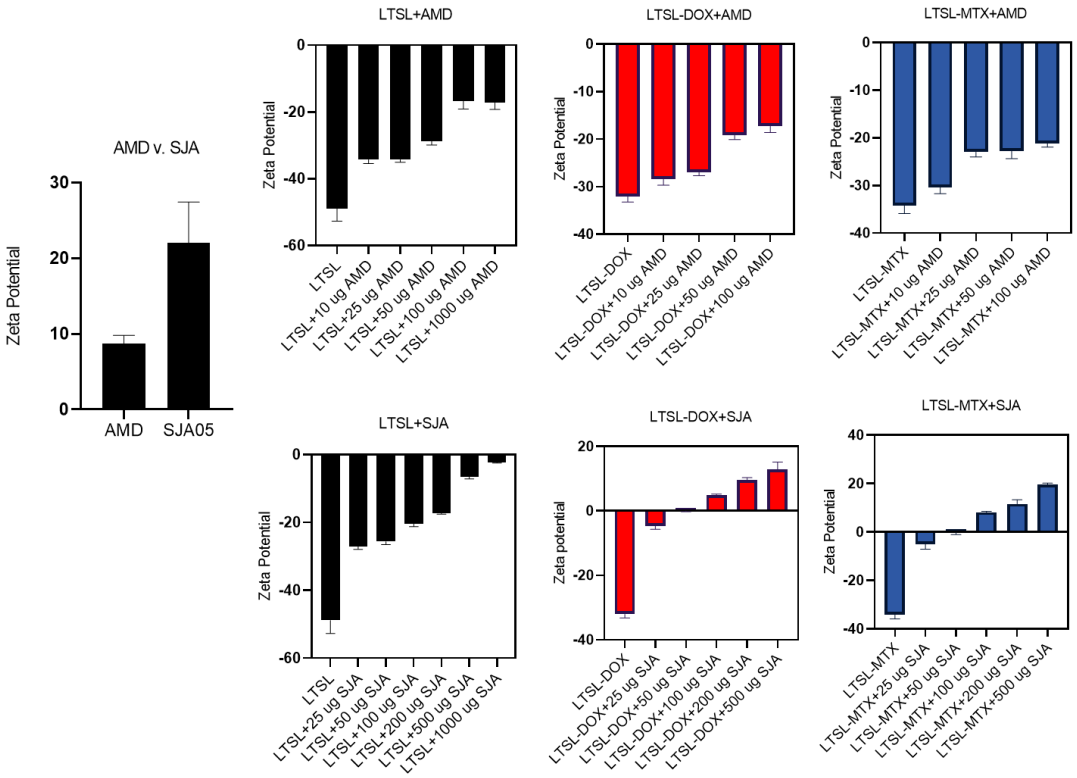

Figure 30. Electrostatic linkage of CXCR4 antagonists to LTSL altered their zeta potential while maintaining size and stability

To compare physicochemical properties of LTSL after addition of cationic CXCR4 antagonists, LTSL (2 mg/100µL) were incubated with various concentrations of AMD-3100 or SJA05 (10-1000 µg of AMD/SJA from 2mg/mL solutions). They were lightly vortexed and incubated for 30 minutes. DLS and PALS characterizations were subsequently performed. Size was maintained (c.a. 200 nm) while zeta potential was increased based upon the amount of CXCR4 antagonist added.

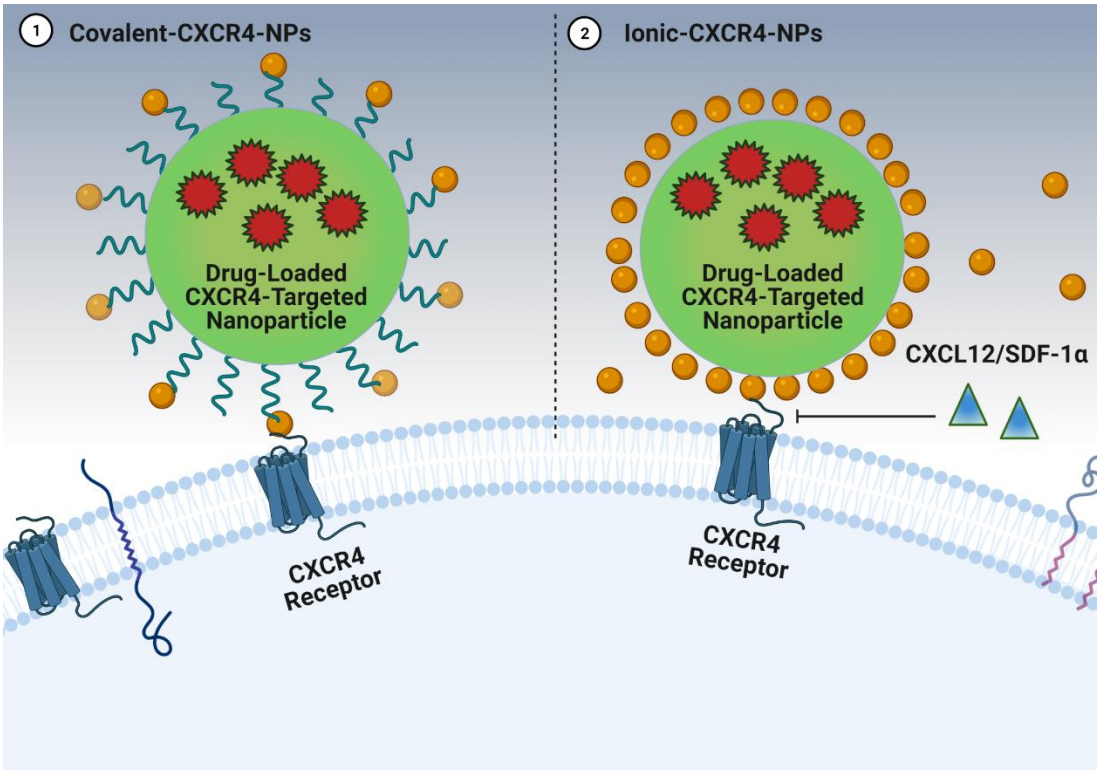

Figure 31. Model concept of CXCR4-NPs made in this study

1) Covalent CXCR4-NPs were synthesized by novel-pendant arm modification and thiol-maleimide crosslinking reaction, 2) Ionic, or electrostatically attached,CXCR4-NPs were synthesized by co-incubating previously published SJA05 and commercially available AMD-3100 with anionic LTSL.

REFERENCES

1 Siegel, R. L., Miller, K. D., Fuchs, H. E. & Jemal, A. Cancer Statistics, 2021. *CA: A Cancer Journal for Clinicians* **71**, 7-33, doi:https://doi.org/10.3322/caac.21654 (2021).

2 Mole, R. Whole body irradiation—radiobiology or medicine? *The British journal of radiology* **26**, 234-241 (1953).

3 Kaminski, J. M. *et al.* The controversial abscopal effect. *Cancer Treatment Reviews* **31**, 159-172, doi:https://doi.org/10.1016/j.ctrv.2005.03.004 (2005).

4 Bramhall, R. J., Mahady, K. & Peach, A. H. S. Spontaneous regression of metastatic melanoma – Clinical evidence of the abscopal effect. *European Journal of Surgical Oncology (EJSO)* **40**, 34-41, doi:https://doi.org/10.1016/j.ejso.2013.09.026 (2014).

5 Okwan-Duodu, D., Pollack, B. P., Lawson, D. & Khan, M. K. Role of radiation therapy as immune activator in the era of modern immunotherapy for metastatic malignant melanoma. *American journal of clinical oncology* **38**, 119-125 (2015).

6 Hidaka, Y., Takeichi, T., Ishikawa, Y., Kawamura, M. & Akiyama, M. Abscopal effect of local irradiation treatment for diffuse large B-cell lymphoma. *Acta dermato-venereologica* **97**, 1140-1141 (2017).

7 Ishiyama, H. *et al.* Spontaneous regression of thoracic metastases while progression of brain metastases after stereotactic radiosurgery and stereotactic body radiotherapy for metastatic renal cell carcinoma: abscopal effect prevented by the blood-brain barrier? *Clinical genitourinary cancer* **10**, 196-198 (2012).

8 Van de Walle, M., Demol, J., Staelens, L. & Rottey, S. Abscopal effect in metastatic renal cell carcinoma. *Acta Clinica Belgica* **72**, 245-249, doi:10.1080/17843286.2016.1201614 (2017).

9 Nakanishi, M., Chuma, M., Hige, S. & Asaka, M. Abscopal effect on hepatocellular carcinoma. *The American journal of gastroenterology* **103**, 1320 (2008).

10 Ohba, K. *et al.* Abscopal regression of hepatocellular carcinoma after radiotherapy for bone metastasis. *Gut* **43**, 575-577 (1998).

11 Yoo, G. S. *et al.* Radiation-induced abscopal effect and its enhancement by programmed cell death 1 blockade in the hepatocellular carcinoma: A murine model study. *Clin Mol Hepatol* **27**, 144-156, doi:10.3350/cmh.2020.0095 (2021).

12 Cong, Y., Shen, G., Wu, S. & Hao, R. Abscopal regression following SABR for non-small-cell-lung cancer: a case report. *Cancer biology & therapy* **18**, 1-3 (2017).

13 Siva, S. *et al.* Abscopal effects after conventional and stereotactic lung irradiation of non–small-cell lung cancer. *Journal of Thoracic Oncology* **8**, e71-e72 (2013).

14 Takaya, M. *et al.* Abscopal effect of radiation on toruliform para-aortic lymph node metastases of advanced uterine cervical carcinoma-a case report. *Anticancer Res* **27**, 499-503 (2007).

15 Azami, A. *et al.* Abscopal effect following radiation monotherapy in breast cancer: A case report. *Mol Clin Oncol* **9**, 283-286, doi:10.3892/mco.2018.1677 (2018).

16 Smyth, M. J., Dunn, G. P. & Schreiber, R. D. in *Advances in Immunology* Vol. 90 1-50 (Academic Press, 2006).

17 Shankaran, V. *et al.* IFNγ and lymphocytes prevent primary tumour development and shape tumour immunogenicity. *Nature* **410**, 1107-1111 (2001).

18 Siu, L. L. *et al.* Challenges and Opportunities in Adapting Clinical Trial Design for Immunotherapies. *Clinical Cancer Research* **23**, 4950-4958, doi:10.1158/1078-0432.Ccr-16-3079 (2017).

19 Krishna, R. & Mayer, L. D. Multidrug resistance (MDR) in cancer: Mechanisms, reversal using modulators of MDR and the role of MDR modulators in influencing the pharmacokinetics of anticancer drugs. *European Journal of Pharmaceutical Sciences* **11**, 265-283, doi:https://doi.org/10.1016/S0928-0987(00)00114-7 (2000).
20 Baguley, B. C. Multiple drug resistance mechanisms in cancer. *Molecular biotechnology* **46**, 308-316 (2010).
21 Wu, Q., Yang, Z., Nie, Y., Shi, Y. & Fan, D. Multi-drug resistance in cancer chemotherapeutics: Mechanisms and lab approaches. *Cancer letters* **347**, 159-166, doi:https://doi.org/10.1016/j.canlet.2014.03.013 (2014).
22 Pollack, A. & Zagars, G. K. External beam radiotherapy dose response of prostate cancer. *International journal of radiation oncology, biology, physics* **39**, 1011-1018 (1997).
23 Kupelian, P. A. *et al.* Radical prostatectomy, external beam radiotherapy< 72 Gy, external beam radiotherapy⩾ 72 Gy, permanent seed implantation, or combined seeds/external beam radiotherapy for stage T1 – T2 prostate cancer. *International Journal of Radiation Oncology* Biology* Physics* **58**, 25-33 (2004).
24 Mijnheer, B., Beddar, S., Izewska, J. & Reft, C. In vivo dosimetry in external beam radiotherapy. *Medical physics* **40**, 070903 (2013).
25 Marwaha, G., Macklis, R., Singh, A. D. & Wilkinson, A. Brachytherapy. *Dev Ophthalmol* **52**, 29-35, doi:10.1159/000351053 (2013).
26 Nag, S. *et al.* The American Brachytherapy Society recommendations for high-dose-rate brachytherapy for carcinoma of the cervix. *International Journal of Radiation Oncology* Biology* Physics* **48**, 201-211 (2000).
27 Devlin, P. M. *Brachytherapy: applications and techniques*. (Springer Publishing Company, 2015).
28 Nag, S. *et al.* The American Brachytherapy Society recommendations for brachytherapy of uveal melanomas. *International Journal of Radiation Oncology* Biology* Physics* **56**, 544-555 (2003).
29 Kennedy, A. Selective internal radiation therapy dosimetry. *Future Oncol* **10**, 77-81, doi:10.2217/fon.14.230 (2014).
30 Stubbs, R. & Wickremesekera, S. Selective internal radiation therapy (SIRT): a new modality for treating patients with colorectal liver metastases. *Hpb* **6**, 133-139 (2004).
31 Welsh, J. S., Kennedy, A. S. & Thomadsen, B. Selective internal radiation therapy (SIRT) for liver metastases secondary to colorectal adenocarcinoma. *International Journal of Radiation Oncology* Biology* Physics* **66**, S62-S73 (2006).
32 Stubbs, R. S., Cannan, R. J. & Mitchell, A. W. Selective internal radiation therapy (SIRT) with 90Yttrium microspheres for extensive colorectal liver metastases. *Hepato-gastroenterology* **48**, 333-337 (2001).
33 Pöpperl, G. *et al.* Selective internal radiation therapy with SIR-Spheres® in patients with nonresectable liver tumors. *Cancer biotherapy & radiopharmaceuticals* **20**, 200-208 (2005).
34 Jackson, S. P. & Bartek, J. The DNA-damage response in human biology and disease. *Nature* **461**, 1071-1078, doi:10.1038/nature08467 (2009).
35 Baskar, R., Lee, K. A., Yeo, R. & Yeoh, K.-W. Cancer and radiation therapy: current advances and future directions. *Int J Med Sci* **9**, 193-199, doi:10.7150/ijms.3635 (2012).
36 Delaney, G., Jacob, S., Featherstone, C. & Barton, M. The role of radiotherapy in cancer treatment. *Cancer* **104**, 1129-1137, doi:https://doi.org/10.1002/cncr.21324 (2005).
37 Kim, W. *et al.* Cellular Stress Responses in Radiotherapy. *Cells* **8**, 1105 (2019).

38 Medler, T. R., Blair, T. C., Crittenden, M. R. & Gough, M. J. Defining immunogenic and radioimmunogenic tumors. *Front Oncol* **11**, 839 (2021).
39 Dewan, M. Z. *et al.* Fractionated but Not Single-Dose Radiotherapy Induces an Immune-Mediated Abscopal Effect when Combined with Anti–CTLA-4 Antibody. *Clinical Cancer Research* **15**, 5379, doi:10.1158/1078-0432.CCR-09-0265 (2009).
40 Nauts, H. C., Fowler, G. A. & Bogatko, F. H. A review of the influence of bacterial infection and of bacterial products (Coley's toxins) on malignant tumors in man; a critical analysis of 30 inoperable cases treated by Coley's mixed toxins, in which diagnosis was confirmed by microscopic examination selected for special study. *Acta Med Scand Suppl* **276**, 1-103 (1953).
41 McCarthy, E. F. The toxins of William B. Coley and the treatment of bone and soft-tissue sarcomas. *Iowa Orthop J* **26**, 154-158 (2006).
42 Kirkwood, J. M. *et al.* Immunotherapy of cancer in 2012. *CA: a cancer journal for clinicians* **62**, 309-335 (2012).
43 Ma, J. *et al.* The M1 form of tumor-associated macrophages in non-small cell lung cancer is positively associated with survival time. *BMC cancer* **10**, 1-9 (2010).
44 Cai, X. *et al.* Re-polarization of tumor-associated macrophages to pro-inflammatory M1 macrophages by microRNA-155. *Journal of Molecular Cell Biology* **4**, 341-343, doi:10.1093/jmcb/mjs044 (2012).
45 Klug, F. *et al.* Low-dose irradiation programs macrophage differentiation to an iNOS+/M1 phenotype that orchestrates effective T cell immunotherapy. *Cancer cell* **24**, 589-602 (2013).
46 Fernandez, N. C. *et al.* Dendritic cells directly trigger NK cell functions: cross-talk relevant in innate anti-tumor immune responses in vivo. *Nature medicine* **5**, 405-411 (1999).
47 Alsaab, H. O. *et al.* PD-1 and PD-L1 checkpoint signaling inhibition for cancer immunotherapy: mechanism, combinations, and clinical outcome. *Frontiers in pharmacology* **8**, 561 (2017).
48 Walunas, T. L. *et al.* CTLA-4 can function as a negative regulator of T cell activation. *Immunity* **1**, 405-413, doi:https://doi.org/10.1016/1074-7613(94)90071-X (1994).
49 Haslam, A. & Prasad, V. Estimation of the Percentage of US Patients With Cancer Who Are Eligible for and Respond to Checkpoint Inhibitor Immunotherapy Drugs. *JAMA Network Open* **2**, e192535-e192535, doi:10.1001/jamanetworkopen.2019.2535 (2019).
50 Hamid, O. *et al.* Five-year survival outcomes for patients with advanced melanoma treated with pembrolizumab in KEYNOTE-001. *Annals of Oncology* **30**, 582-588, doi:https://doi.org/10.1093/annonc/mdz011 (2019).
51 Kim, J. M. & Chen, D. S. Immune escape to PD-L1/PD-1 blockade: seven steps to success (or failure). *Annals of Oncology* **27**, 1492-1504, doi:https://doi.org/10.1093/annonc/mdw217 (2016).
52 Hegde, P. S. & Chen, D. S. Top 10 Challenges in Cancer Immunotherapy. *Immunity* **52**, 17-35, doi:https://doi.org/10.1016/j.immuni.2019.12.011 (2020).
53 Chabner, B. A. & Roberts, T. G. Chemotherapy and the war on cancer. *Nature Reviews Cancer* **5**, 65-72, doi:10.1038/nrc1529 (2005).
54 Gilman, A. The initial clinical trial of nitrogen mustard. *The American Journal of Surgery* **105**, 574-578 (1963).
55 Farber, S., Diamond, L. K., Mercer, R. D., Sylvester Jr, R. F. & Wolff, J. A. Temporary remissions in acute leukemia in children produced by folic acid antagonist, 4-

aminopteroyl-glutamic acid (aminopterin). *New England Journal of Medicine* **238**, 787-793 (1948).
56 Minocha, A. & Long, B. H. Inhibition of the DNA catenation activity of type II topoisomerase by VP16-213 and VM26. *Biochemical and biophysical research communications* **122**, 165-170 (1984).
57 Bae, Y. H. & Park, K. Targeted drug delivery to tumors: myths, reality and possibility. *Journal of controlled release : official journal of the Controlled Release Society* **153**, 198-205, doi:10.1016/j.jconrel.2011.06.001 (2011).
58 Gottesman, M. M. Mechanisms of cancer drug resistance. *Annual review of medicine* **53**, 615-627 (2002).
59 Elsaid, K. A., Garguilo, S. & Collins, C. M. Chemotherapy e-prescribing: opportunities and challenges. *Integr Pharm Res Pract* **4**, 39-48, doi:10.2147/IPRP.S84232 (2015).
60 Wu, Q., Yang, Z., Nie, Y., Shi, Y. & Fan, D. Multi-drug resistance in cancer chemotherapeutics: mechanisms and lab approaches. *Cancer Lett* **347**, 159-166, doi:10.1016/j.canlet.2014.03.013 (2014).
61 Bao, L. *et al.* Increased expression of P-glycoprotein is associated with doxorubicin chemoresistance in the metastatic 4T1 breast cancer model. *Am J Pathol* **178**, 838-852, doi:10.1016/j.ajpath.2010.10.029 (2011).
62 Roundhill, E. & Burchill, S. Detection and characterisation of multi-drug resistance protein 1 (MRP-1) in human mitochondria. *British journal of cancer* **106**, 1224-1233 (2012).
63 Young, L. C. *et al.* Expression of multidrug resistance protein-related genes in lung cancer: correlation with drug response. *Clin Cancer Res* **5**, 673-680 (1999).
64 Tada, Y. *et al.* Increased expression of multidrug resistance‐associated proteins in bladder cancer during clinical course and drug resistance to doxorubicin. *International journal of cancer* **98**, 630-635 (2002).
65 Grimm, A., Madduri, K., Ali, A. & Hutchinson, C. R. Characterization of the Streptomyces peucetius ATCC 29050 genes encoding doxorubicin polyketide synthase. *Gene* **151**, 1-10, doi:https://doi.org/10.1016/0378-1119(94)90625-4 (1994).
66 Dickens, M. L. & Strohl, W. R. Isolation and characterization of a gene from Streptomyces sp. strain C5 that confers the ability to convert daunomycin to doxorubicin on Streptomyces lividans TK24. *Journal of Bacteriology* **178**, 3389-3395, doi:10.1128/jb.178.11.3389-3395.1996 (1996).
67 Damiani, R. M. *et al.* Pathways of cardiac toxicity: comparison between chemotherapeutic drugs doxorubicin and mitoxantrone. *Archives of Toxicology* **90**, 2063-2076, doi:10.1007/s00204-016-1759-y (2016).
68 Tsutsui, H., Kinugawa, S. & Matsushima, S. Oxidative stress and mitochondrial DNA damage in heart failure. *Circulation Journal* **72**, A31-A37 (2008).
69 Costa, V. M., Carvalho, F., Duarte, J. A., Bastos, M. d. L. & Remião, F. The Heart As a Target for Xenobiotic Toxicity: The Cardiac Susceptibility to Oxidative Stress. *Chemical research in toxicology* **26**, 1285-1311, doi:10.1021/tx400130v (2013).
70 Timolati, F. *et al.* Neuregulin-1 beta attenuates doxorubicin-induced alterations of excitation–contraction coupling and reduces oxidative stress in adult rat cardiomyocytes. *Journal of Molecular and Cellular Cardiology* **41**, 845-854, doi:https://doi.org/10.1016/j.yjmcc.2006.08.002 (2006).

71 Arnaiz, S. L. & Llesuy, S. Oxidative stress in mouse heart by antitumoral drugs: a comparative study of doxurobicin and mitoxantrone. *Toxicology* **77**, 31-38, doi:https://doi.org/10.1016/0300-483X(93)90135-F (1993).
72 Durr, F., Wallace, R. & Citarella, R. Molecular and biochemical pharmacology of mitoxantrone. *Cancer treatment reviews* **10**, 9-11 (1983).
73 Brück, T. B. & Brück, D. W. Oxidative metabolism of the anti-cancer agent mitoxantrone by horseradish, lacto-and lignin peroxidase. *Biochimie* **93**, 217-226, doi:https://doi.org/10.1016/j.biochi.2010.09.015 (2011).
74 Chen, Y., Jungsuwadee, P., Vore, M., Butterfield, D. A. & St Clair, D. K. Collateral damage in cancer chemotherapy: oxidative stress in nontargeted tissues. *Molecular interventions* **7**, 147 (2007).
75 Seiter, K. Toxicity of the topoisomerase II inhibitors. *Expert opinion on drug safety* **4**, 219-234 (2005).
76 Cavalcante, R. P. *et al.* Application of Fenton, photo-Fenton, solar photo-Fenton, and UV/H 2 O 2 to degradation of the antineoplastic agent mitoxantrone and toxicological evaluation. *Environmental Science and Pollution Research* **20**, 2352-2361 (2013).
77 Stewart, D. J. *et al.* Human autopsy tissue concentrations of mitoxantrone. *Cancer Treat Rep* **70**, 1255-1261 (1986).
78 Lechner, M. G. *et al.* Immunogenicity of murine solid tumor models as a defining feature of in vivo behavior and response to immunotherapy. *J Immunother* **36**, 477-489, doi:10.1097/01.cji.0000436722.46675.4a (2013).
79 Pitt, J. M., Kroemer, G. & Zitvogel, L. Immunogenic and Non-immunogenic Cell Death in the Tumor Microenvironment. *Adv Exp Med Biol* **1036**, 65-79, doi:10.1007/978-3-319-67577-0_5 (2017).
80 Pinho, S. S., Carvalho, S., Cabral, J., Reis, C. A. & Gärtner, F. Canine tumors: a spontaneous animal model of human carcinogenesis. *Translational Research* **159**, 165-172, doi:https://doi.org/10.1016/j.trsl.2011.11.005 (2012).
81 Albanese, A., Tang, P. S. & Chan, W. C. W. The Effect of Nanoparticle Size, Shape, and Surface Chemistry on Biological Systems. *Annual Review of Biomedical Engineering* **14**, 1-16, doi:10.1146/annurev-bioeng-071811-150124 (2012).
82 Jurney, P. *et al.* Unique size and shape-dependent uptake behaviors of non-spherical nanoparticles by endothelial cells due to a shearing flow. *Journal of Controlled Release* **245**, 170-176 (2017).
83 Truong, N. P., Whittaker, M. R., Mak, C. W. & Davis, T. P. The importance of nanoparticle shape in cancer drug delivery. *Expert opinion on drug delivery* **12**, 129-142 (2015).
84 Fischer, N. O., Rasley, A. & Blanchette, C. Nanoparticles and antigen delivery: understanding the benefits and drawbacks of different delivery platforms. *Nanomedicine (London, England)* **9**, 373-376, doi:10.2217/nnm.14.16 (2014).
85 Baetke, S. C., Lammers, T. & Kiessling, F. Applications of nanoparticles for diagnosis and therapy of cancer. *The British journal of radiology* **88**, 20150207, doi:10.1259/bjr.20150207 (2015).
86 Ward, A. E. & Rosenthal, B. M. Evolutionary responses of innate immunity to adaptive immunity. *Infection, genetics and evolution : journal of molecular epidemiology and evolutionary genetics in infectious diseases* **21**, 492-496, doi:10.1016/j.meegid.2013.12.021 (2014).
87 Prabha, S., Arya, G., Chandra, R., Ahmed, B. & Nimesh, S. Effect of size on biological properties of nanoparticles employed in gene delivery. *Artificial cells, nanomedicine, and biotechnology (Print)* **44**, 1-9, doi:10.3109/21691401.2014.913054 (2014).

88 Oh, W.-K. *et al.* Cellular uptake, cytotoxicity, and innate immune response of silica–titania hollow nanoparticles based on size and surface functionality. *ACS nano* **4**, 5301-5313 (2010).
89 Jia, J. *et al.* Interactions between nanoparticles and dendritic cells: from the perspective of cancer immunotherapy. *Front Oncol* **8**, 404 (2018).
90 Shima, F., Akagi, T. & Akashi, M. Effect of hydrophobic side chains in the induction of immune responses by nanoparticle adjuvants consisting of amphiphilic poly (γ-glutamic acid). *Bioconjugate chemistry* **26**, 890-898 (2015).
91 Moyano, D. F. *et al.* Nanoparticle hydrophobicity dictates immune response. *Journal of the American Chemical Society* **134**, 3965-3967 (2012).
92 Oh, J. Y. *et al.* Cloaking nanoparticles with protein corona shield for targeted drug delivery. *Nature Communications* **9**, 4548, doi:10.1038/s41467-018-06979-4 (2018).
93 Saha, K. *et al.* Regulation of macrophage recognition through the interplay of nanoparticle surface functionality and protein corona. *ACS nano* **10**, 4421-4430 (2016).
94 Amoozgar, Z. & Yeo, Y. Recent advances in stealth coating of nanoparticle drug delivery systems. *Wiley interdisciplinary reviews. Nanomedicine and nanobiotechnology* **4**, 219-233, doi:10.1002/wnan.1157 (2012).
95 Jang, H.-J., Shin, C. Y. & Kim, K.-B. Safety Evaluation of Polyethylene Glycol (PEG) Compounds for Cosmetic Use. *Toxicol Res* **31**, 105-136, doi:10.5487/TR.2015.31.2.105 (2015).
96 Klibanov, A. L., Maruyama, K., Torchilin, V. P. & Huang, L. Amphipathic polyethyleneglycols effectively prolong the circulation time of liposomes. *FEBS Letters* **268**, 235-237, doi:https://doi.org/10.1016/0014-5793(90)81016-H (1990).
97 Wu, W.-d. *et al.* The targeted-liposome delivery system of antitumor drugs. *Current drug metabolism* **16**, 894-910 (2015).
98 Xing, M., Yan, F., Yu, S. & Shen, P. Efficacy and Cardiotoxicity of Liposomal Doxorubicin-Based Chemotherapy in Advanced Breast Cancer: A Meta-Analysis of Ten Randomized Controlled Trials. *PloS one* **10**, e0133569, doi:10.1371/journal.pone.0133569 (2015).
99 Kong, G. & Dewhirst, M. W. Hyperthermia and liposomes. *International journal of hyperthermia : the official journal of European Society for Hyperthermic Oncology, North American Hyperthermia Group* **15**, 345-370 (1999).
100 Vangasseri, D. P. *et al.* Immunostimulation of dendritic cells by cationic liposomes. *Molecular membrane biology* **23**, 385-395 (2006).
101 Collins, D. S., Findlay, K. & Harding, C. Processing of exogenous liposome-encapsulated antigens in vivo generates class I MHC-restricted T cell responses. *The Journal of Immunology* **148**, 3336-3341 (1992).
102 Harding, C. V., Collins, D. S., Kanagawa, O. & Unanue, E. R. Liposome-encapsulated antigens engender lysosomal processing for class II MHC presentation and cytosolic processing for class I presentation. *The Journal of Immunology* **147**, 2860-2863 (1991).
103 Suzuki, Y. *et al.* Liposome-encapsulated CpG oligodeoxynucleotides as a potent adjuvant for inducing type 1 innate immunity. *Cancer research* **64**, 8754-8760, doi:10.1158/0008-5472.can-04-1691 (2004).
104 Ross, P. C. & Hui, S. W. Lipoplex size is a major determinant of in vitro lipofection efficiency. *Gene Therapy* **6**, 651-659, doi:10.1038/sj.gt.3300863 (1999).
105 Sayour, E. J., Mendez-Gomez, H. R. & Mitchell, D. A. Cancer vaccine immunotherapy with RNA-loaded liposomes. *International journal of molecular sciences* **19**, 2890 (2018).

106 Schoenmaker, L. *et al.* mRNA-lipid nanoparticle COVID-19 vaccines: Structure and stability. *International journal of pharmaceutics* **601**, 120586, doi:https://doi.org/10.1016/j.ijpharm.2021.120586 (2021).
107 Moon, J. J. *et al.* Interbilayer-crosslinked multilamellar vesicles as synthetic vaccines for potent humoral and cellular immune responses. *Nature materials* **10**, 243-251, doi:10.1038/nmat2960 (2011).
108 Seow, Y. & Wood, M. J. Biological gene delivery vehicles: beyond viral vectors. *Molecular Therapy* **17**, 767-777 (2009).
109 Madhusudan, S. *et al.* A multicenter Phase I gene therapy clinical trial involving intraperitoneal administration of E1A-lipid complex in patients with recurrent epithelial ovarian cancer overexpressing HER-2/neu oncogene. *Clinical Cancer Research* **10**, 2986-2996 (2004).
110 Wakabayashi, T. *et al.* A phase I clinical trial of interferon‐beta gene therapy for high‐grade glioma: novel findings from gene expression profiling and autopsy. *The Journal of Gene Medicine: A cross‐disciplinary journal for research on the science of gene transfer and its clinical applications* **10**, 329-339 (2008).
111 Wang, D., Sun, Y., Liu, Y., Meng, F. & Lee, R. J. Clinical translation of immunoliposomes for cancer therapy: Recent perspectives. *Expert opinion on drug delivery* **15**, 893-903 (2018).
112 Yoo, G. H. *et al.* Phase I trial of intratumoral liposome E1A gene therapy in patients with recurrent breast and head and neck cancer. *Clinical cancer research* **7**, 1237-1245 (2001).
113 Yadav, A., Murthy, M., Shete, A. & Sakhare, S. Stability aspects of liposomes. *Indian Journal of Pharmaceutical Education and Research* **45**, 402-413 (2011).
114 Olusanya, T. O. B., Haj Ahmad, R. R., Ibegbu, D. M., Smith, J. R. & Elkordy, A. A. Liposomal Drug Delivery Systems and Anticancer Drugs. *Molecules* **23**, 907, doi:10.3390/molecules23040907 (2018).
115 Briuglia, M.-L., Rotella, C., McFarlane, A. & Lamprou, D. A. Influence of cholesterol on liposome stability and on in vitro drug release. *Drug delivery and translational research* **5**, 231-242 (2015).
116 Rideau, E., Dimova, R., Schwille, P., Wurm, F. R. & Landfester, K. Liposomes and polymersomes: a comparative review towards cell mimicking. *Chemical Society reviews* **47**, 8572-8610, doi:10.1039/C8CS00162F (2018).
117 Massignani, M., Lomas, H. & Battaglia, G. Polymersomes: a synthetic biological approach to encapsulation and delivery. *Modern techniques for nano-and microreactors/-reactions*, 115-154 (2010).
118 Ahmed, F. *et al.* Shrinkage of a rapidly growing tumor by drug-loaded polymersomes: pH-triggered release through copolymer degradation. *Molecular pharmaceutics* **3**, 340-350 (2006).
119 Ahmed, F. *et al.* Biodegradable polymersomes loaded with both paclitaxel and doxorubicin permeate and shrink tumors, inducing apoptosis in proportion to accumulated drug. *Journal of Controlled Release* **116**, 150-158 (2006).
120 Choucair, A., Lim Soo, P. & Eisenberg, A. Active loading and tunable release of doxorubicin from block copolymer vesicles. *Langmuir : the ACS journal of surfaces and colloids* **21**, 9308-9313 (2005).

121 Xiaoli, S. & Na, Z. Cationic Polymer Optimization for Efficient Gene Delivery. *Mini-Reviews in Medicinal Chemistry* **10**, 108-125, doi:http://dx.doi.org/10.2174/138955710791185109 (2010).
122 Boussif, O. *et al.* A versatile vector for gene and oligonucleotide transfer into cells in culture and in vivo: polyethylenimine. *Proceedings of the National Academy of Sciences* **92**, 7297-7301 (1995).
123 Pack, D. W., Hoffman, A. S., Pun, S. & Stayton, P. S. Design and development of polymers for gene delivery. *Nature reviews Drug discovery* **4**, 581-593 (2005).
124 Wei, P., Sun, M., Yang, B., Xiao, J. & Du, J. Ultrasound-responsive polymersomes capable of endosomal escape for efficient cancer therapy. *Journal of controlled release : official journal of the Controlled Release Society* **322**, 81-94, doi:10.1016/j.jconrel.2020.03.013 (2020).
125 Lim, S. K., De Hoog, H.-P., Parikh, A. N., Nallani, M. & Liedberg, B. Hybrid, nanoscale phospholipid/block copolymer vesicles. *Polymers* **5**, 1102-1114 (2013).
126 Nam, J., Vanderlick, T. K. & Beales, P. A. Formation and dissolution of phospholipid domains with varying textures in hybrid lipo-polymersomes. *Soft Matter* **8**, 7982-7988 (2012).
127 Cheng, Z. *et al.* Improved tumor targeting of polymer-based nanovesicles using polymer–lipid blends. *Bioconjugate chemistry* **22**, 2021-2029 (2011).
128 Wei, P., Sun, M., Yang, B., Xiao, J. & Du, J. Ultrasound-responsive polymersomes capable of endosomal escape for efficient cancer therapy. *Journal of Controlled Release* **322**, 81-94, doi:https://doi.org/10.1016/j.jconrel.2020.03.013 (2020).
129 Stride, E. *et al.* Microbubble Agents: New Directions. *Ultrasound in Medicine & Biology* **46**, 1326-1343, doi:https://doi.org/10.1016/j.ultrasmedbio.2020.01.027 (2020).
130 Cai, W. B. *et al.* The optimized fabrication of nanobubbles as ultrasound contrast agents for tumor imaging. *Scientific reports* **5**, 1-11 (2015).
131 Endo-Takahashi, Y. & Negishi, Y. Microbubbles and Nanobubbles with Ultrasound for Systemic Gene Delivery. *Pharmaceutics* **12**, doi:10.3390/pharmaceutics12100964 (2020).
132 VanOsdol, J. *et al.* Sequential HIFU heating and nanobubble encapsulation provide efficient drug penetration from stealth and temperature sensitive liposomes in colon cancer. *Journal of Controlled Release* **247**, 55-63, doi:https://doi.org/10.1016/j.jconrel.2016.12.033 (2017).
133 Ferrara, K., Pollard, R. & Borden, M. Ultrasound microbubble contrast agents: fundamentals and application to gene and drug delivery. *Annu Rev Biomed Eng* **9**, 415-447, doi:10.1146/annurev.bioeng.8.061505.095852 (2007).
134 Perrault, S. D., Walkey, C., Jennings, T., Fischer, H. C. & Chan, W. C. W. Mediating Tumor Targeting Efficiency of Nanoparticles Through Design. *Nano Letters* **9**, 1909-1915, doi:10.1021/nl900031y (2009).
135 Fischer, H. C., Hauck, T. S., Gómez-Aristizábal, A. & Chan, W. C. W. Exploring Primary Liver Macrophages for Studying Quantum Dot Interactions with Biological Systems. *Advanced Materials* **22**, 2520-2524, doi:https://doi.org/10.1002/adma.200904231 (2010).
136 Vaupel, P., Höckel, M. & Mayer, A. Detection and characterization of tumor hypoxia using pO2 histography. *Antioxid Redox Signal* **9**, 1221-1235, doi:10.1089/ars.2007.1628 (2007).

137 Kwon, I. K., Lee, S. C., Han, B. & Park, K. Analysis on the current status of targeted drug delivery to tumors. *Journal of Controlled Release* **164**, 108-114, doi:https://doi.org/10.1016/j.jconrel.2012.07.010 (2012).
138 Xiang, Y., Bernards, N., Hoang, B., Zheng, J. & Matsuura, N. Perfluorocarbon nanodroplets can reoxygenate hypoxic tumors in vivo without carbogen breathing. *Nanotheranostics* **3**, 135-144, doi:10.7150/ntno.29908 (2019).
139 Subramanian, S. *et al.* Reporting of quantitative oxygen mapping in EPR imaging. *J Magn Reson* **214**, 244-251, doi:10.1016/j.jmr.2011.11.013 (2012).
140 Duan, L. *et al.* Micro/nano-bubble-assisted ultrasound to enhance the EPR effect and potential theranostic applications. *Theranostics* **10**, 462-483, doi:10.7150/thno.37593 (2020).
141 Buerki-Thurnherr, T. *et al.* In vitro mechanistic study towards a better understanding of ZnO nanoparticle toxicity. *Nanotoxicology* **7**, 402-416, doi:10.3109/17435390.2012.666575 (2013).
142 Bakand, S., Hayes, A. & Dechsakulthorn, F. Nanoparticles: a review of particle toxicology following inhalation exposure. *Inhalation toxicology* **24**, 125-135, doi:10.3109/08958378.2010.642021 (2012).
143 Sutunkova, M. P. *et al.* The most important inferences from the Ekaterinburg nanotoxicology team's animal experiments assessing adverse health effects of metallic and metal oxide nanoparticles. *Toxicology reports* **5**, 363-376, doi:10.1016/j.toxrep.2018.03.008 (2018).
144 de Smet, M., Heijman, E., Langereis, S., Hijnen, N. M. & Grüll, H. Magnetic resonance imaging of high intensity focused ultrasound mediated drug delivery from temperature-sensitive liposomes: An in vivo proof-of-concept study. *Journal of Controlled Release* **150**, 102-110, doi:https://doi.org/10.1016/j.jconrel.2010.10.036 (2011).
145 Amidi, M., de Raad, M., Crommelin, D. J., Hennink, W. E. & Mastrobattista, E. Antigen-expressing immunostimulatory liposomes as a genetically programmable synthetic vaccine. *Systems and synthetic biology* **5**, 21-31 (2011).
146 Kanaoka, E. *et al.* A novel and simple type of liposome carrier for recombinant interleukin‐2. *Journal of pharmacy and pharmacology* **53**, 295-302 (2001).
147 Kanaoka, E. *et al.* Continuous release of interleukin-2 from liposomal IL-2 (mixture of interleukin-2 and liposomes) after subcutaneous administration to mice. *Drug development and industrial pharmacy* **29**, 1149-1153 (2003).
148 Anderson, P. M. *et al.* Depot characteristics and biodistribution of interleukin-2 liposomes: importance of route of administration. *Journal of immunotherapy: official journal of the Society for Biological Therapy* **12**, 19-31 (1992).
149 Iyoda, T. *et al.* Optimal therapeutic strategy using antigen‐containing liposomes selectively delivered to antigen‐presenting cells. *Cancer science* **110**, 875-887 (2019).
150 Jain, S., Tran, T.-H. & Amiji, M. Macrophage repolarization with targeted alginate nanoparticles containing IL-10 plasmid DNA for the treatment of experimental arthritis. *Biomaterials* **61**, 162-177 (2015).
151 Wang, Y. *et al.* Polymeric nanoparticles promote macrophage reversal from M2 to M1 phenotypes in the tumor microenvironment. *Biomaterials* **112**, 153-163 (2017).
152 Mahon, O. R. *et al.* Nano-particle mediated M2 macrophage polarization enhances bone formation and MSC osteogenesis in an IL-10 dependent manner. *Biomaterials* **239**, 119833 (2020).

153 Harrington, K. J. *et al.* Pegylated liposomes have potential as vehicles for intratumoral and subcutaneous drug delivery. *Clinical cancer research* **6**, 2528-2537 (2000).
154 Sethuraman, S. N. *et al.* Novel calreticulin-nanoparticle in combination with focused ultrasound induces immunogenic cell death in melanoma to enhance antitumor immunity. *Theranostics* **10**, 3397-3412, doi:10.7150/thno.42243 (2020).
155 Meraz, I. M. *et al.* Adjuvant cationic liposomes presenting MPL and IL-12 induce cell death, suppress tumor growth, and alter the cellular phenotype of tumors in a murine model of breast cancer. *Molecular pharmaceutics* **11**, 3484-3491 (2014).
156 Francian, A. *et al.* Intratumoral delivery of antigen with complement C3-bound liposomes reduces tumor growth in mice. *Nanomedicine: Nanotechnology, Biology and Medicine* **18**, 326-335 (2019).
157 Nomura, T., Koreeda, N., Yamashita, F., Takakura, Y. & Hashida, M. Effect of particle size and charge on the disposition of lipid carriers after intratumoral injection into tissue-isolated tumors. *Pharmaceutical research* **15**, 128-132, doi:10.1023/a:1011921324952 (1998).
158 Cubillos-Ruiz, J. R. *et al.* Polyethylenimine-based siRNA nanocomplexes reprogram tumor-associated dendritic cells via TLR5 to elicit therapeutic antitumor immunity. *The Journal of clinical investigation* **119**, 2231-2244 (2009).
159 He, W. *et al.* Re-polarizing myeloid-derived suppressor cells (MDSCs) with cationic polymers for cancer immunotherapy. *Scientific reports* **6**, 1-13 (2016).
160 Nikitczuk, K. P., Schloss, R. S., Yarmush, M. L. & Lattime, E. C. PLGA-polymer encapsulating tumor antigen and CpG DNA administered into the tumor microenvironment elicits a systemic antigen-specific IFN-γ response and enhances survival. *Journal of cancer therapy* **4**, 280 (2013).
161 Da Silva, C. G. *et al.* Effective chemoimmunotherapy by co-delivery of doxorubicin and immune adjuvants in biodegradable nanoparticles. *Theranostics* **9**, 6485 (2019).
162 Min, Y. *et al.* Antigen-capturing nanoparticles improve the abscopal effect and cancer immunotherapy. *Nature nanotechnology* **12**, 877-882 (2017).
163 ter Haar, G. & Coussios, C. High intensity focused ultrasound: physical principles and devices. *International journal of hyperthermia* **23**, 89-104 (2007).
164 Kannadorai, R. K. & Liu, Q. Optimization in interstitial plasmonic photothermal therapy for treatment planning. *Medical physics* **40**, 103301 (2013).
165 Kang, H., Jia, B., Li, J., Morrish, D. & Gu, M. Enhanced photothermal therapy assisted with gold nanorods using a radially polarized beam. *Applied physics letters* **96**, 063702 (2010).
166 Golovin, Y. I. *et al.* The dynamics of magnetic nanoparticles exposed to non-heating alternating magnetic field in biochemical applications: theoretical study. *Journal of Nanoparticle Research* **19**, 59 (2017).
167 Skalina, K. A., Singh, S., Chavez, C. G., Macian, F. & Guha, C. Low intensity focused ultrasound (LOFU)-mediated acoustic immune priming and ablative radiation therapy for in situ tumor vaccines. *Scientific reports* **9**, 1-12 (2019).
168 Staruch, R. M., Hynynen, K. & Chopra, R. Hyperthermia-mediated doxorubicin release from thermosensitive liposomes using MR-HIFU: Therapeutic effect in rabbit Vx2 tumours. *International Journal of Hyperthermia* **31**, 118-133 (2015).
169 Haemmerich, D. & Laeseke, P. F. Thermal tumour ablation: devices, clinical applications and future directions. *International journal of hyperthermia : the official journal of European Society for Hyperthermic Oncology, North American Hyperthermia Group* **21**, 755-760, doi:10.1080/02656730500226423 (2005).

170 van den Bijgaart, R. J. *et al.* Thermal and mechanical high-intensity focused ultrasound: perspectives on tumor ablation, immune effects and combination strategies. *Cancer immunology, immunotherapy : CII* **66**, 247-258, doi:10.1007/s00262-016-1891-9 (2017).
171 Steinke, K. *et al.* Pulmonary radiofrequency ablation--an international study survey. *Anticancer Res* **24**, 339-343 (2004).
172 Yasui, K. *et al.* Thoracic tumors treated with CT-guided radiofrequency ablation: initial experience. *Radiology* **231**, 850-857, doi:10.1148/radiol.2313030347 (2004).
173 Schiller, J. D., Gervais, D. A. & Mueller, P. R. Radiofrequency ablation of renal cell carcinoma. *Abdom Imaging* **30**, 442-450, doi:10.1007/s00261-004-0259-3 (2005).
174 Hori, T. *et al.* Risk factors for the local recurrence of hepatocellular carcinoma after a single session of percutaneous radiofrequency ablation. *J Gastroenterol* **38**, 977-981, doi:10.1007/s00535-003-1181-0 (2003).
175 Maxwell, A. *et al.* Disintegration of tissue using high intensity focused ultrasound: Two approaches that utilize shock waves. *Acoustics Today* **8**, 24-36 (2012).
176 Qu, S. *et al.* Non-thermal histotripsy tumor ablation promotes abscopal immune responses that enhance cancer immunotherapy. *Journal for immunotherapy of cancer* **8**, e000200, doi:10.1136/jitc-2019-000200 (2020).
177 Schade, G. R. Evaluation of the Systemic Response to Boiling Histotripsy Treatment for Renal Carcinoma.
178 Hu, Z. *et al.* Release of endogenous danger signals from HIFU-treated tumor cells and their stimulatory effects on APCs. *Biochemical and biophysical research communications* **335**, 124-131, doi:https://doi.org/10.1016/j.bbrc.2005.07.071 (2005).
179 Issels, R. D. *et al.* Neo-adjuvant chemotherapy alone or with regional hyperthermia for localised high-risk soft-tissue sarcoma: a randomised phase 3 multicentre study. *Lancet Oncol* **11**, 561-570, doi:10.1016/s1470-2045(10)70071-1 (2010).
180 Kaur, P., Hurwitz, M. D., Krishnan, S. & Asea, A. Combined hyperthermia and radiotherapy for the treatment of cancer. *Cancers* **3**, 3799-3823 (2011).
181 Hainfeld, J. F. *et al.* Gold nanoparticle hyperthermia reduces radiotherapy dose. *Nanomedicine: Nanotechnology, Biology and Medicine* **10**, 1609-1617 (2014).
182 Mortezaee, K. *et al.* Synergic effects of nanoparticles-mediated hyperthermia in radiotherapy/chemotherapy of cancer. *Life Sciences* **269**, 119020, doi:https://doi.org/10.1016/j.lfs.2021.119020 (2021).
183 Datta, N. R. *et al.* Hyperthermia and radiotherapy with or without chemotherapy in locally advanced cervical cancer: a systematic review with conventional and network meta-analyses. *International Journal of Hyperthermia* **32**, 809-821 (2016).
184 van der Zee, J. *et al.* Comparison of radiotherapy alone with radiotherapy plus hyperthermia in locally advanced pelvic tumours: a prospective, randomised, multicentre trial. *The Lancet* **355**, 1119-1125 (2000).
185 Vasanthan, A. *et al.* Regional hyperthermia combined with radiotherapy for uterine cervical cancers: a multi-institutional prospective randomized trial of the international atomic energy agency. *International Journal of Radiation Oncology* Biology* Physics* **61**, 145-153 (2005).
186 Storm, F. K. Clinical hyperthermia and chemotherapy. *Radiologic clinics of North America* **27**, 621-627 (1989).
187 Nguyen, H. T. *et al.* Combined hyperthermia and chemotherapy as a synergistic anticancer treatment. *Journal of Pharmaceutical Investigation* **49**, 519-526 (2019).

188 Liu, D. *et al.* Targeted destruction of cancer stem cells using multifunctional magnetic nanoparticles that enable combined hyperthermia and chemotherapy. *Theranostics* **10**, 1181 (2020).
189 Hurwitz, M. D. *et al.* Hyperthermia combined with radiation for the treatment of locally advanced prostate cancer: Long‐term results from Dana‐Farber Cancer Institute study 94‐153. *Cancer* **117**, 510-516 (2011).
190 Colombo, R. *et al.* Multicentric Study Comparing Intravesical Chemotherapy Alone and With Local Microwave Hyperthermia for Prophylaxis of Recurrence of Superficial Transitional Cell Carcinoma. *Journal of Clinical Oncology* **21**, 4270-4276, doi:10.1200/jco.2003.01.089 (2003).
191 Colombo, R., Salonia, A., Leib, Z., Pavone‐Macaluso, M. & Engelstein, D. Long‐term outcomes of a randomized controlled trial comparing thermochemotherapy with mitomycin‐C alone as adjuvant treatment for non‐muscle‐invasive bladder cancer (NMIBC). *BJU International-British Journal of Urology* **107**, 912 (2011).
192 Young, J. K., Figueroa, E. R. & Drezek, R. A. Tunable nanostructures as photothermal theranostic agents. *Annals of biomedical engineering* **40**, 438-459 (2012).
193 Zhang, Z., Wang, J. & Chen, C. Near‐infrared light‐mediated nanoplatforms for cancer thermo‐chemotherapy and optical imaging. *Advanced Materials* **25**, 3869-3880 (2013).
194 Zhou, F. *et al.* InCVAX–a novel strategy for treatment of late-stage, metastatic cancers through photoimmunotherapy induced tumor-specific immunity. *Cancer letters* **359**, 169-177 (2015).
195 Zhang, Z. *et al.* Near infrared laser-induced targeted cancer therapy using thermoresponsive polymer encapsulated gold nanorods. *Journal of the American Chemical Society* **136**, 7317-7326 (2014).
196 Wang, C. *et al.* Immunological responses triggered by photothermal therapy with carbon nanotubes in combination with anti‐CTLA‐4 therapy to inhibit cancer metastasis. *Advanced Materials* **26**, 8154-8162 (2014).
197 Vines, J. B., Yoon, J.-H., Ryu, N.-E., Lim, D.-J. & Park, H. Gold Nanoparticles for Photothermal Cancer Therapy. *Frontiers in chemistry* **7**, doi:10.3389/fchem.2019.00167 (2019).
198 Cano-Mejia, J. *et al.* Prussian blue nanoparticle-based photothermal therapy combined with checkpoint inhibition for photothermal immunotherapy of neuroblastoma. *Nanomedicine: Nanotechnology, Biology and Medicine* **13**, 771-781, doi:https://doi.org/10.1016/j.nano.2016.10.015 (2017).
199 Elsherbini, A. A. M., Saber, M., Aggag, M., El-Shahawy, A. & Shokier, H. A. A. Magnetic nanoparticle-induced hyperthermia treatment under magnetic resonance imaging. *Magnetic Resonance Imaging* **29**, 272-280, doi:https://doi.org/10.1016/j.mri.2010.08.010 (2011).
200 Yang, L. *et al.* Receptor-Targeted Nanoparticles for In vivo Imaging of Breast Cancer. *Clinical Cancer Research* **15**, 4722-4732, doi:10.1158/1078-0432.Ccr-08-3289 (2009).
201 Maya, S. *et al.* Chitosan cross-linked docetaxel loaded EGF receptor targeted nanoparticles for lung cancer cells. *International Journal of Biological Macromolecules* **69**, 532-541, doi:https://doi.org/10.1016/j.ijbiomac.2014.06.009 (2014).
202 Kumari, M. *et al.* Curcumin loaded selenium nanoparticles synergize the anticancer potential of doxorubicin contained in self-assembled, cell receptor targeted

nanoparticles. *European Journal of Pharmaceutics and Biopharmaceutics* **130**, 185-199, doi:https://doi.org/10.1016/j.ejpb.2018.06.030 (2018).
203 Zhou, H. *et al.* IGF1 Receptor Targeted Theranostic Nanoparticles for Targeted and Image-Guided Therapy of Pancreatic Cancer. *ACS nano* **9**, 7976-7991, doi:10.1021/acsnano.5b01288 (2015).
204 Gao, D.-Y. *et al.* CXCR4-targeted lipid-coated PLGA nanoparticles deliver sorafenib and overcome acquired drug resistance in liver cancer. *Biomaterials* **67**, 194-203, doi:https://doi.org/10.1016/j.biomaterials.2015.07.035 (2015).
205 Yu, M. *et al.* AMD3100 sensitizes acute lymphoblastic leukemia cells to chemotherapy in vivo. *Blood Cancer Journal* **1**, e14-e14, doi:10.1038/bcj.2011.13 (2011).
206 Domanska, U. M. *et al.* CXCR4 inhibition with AMD3100 sensitizes prostate cancer to docetaxel chemotherapy. *Neoplasia* **14**, 709-718 (2012).
207 Chen, Y. *et al.* Differential effects of sorafenib on liver versus tumor fibrosis mediated by stromal‐derived factor 1 alpha/C‐X‐C receptor type 4 axis and myeloid differentiation antigen‐positive myeloid cell infiltration in mice. *Hepatology* **59**, 1435-1447 (2014).
208 Vila-Coro, A. J. *et al.* The chemokine SDF-lα triggers CXCR4 receptor dimerization and activates the JAK/STAT pathway. *The FASEB Journal* **13**, 1699-1710, doi:https://doi.org/10.1096/fasebj.13.13.1699 (1999).
209 Pfeiffer, M. *et al.* Alternative implication of CXCR4 in JAK2/STAT3 activation in small cell lung cancer. *Br J Cancer* **100**, 1949-1956, doi:10.1038/sj.bjc.6605068 (2009).
210 McDonald, D. M. & Baluk, P. Significance of Blood Vessel Leakiness in Cancer. *Cancer research* **62**, 5381-5385 (2002).
211 Maeda, H., Wu, J., Sawa, T., Matsumura, Y. & Hori, K. Tumor vascular permeability and the EPR effect in macromolecular therapeutics: a review. *Journal of Controlled Release* **65**, 271-284, doi:https://doi.org/10.1016/S0168-3659(99)00248-5 (2000).
212 Maeda, H. The enhanced permeability and retention (EPR) effect in tumor vasculature: the key role of tumor-selective macromolecular drug targeting. *Advances in enzyme regulation* (2001).
213 Fang, J., Nakamura, H. & Maeda, H. The EPR effect: unique features of tumor blood vessels for drug delivery, factors involved, and limitations and augmentation of the effect. *Advanced drug delivery reviews* **63**, 136-151 (2011).
214 Chang, B. *et al.* Thermo and pH dual responsive, polymer shell coated, magnetic mesoporous silica nanoparticles for controlled drug release. *Journal of materials chemistry* **21**, 9239-9247 (2011).
215 Deka, S. R. *et al.* Acidic pH-responsive nanogels as smart cargo systems for the simultaneous loading and release of short oligonucleotides and magnetic nanoparticles. *Langmuir : the ACS journal of surfaces and colloids* **26**, 10315-10324 (2010).
216 Bae, Y., Nishiyama, N. & Kataoka, K. In vivo antitumor activity of the folate-conjugated pH-sensitive polymeric micelle selectively releasing adriamycin in the intracellular acidic compartments. *Bioconjugate chemistry* **18**, 1131-1139 (2007).
217 Bae, Y., Fukushima, S., Harada, A. & Kataoka, K. Design of environment‐sensitive supramolecular assemblies for intracellular drug delivery: Polymeric micelles that are responsive to intracellular pH change. *Angewandte Chemie* **115**, 4788-4791 (2003).
218 Lee, E. S., Na, K. & Bae, Y. H. Doxorubicin loaded pH-sensitive polymeric micelles for reversal of resistant MCF-7 tumor. *Journal of controlled release* **103**, 405-418 (2005).

219 Yu, S. *et al.* Magnetic and pH-sensitive nanoparticles for antitumor drug delivery. *Colloids and Surfaces B: Biointerfaces* **103**, 15-22, doi:https://doi.org/10.1016/j.colsurfb.2012.10.041 (2013).
220 Xie, G. *et al.* On-demand release of CO2 from photothermal hydrogels for accelerating skin wound healing. *Chemical Engineering Journal* **403**, 126353, doi:https://doi.org/10.1016/j.cej.2020.126353 (2021).
221 Wilson, W. R. & Hay, M. P. Targeting hypoxia in cancer therapy. *Nature Reviews Cancer* **11**, 393-410, doi:10.1038/nrc3064 (2011).
222 Brown, J. M. SR 4233 (Tirapazamine): a new anticancer drug exploiting hypoxia in solid tumours. *Br J Cancer* **67**, 1163-1170, doi:10.1038/bjc.1993.220 (1993).
223 Gu, Y. *et al.* Roles of DNA repair and reductase activity in the cytotoxicity of the hypoxia-activated dinitrobenzamide mustard PR-104A. *Molecular cancer therapeutics* **8**, 1714-1723, doi:10.1158/1535-7163.Mct-08-1209 (2009).
224 Thambi, T. *et al.* Hypoxia-responsive polymeric nanoparticles for tumor-targeted drug delivery. *Biomaterials* **35**, 1735-1743, doi:https://doi.org/10.1016/j.biomaterials.2013.11.022 (2014).
225 Liu, H. *et al.* Development of a hypoxia-triggered and hypoxic radiosensitized liposome as a doxorubicin carrier to promote synergetic chemo-/radio-therapy for glioma. *Biomaterials* **121**, 130-143, doi:https://doi.org/10.1016/j.biomaterials.2017.01.001 (2017).
226 Wang, Y., Shang, W., Niu, M., Tian, J. & Xu, K. Hypoxia-active nanoparticles used in tumor theranostic. *International journal of nanomedicine* **14**, 3705-3722, doi:10.2147/IJN.S196959 (2019).
227 Xavierselvan, M. *et al.* Photoacoustic Nanodroplets for Oxygen Enhanced Photodynamic Therapy of Cancer. *Photoacoustics*, 100306, doi:https://doi.org/10.1016/j.pacs.2021.100306 (2021).
228 Plenderleith, I. H. Treating the treatment: toxicity of cancer chemotherapy. *Can Fam Physician* **36**, 1827-1830 (1990).
229 Ullah, M. F. Cancer multidrug resistance (MDR): a major impediment to effective chemotherapy. *Asian Pacific journal of cancer prevention : APJCP* **9**, 1-6 (2008).
230 Liang, X.-J., Chen, C., Zhao, Y. & Wang, P. C. in *Multi-Drug Resistance in Cancer* (ed Jun Zhou) 467-488 (Humana Press, 2010).
231 Hainfeld, J. F. *et al.* Gold nanoparticle hyperthermia reduces radiotherapy dose. *Nanomedicine : nanotechnology, biology, and medicine* **10**, 1609-1617, doi:10.1016/j.nano.2014.05.006 (2014).
232 Fox, E. J. Mechanism of action of mitoxantrone. *Neurology* **63**, S15-18, doi:10.1212/wnl.63.12_suppl_6.s15 (2004).
233 Ehninger, G., Schuler, U., Proksch, B., Zeller, K.-P. & Blanz, J. Pharmacokinetics and Metabolism of Mitoxantrone A Review. *Clinical Pharmacokinetics* **18**, 365-380, doi:10.2165/00003088-199018050-00003 (1990).
234 Henderson, I. C. *et al.* Randomized clinical trial comparing mitoxantrone with doxorubicin in previously treated patients with metastatic breast cancer. *Journal of Clinical Oncology* **7**, 560-571, doi:10.1200/JCO.1989.7.5.560 (1989).
235 Rossato, L. G. *et al.* The metabolic profile of mitoxantrone and its relation with mitoxantrone-induced cardiotoxicity. *Archives of toxicology* **87**, 1809-1820 (2013).
236 Li, C. *et al.* Encapsulation of mitoxantrone into pegylated SUVs enhances its antineoplastic efficacy. *European Journal of Pharmaceutics and Biopharmaceutics* **70**, 657-665, doi:https://doi.org/10.1016/j.ejpb.2008.05.019 (2008).

237 Kashiwayanagi, M., Suenaga, A., Enomoto, S. & Kurihara, K. Membrane fluidity changes of liposomes in response to various odorants. Complexity of membrane composition and variety of adsorption sites for odorants. *Biophys J* **58**, 887-895, doi:10.1016/S0006-3495(90)82433-4 (1990).
238 Discher, D. E. & Ahmed, F. POLYMERSOMES. *Annual Review of Biomedical Engineering* **8**, 323-341, doi:10.1146/annurev.bioeng.8.061505.095838 (2006).
239 Elhelf, I. A. S. *et al.* High intensity focused ultrasound: The fundamentals, clinical applications and research trends. *Diagnostic and Interventional Imaging* **99**, 349-359, doi:https://doi.org/10.1016/j.diii.2018.03.001 (2018).
240 Negussie, A. H. *et al.* Formulation and characterisation of magnetic resonance imageable thermally sensitive liposomes for use with magnetic resonance-guided high intensity focused ultrasound. *International Journal of Hyperthermia* **27**, 140-155 (2011).
241 Mayer, L., Bally, M. & Cullis, P. Uptake of adriamycin into large unilamellar vesicles in response to a pH gradient. *Biochimica et Biophysica Acta (BBA)-Biomembranes* **857**, 123-126 (1986).
242 Maples, D. *et al.* Synthesis and characterisation of ultrasound imageable heat-sensitive liposomes for HIFU therapy. *International journal of hyperthermia : the official journal of European Society for Hyperthermic Oncology, North American Hyperthermia Group* **31**, 674-685, doi:10.3109/02656736.2015.1057622 (2015).
243 Li, S., Byrne, B., Welsh, J. & Palmer, A. F. Self‐Assembled Poly (butadiene)‐b‐poly (ethylene oxide) Polymersomes as Paclitaxel Carriers. *Biotechnology progress* **23**, 278-285 (2007).
244 Dou, Y., Hynynen, K. & Allen, C. To heat or not to heat: Challenges with clinical translation of thermosensitive liposomes. *Journal of controlled release : official journal of the Controlled Release Society* **249**, 63-73, doi:10.1016/j.jconrel.2017.01.025 (2017).
245 Danaei, M. *et al.* Impact of Particle Size and Polydispersity Index on the Clinical Applications of Lipidic Nanocarrier Systems. *Pharmaceutics* **10**, doi:10.3390/pharmaceutics10020057 (2018).
246 Anajafi, T. & Mallik, S. Polymersome-based drug-delivery strategies for cancer therapeutics. *Ther Deliv* **6**, 521-534, doi:10.4155/tde.14.125 (2015).
247 Shuwen, G. *et al.* Supramoleculr Polymersomes Constucted from Water-soluble Pillar[5]arene and Cationic Poly(glutamamide)s and Their Applications for Targeted Anticancer Drug Delivery. *Polym. Chem.* **8**, doi:10.1039/C7PY01259D (2017).
248 Kulkarni, P. *et al.* Tissue-Penetrating, Hypoxia-Responsive Echogenic Polymersomes For Drug Delivery To Solid Tumors. *Chemistry* **24**, 12490-12494, doi:10.1002/chem.201802229 (2018).
249 Xia, L. *et al.* Acoustic Characterization of Echogenic Polymersomes Prepared From Amphiphilic Block Copolymers. *Ultrasound Med Biol* **44**, 447-457, doi:10.1016/j.ultrasmedbio.2017.10.011 (2018).
250 Karandish, F. *et al.* Nucleus-Targeted, Echogenic Polymersomes for Delivering a Cancer Stemness Inhibitor to Pancreatic Cancer Cells. *Biomacromolecules* **19**, 4122-4132, doi:10.1021/acs.biomac.8b01133 (2018).
251 Bader, K. B., Vlaisavljevich, E. & Maxwell, A. D. For Whom the Bubble Grows: Physical Principles of Bubble Nucleation and Dynamics in Histotripsy Ultrasound Therapy. *Ultrasound Med Biol* **45**, 1056-1080, doi:10.1016/j.ultrasmedbio.2018.10.035 (2019).
252 Thi, T. T. H. *et al.* Lipid-Based Nanoparticles in the Clinic and Clinical Trials: From Cancer Nanomedicine to COVID-19 Vaccines. *Vaccines* **9**, doi:10.3390/vaccines9040359 (2021).

253 Hayes, D. F. *et al.* Tumor Marker Utility Grading System: a Framework to Evaluate Clinical Utility of Tumor Markers. *JNCI: Journal of the National Cancer Institute* **88**, 1456-1466, doi:10.1093/jnci/88.20.1456 (1996).
254 McKenna, R. J. Clinical aspects of cancer in the elderly. Treatment decisions, treatment choices, and follow‐up. *Cancer* **74**, 2107-2117 (1994).
255 Hammerich, L., Bhardwaj, N., Kohrt, H. E. & Brody, J. D. In situ vaccination for the treatment of cancer. *Immunotherapy* **8**, 315-330 (2016).
256 Hammerich, L., Binder, A. & Brody, J. D. In situ vaccination: Cancer immunotherapy both personalized and off-the-shelf. *Molecular oncology* **9**, 1966-1981, doi:10.1016/j.molonc.2015.10.016 (2015).
257 Suresh, M. *et al.* Role of CD28-B7 interactions in generation and maintenance of CD8 T cell memory. *The Journal of Immunology* **167**, 5565-5573 (2001).
258 Krysko, D. V. *et al.* Immunogenic cell death and DAMPs in cancer therapy. *Nature Reviews Cancer* **12**, 860-875, doi:10.1038/nrc3380 (2012).
259 Li, C. *et al.* Mitoxantrone triggers immunogenic prostate cancer cell death via p53-dependent PERK expression. *Cellular Oncology* **43**, 1099-1116, doi:10.1007/s13402-020-00544-2 (2020).
260 Workenhe, S. T., Pol, J. G., Lichty, B. D., Cummings, D. T. & Mossman, K. L. Combining oncolytic HSV-1 with immunogenic cell death-inducing drug mitoxantrone breaks cancer immune tolerance and improves therapeutic efficacy. *Cancer immunology research* **1**, 309-319 (2013).
261 Ratschker, T. *et al.* Mitoxantrone-Loaded Nanoparticles for Magnetically Controlled Tumor Therapy–Induction of Tumor Cell Death, Release of Danger Signals and Activation of Immune Cells. *Pharmaceutics* **12**, 923 (2020).
262 Alev, M. *et al.* Targeting of drug-loaded nanoparticles to tumor sites increases cell death and release of danger signals. *Journal of Controlled Release* **285**, 67-80, doi:https://doi.org/10.1016/j.jconrel.2018.07.007 (2018).
263 Danhier, F. To exploit the tumor microenvironment: Since the EPR effect fails in the clinic, what is the future of nanomedicine? *Journal of Controlled Release* **244**, 108-121 (2016).
264 Lee, H. L. *et al.* Redox- and pH-Responsive Nanoparticles Release Piperlongumine in a Stimuli-Sensitive Manner to Inhibit Pulmonary Metastasis of Colorectal Carcinoma Cells. *J Pharm Sci* **107**, 2702-2712, doi:10.1016/j.xphs.2018.06.011 (2018).
265 Maxwell, A. D. *et al.* Disintegration of tissue using high intensity focused ultrasound: Two approaches that utilize shock waves. *Acoustics Today* **8**, 24-36 (2012).
266 Roberts, W. W. Development and translation of histotripsy: current status and future directions. *Curr Opin Urol* **24**, 104-110, doi:10.1097/mou.0000000000000001 (2014).
267 Newman, C. M. H. & Bettinger, T. Gene therapy progress and prospects: Ultrasound for gene transfer. *Gene Therapy* **14**, 465-475, doi:10.1038/sj.gt.3302925 (2007).
268 Rapoport, N. Combined cancer therapy by micellar-encapsulated drug and ultrasound. *International journal of pharmaceutics* **277**, 155-162 (2004).
269 Sung, H. H. *et al.* Seven years of experience with high‐intensity focused ultrasound for prostate cancer: Advantages and limitations. *The Prostate* **72**, 1399-1406 (2012).
270 Rapoport, N. *et al.* Ultrasound-mediated tumor imaging and nanotherapy using drug loaded, block copolymer stabilized perfluorocarbon nanoemulsions. *Journal of controlled release : official journal of the Controlled Release Society* **153**, 4-15, doi:10.1016/j.jconrel.2011.01.022 (2011).

271 Huang, F. Y. *et al.* Induction of enhanced immunogenic cell death through ultrasound-controlled release of doxorubicin by liposome-microbubble complexes. *Oncoimmunology* **7**, e1446720, doi:10.1080/2162402x.2018.1446720 (2018).
272 Ulvé, R. *et al.* Discovery of Human-Similar Gene Fusions in Canine Cancers. *Cancer research* **77**, 5721, doi:10.1158/0008-5472.CAN-16-2691 (2017).
273 Selting, K. A. *et al.* Outcome of dogs with high-grade soft tissue sarcomas treated with and without adjuvant doxorubicin chemotherapy: 39 cases (1996–2004). *Journal of the American Veterinary Medical Association* **227**, 1442-1448, doi:10.2460/javma.2005.227.1442 (2005).
274 Yu, W., Tang, L., Lin, F., Jiang, L. & Shen, Z. Significance of HIFU in local unresectable recurrence of soft tissue sarcoma, a single-center, respective, case series in China. *Surg Oncol* **30**, 117-121, doi:10.1016/j.suronc.2019.06.004 (2019).
275 Von Hoff, D. D., Coltman, C. A., Jr. & Forseth, B. Activity of mitoxantrone in a human tumor cloning system. *Cancer research* **41**, 1853-1855 (1981).
276 Bull, F. E., Von Hoff, D. D., Balcerzak, S. P., Stephens, R. L. & Panettiere, F. J. Phase II trial of mitoxantrone in advanced sarcomas: a Southwest Oncology Group study. *Cancer Treat Rep* **69**, 231-233 (1985).
277 Manickavasagam, D. & Oyewumi, M. O. Internalization of particulate delivery systems by activated microglia influenced the therapeutic efficacy of simvastatin repurposing for neuroinflammation. *International journal of pharmaceutics* **570**, 118690, doi:https://doi.org/10.1016/j.ijpharm.2019.118690 (2019).
278 Lee, J. *et al.* Caveolae‐M ediated Endocytosis of Conjugated Polymer Nanoparticles. *Macromolecular bioscience* **13**, 913-920 (2013).
279 Fittipaldi, A. *et al.* Cell membrane lipid rafts mediate caveolar endocytosis of HIV-1 Tat fusion proteins. *Journal of Biological Chemistry* **278**, 34141-34149 (2003).
280 Hahn, O. *et al.* Modulating the Heat Sensitivity of Prostate Cancer Cell Lines In Vitro: A New Impact for Focal Therapies. *Biomedicines* **8**, doi:10.3390/biomedicines8120585 (2020).
281 Xin, Y., Qi, Q., Mao, Z. & Zhan, X. PLGA nanoparticles introduction into mitoxantrone-loaded ultrasound-responsive liposomes: In vitro and in vivo investigations. *International journal of pharmaceutics* **528**, 47-54, doi:https://doi.org/10.1016/j.ijpharm.2017.05.059 (2017).
282 Batschinski, K. *et al.* Canine visceral hemangiosarcoma treated with surgery alone or surgery and doxorubicin: 37 cases (2005-2014). *Can Vet J* **59**, 967-972 (2018).
283 Gameiro, S. R. *et al.* Radiation-induced immunogenic modulation of tumor enhances antigen processing and calreticulin exposure, resulting in enhanced T-cell killing. *Oncotarget* **5**, 403-416, doi:10.18632/oncotarget.1719 (2014).
284 Kaye, S. B. The multidrug resistance phenotype. *Br J Cancer* **58**, 691-694, doi:10.1038/bjc.1988.291 (1988).
285 Fojo, A., Hamilton, T. C., Young, R. C. & Ozols, R. F. Multidrug resistance in ovarian cancer. *Cancer* **60**, 2075-2080, doi:https://doi.org/10.1002/1097-0142(19901015)60:8+<2075::AID-CNCR2820601521>3.0.CO;2-F (1987).
286 Song, X. *et al.* Hypoxia-induced resistance to cisplatin and doxorubicin in non-small cell lung cancer is inhibited by silencing of HIF-1alpha gene. *Cancer Chemother Pharmacol* **58**, 776-784, doi:10.1007/s00280-006-0224-7 (2006).

287 Frederiksen, L. J. *et al.* Hypoxia induced resistance to doxorubicin in prostate cancer cells is inhibited by low concentrations of glyceryl trinitrate. *The Journal of urology* **170**, 1003-1007 (2003).
288 Liang, Z. *et al.* CXCR4/CXCL12 axis promotes VEGF-mediated tumor angiogenesis through Akt signaling pathway. *Biochemical and biophysical research communications* **359**, 716-722, doi:10.1016/j.bbrc.2007.05.182 (2007).
289 Ishikawa, T. *et al.* Hypoxia enhances CXCR4 expression by activating HIF-1 in oral squamous cell carcinoma. *Oncology reports* **21**, 707-712 (2009).
290 Liu, Y.-L. *et al.* Regulation of the chemokine receptor CXCR4 and metastasis by hypoxia-inducible factor in non small cell lung cancer cell lines. *Cancer biology & therapy* **5**, 1320-1326 (2006).
291 Domanska, U. M. *et al.* A review on CXCR4/CXCL12 axis in oncology: no place to hide. *Eur. J. Cancer* **49**, 219-230 (2013).
292 Darash-Yahana, M. *et al.* Role of high expression levels of CXCR4 in tumor growth, vascularization, and metastasis. *FASEB J.* **18**, 1240-1242 (2004).
293 Zlotnik, A., Burkhardt, A. M. & Homey, B. Homeostatic chemokine receptors and organ-specific metastasis. *Nature Rev. Immunology* **11**, 597-606 (2011).
294 Ramsey, D. M. & McAlpine, S. R. Halting metastasis through CXCR4 inhibition. *Bioorganic & Med. Chem. Lett.* **23**, 20-25 (2013).
295 Beji, S. *et al.* Doxorubicin upregulates CXCR4 via miR-200c/ZEB1-dependent mechanism in human cardiac mesenchymal progenitor cells. *Cell Death & Disease* **8**, e3020-e3020, doi:10.1038/cddis.2017.409 (2017).
296 Domanska, U. M. *et al.* CXCR4 inhibition with AMD3100 sensitizes prostate cancer to docetaxel chemotherapy. *Neoplasia* **14**, 709-718, doi:10.1593/neo.12324 (2012).
297 Dragoj, M. *et al.* Targeting CXCR4 and FAK reverses doxorubicin resistance and suppresses invasion in non-small cell lung carcinoma. *Cell Oncol (Dordr)* **40**, 47-62, doi:10.1007/s13402-016-0304-6 (2017).
298 Ramsey, D. M. & McAlpine, S. R. Halting metastasis through CXCR4 inhibition. *Bioorg Med Chem Lett* **23**, 20-25, doi:10.1016/j.bmcl.2012.10.138 (2013).
299 Weich, A. *et al.* Wnt/β-Catenin Signaling Regulates CXCR4 Expression and [(68)Ga] Pentixafor Internalization in Neuroendocrine Tumor Cells. *Diagnostics (Basel)* **11**, doi:10.3390/diagnostics11020367 (2021).
300 Hubin, T. J., McCormick, J. M., Collinson, S. R., Alcock, N. W. & Busch, D. H. Ultra rigid cross-bridged tetraazamacrocycles as ligands--the challenge and the solution. *Chem. Commun.*, 1675-1676 (1998).
301 Hubin, T. J., McCormick, J. M., Alcock, N. W., Clase, H. J. & Busch, D. H. Crystallographic Characterization of Stepwise Changes in Ligand Conformations as Their Internal Topology Changes and Two Novel Cross-Bridged Tetraazamacrocyclic Copper(II) Complexes. *Inorg. Chem.* **38**, 4435-4446 (1999).
302 Hubin, T. J. *et al.* New iron(II) and manganese(II) complexes of two ultra-rigid, cross-bridged tetraazamacrocycles for catalysis and biomimicry. *J. Am. Chem. Soc.* **122**, 2512-2522 (2000).
303 Hubin, T. J. Synthesis and coordination chemistry of topologically constrained azamacrocycles. *Coord. Chem. Rev.* **241**, 27-46 (2003).
304 Valks, G. C. *et al.* Configurationally restricted bismacrocyclic CXCR4 receptor antagonists. *Journal of Medicinal Chemistry* **49**, 6162-6165, doi:10.1021/jm0607810 (2006).

305 Khan, A. *et al.* Binding optimization through coordination chemistry: CXCR4 chemokine receptor antagonists from ultrarigid metal complexes. *J. Am. Chem. Soc.* **131**, 3416-3417 (2009).
306 Smith, R. *et al.* CXCR4 chemokine receptor antagonists: nickel(II) complexes of configurationally restricted macrocycles. *Dalton Trans.* **41**, 11369-11377 (2012).
307 Maples, R. D. *et al.* Aspartate-based CXCR4 chemokine receptor binding of cross-bridged tetraazamacrocyclic copper(II) and zinc(II) complexes. *Chemistry: A European Journal* **22**, 12916-12930 (2016).
308 Wang, H., Yu, J., Lu, X. & He, X. Nanoparticle systems reduce systemic toxicity in cancer treatment. *Nanomedicine : nanotechnology, biology, and medicine* **11**, 103-106 (2016).
309 Hall, M. D., Okabe, M., Shen, D.-W., Liang, X.-J. & Gottesman, M. M. The role of cellular accumulation in determining sensitivity to platinum-based chemotherapy. *Annu. Rev. Pharmacol. Toxicol.* **48**, 495-535 (2008).
310 Luqmani, Y. Mechanisms of drug resistance in cancer chemotherapy. *Medical principles and practice* **14**, 35-48 (2005).
311 DeVita Jr, V. T., Serpick, A. A. & Carbone, P. P. Combination chemotherapy in the treatment of advanced Hodgkin's disease. *Annals of internal medicine* **73**, 881-895 (1970).
312 Fassnacht, M. *et al.* Combination chemotherapy in advanced adrenocortical carcinoma. *New England Journal of Medicine* **366**, 2189-2197 (2012).
313 Khan, A. *et al.* Binding optimization through coordination chemistry: CXCR4 chemokine receptor antagonists from ultrarigid metal complexes. *Journal of the American Chemical Society* **131**, 3416-3417, doi:10.1021/ja807921k (2009).
314 Le Baccon, M. *et al.* Bis-aminals: efficient tools for bis-macrocycle synthesis. *New Journal of Chemistry* **25**, 1168-1174 (2001).
315 Smith, R. *et al.* CXCR4 chemokine receptor antagonists: nickel (II) complexes of configurationally restricted macrocycles. *Dalton Transactions* **41**, 11369-11377 (2012).
316 Khalil, D. N. *et al.* In situ vaccination with defined factors overcomes T cell exhaustion in distant tumors. *J Clin Invest* **129**, 3435-3447, doi:10.1172/jci128562 (2019).
317 Liao, Y. X. *et al.* CXCR4 blockade sensitizes osteosarcoma to doxorubicin by inducing autophagic cell death via PI3K-Akt-mTOR pathway inhibition. *Int J Oncol* **59**, doi:10.3892/ijo.2021.5229 (2021).
318 Pallarès, V. *et al.* An Auristatin nanoconjugate targeting CXCR4+ leukemic cells blocks acute myeloid leukemia dissemination. *Journal of Hematology & Oncology* **13**, 36, doi:10.1186/s13045-020-00863-9 (2020).
319 Liu, J.-Y. *et al.* Delivery of siRNA Using CXCR4-targeted Nanoparticles Modulates Tumor Microenvironment and Achieves a Potent Antitumor Response in Liver Cancer. *Molecular Therapy* **23**, 1772-1782, doi:https://doi.org/10.1038/mt.2015.147 (2015).
320 Liu, J. Y. *et al.* Delivery of siRNA Using CXCR4-targeted Nanoparticles Modulates Tumor Microenvironment and Achieves a Potent Antitumor Response in Liver Cancer. *Molecular therapy : the journal of the American Society of Gene Therapy* **23**, 1772-1782, doi:10.1038/mt.2015.147 (2015).

VITA

MICHAEL-JOSEPH GORBET

Candidate for the Degree of

Doctor of Philosophy

Thesis: DEVELOPMENT OF BUBBLE AND LIGAND-BASED TARGETED NANOPARTICLES FOR SOLID TUMOR THERAPY

Major Field: COMPARATIVE BIOMEDICAL SCIENCES

Biographical:

Education:

Completed the requirements for the Doctor of Philosophy/Education in your major at Oklahoma State University, Stillwater, Oklahoma in December, 2021.

Completed the requirements for the Bachelor of Science in Chemistry at Southwestern Oklahoma State University, Weatherford, OK in 2016.

Experience:

Graduate Research Assistant
(August 2017- Dec 2021)

Professional Memberships:

American Chemical Society